THE PERTURBATION OF 3D PRINTED LONG-PERIOD FIBER GRATING DEVICE FOR TUNABLE OPTICAL FILTER INSIDE SINGLE-MODE FIBER

RAVIVUDH KHUN-IN

Student ID: NB17509

Major: Functional Control Systems

Supervisor

Prof. Hideki Yokoi

A thesis submitted in fulfilment of the

Requirements for the award of the degree of

Doctor of Engineering

Shibaura Institute of Technology

CANDIDATE'S DECLARATION

It is hereby declared that this dissertation or any part of it has not been submitted elsewhere for the award of any degree or diploma.

Signed: _____

(Ravivudh Khun-in)

Student no.: NB17509

Certified by: _____

(Prof. Hideki Yokoi)

Dedicated

To

My Honorable Supervisor

ACKNOWLEDGEMENTS

Beyond anything, I would like to express my appreciation and gratitude to many individuals for their assistance and contributions towards the success of this research study. Especially I am very delighted to express my gratefulness to my supervisor, ***Prof. Hideki Yokoi***, Department of Electronic Engineering, Shibaura Institute of Technology, Japan, for his valuable time, advices, and supports since the planning throughout the progress of this research work. His willingness and encouragement have been very much appreciated.

I am grateful to ***Prof. Yoshikazu Koike***, ***Prof. Hiroyasu Ishikawa***, ***Prof. Shinichiro Kanoh*** from Shibaura Institute of Technology and ***Assoc. Prof. Yuya Shoji*** from Tokyo Institute of Technology for their kind agreement in reviewing my dissertation.

I would like to offer a very special thanks to ***Assist. Prof. Dr. Apichai Bhatranand*** from the Department of Electronics and Telecommunication Engineering, King Mongkut's University of Technology Thonburi for his valuable time and encouragement to revise the manuscript for the academic publications.

I would like to express my deepest gratitude and sincere appreciation to my parents for their perfect economy support, encouragement, support and love throughout my life, for which mere expression of thanks likewise does not suffice.

Special thanks to all lecturers and staff of Shibaura Institute of Technology, for their great elaborate knowledge and kindness. Finally, for any errors or inadequacies that may remain in this work, of course, the responsibility is entirely of my own.

ABSTRACT

The telecommunication by using an optical fiber as a transmission medium becomes widely popular in several commercial fields and applications. The attenuation of the fiber is possibly lower than 0.14 dB/km in which it is able to transmit the optical power to very long distance with very few losses. There are two major types of the fiber; single-mode and multimode fiber. Single-mode fiber carries only one mode of light to be transmitted through longer distance while multimode fiber can carry several modes of light, but they are transmitted in shorter distance. The fiber type is selected regarding to the appropriate factors of usage such as distance and environment. In addition, an optical fiber is capable for the sensor application to the surrounding environment for the specific measurement. Various sensor types have been developed to response the appropriate usage with the lower price.

One of an interesting sensor type by using an optical fiber is the fiber grating. The fiber grating is the fiber with its structure change at specific point with the period as a grating period along the fiber axis. Fiber grating consists of two main types; fiber Bragg grating (FBG) and long-period fiber grating (LPFG). FBG is also called short-period fiber grating where its period relies in submicron level while LPFG has its grating period between 100 to 1,000 μm. This research focuses only on the LPFG with the single-mode fiber type. The development of the LPFG fabrication techniques on the fiber has been studied all the time. The LPFG first observed as a mode coupling inside the fiber with its periodic perturbation structure along the fiber axis. The mode coupling was detected as the attenuation loss in the form of resonant wavelength. Later, an inscription of LPFG structure into the fiber by using UV irradiation was performed to permanently alter the periodic index of the fiber. The fabrication was then developed by using external device as a mechanically induced technique which temporarily altered the fiber structure only when the fiber was perturbed by that device.

The LPFG fabrication by the perturbation of a 3D printed LPFG device on to the fiber is carried out to observe the coupling characteristics in term of resonant wavelengths as conventional methods did. The modern technology of three-dimensional printing has been increasing and it is benefit to various applications with low cost, but high efficiency. The 3D printing technology inspires the creation of an LPFG device in which the design of the 3D printed LPFG device is controllable. The 3D printed LPFG device has a general dimension of 4.0 cm long, 2.5 cm wide, and 0.5 cm thick. The grating period of the LPFG device begins from 500 to 630 μm with an increment of 10 μm. The perturbation process was taken by direct pressing the LPFG device on to the bare single-mode fiber by using a digital force meter and the perturbation weight can be read as well. The broadband light

source with the maximum power at 1550 nm transmits the light pulse through the fiber and it is received by an OSA.

The spectral output shows the amount of three to four resonant wavelengths for a single perturbation and five resonant wavelengths for a simultaneous perturbation. Each resonant wavelength corresponds to each coupling mode. All resonant wavelengths shift to the longer one when the LPFG device with longer grating period is applied. The relationship between the resonant shift and the grating period is linear function. The constant value referring to that relationship is the differential effective refractive indices between core and cladding mode. From the single perturbation, three resonant wavelengths have the constant value of 1.2857×10^{-3}, 1.5287×10^{-3}, and 1.9406×10^{-3}, respectively. All resonant shifts have the linearity over 0.99 as determined from the coefficient of determination (R^2). In addition, the 550 μm grating period of the LPFG device is slightly expanded by tilting the device from its initial axis. Practically, the fiber is rotated with the support of fiber rotator every 5 degrees. The constant values of three resonant shifts are 1.2666×10^{-3}, 1.4843×10^{-3}, and 1.8194×10^{-3}, respectively and all of them have the linearity higher than 0.99 as well. Those constant values are lower compared with the single perturbation due to larger induced refractive index and smaller grating expansion from tilted LPFG device. The perturbation of the LPFG device with the different specification of the fiber or different surrounding environment especially temperature may result to different results of resonant wavelengths.

Besides the experiment, the characteristic of coupling mode is simulated to observe the electric field distribution through the grating structure along the propagation axis. The finite-difference time-domain (FDTD) technique is used to simulate an electric field in term of TE mode in FullWAVE (Synopsys Inc.) software. The dimension of the fiber is shrunk to few microns and the index difference is setup to very high to decrease the simulation time, but still remain the clear resolution of the simulation results. Four examples of grating period; 5.2, 5.5, 5.8, and 6.1 μm, together with an amount of three grating pitches. The simulation results show that the coupling begins when the light passes the first grating pitch, but not every grating pitches as seen from the contour. The coupling characteristic shows that when the coupling to cladding mode happens, the magnitude of the field inside core layer decreases. When the electric field is in phase with the position of the grating pitch, the coupling at that grating pitch occurs. This causes the LPFG to have many grating pitches to increase the coupling strength. If any parameters are changed such as refractive indices of core and cladding layer, even the grating pitch, the distribution of an electric field will be changed or no coupling occurs on that structure.

The fabrication of an LPFG structure by using 3D printed LPFG device has a potential to filter out partial wavelength from the broadband signal inside an optical link. The advantage of using the

LPFG device is that it temporarily changes the fiber when it is only perturbed on the fiber in which the fiber is able to be used for another purposes. The perturbation of a 3D printed LPFG device can be applied to the tunable filter as it can control the resonant wavelength. Moreover, it is also suitable for weight sensor to the object or an intruder sensor when someone approaches the sensor area.

Keywords: long-period fiber grating, 3D printed LPFG device, perturbation, resonant wavelength, coupling, electric field distribution

CONTENTS

PAGE

CONTENTS (Cont'd)

PAGE

CONTENTS (Cont'd)

PAGE

LIST OF FIGURES

PAGE

LIST OF FIGURES (Cont'd)

PAGE

LIST OF FIGURES (Cont'd

PAGE

LIST OF TABLES

PAGE

LIST OF PUBLICATIONS

Journals

[1] R. Khun-in, Y. Usuda, Y. Jiraraksopakun, A. Bhatranand, and H. Yokoi, “Resin Made Long-Period Fiber Grating Structure for Tunable Optical Filter inside Single-Mode Fiber”: *Key Engineering Materials*, accepted for publication, 2020.

[2] R. Khun-in, Y. Usuda, Y. Jiraraksopakun, A. Bhatranand, and H. Yokoi, “Coupled mode characteristics from the perturbation of 3D printed long-period fiber grating devices”: *Photonic Sensors*, vol. 10, no. 3, pp. 195-203, May 2020.

International Conferences

[1] R. Khun-in, Y. Usuda, A. Bhatranand, and H. Yokoi, “The study of coupled-mode characteristics from resonant wavelengths inside fiber grating structures”: Proc. 19th International Conference on Numerical Simulation of Optoelectronic Devices, MP02, pp. 23-24, July 2019. 査読有り

[2] R. Khun-in, M. Takagi, Y. Usuda, A. Bhatranand, and H. Yokoi, “Simultaneous Perturbation of 3D Printed Long-Period Fiber Grating Devices for Controllable Resonant Wavelengths”: Optical Sensors and Sensing Congress, SW6C.5, June 2019. 査読有り

[3] M. Takagi, R. Khun-in, Y. Jiraraksopakun, A. Bhatranand, and H. Yokoi, “Evaluation of resonant wavelength from mechanically induced long-period fiber grating fabricated by 3D printer”: 23rd Microoptics Conference, P-69, October 2018. 査読有り

[4] R. Khun-in, M. Takagi, K. Nanjo, Y. Jiraraksopakun, A. Bhatranand, and H. Yokoi, “Resonant wavelength observation by 3D printed mechanically induced long-period fiber grating device”: Advanced Photonics Congress 2018, JTu2A.48, July 2018. 査読有り

[5] R. Khun-in, K. Nanjo, Y. Jiraraksopakun, A. Bhatranand, and H. Yokoi, “Weight Sensor by 3D Printed Mechanically Induced Long-Period Fiber Grating for Power Control inside Single-mode Fiber”: 22nd Microoptics Conference, P-55, pp. 246-247, November 2017. 査読有り

Domestic Conferences

[1] 臼田侑史, R.Khun-in, 高木真寛, 横井秀樹, “長周期光ファイバグレーティングを用いた多点計測”: 第 6 回グリーンイノベーションシンポジウム, pp. 71-73, February 2019.

[2] M. Takagi, K. Nanjo, R. Khun-in, Y. Jiraraksopakun, A. Bhatranand, and H. Yokoi, “Fabrication of mechanically induced long-period fiber grating by using 3D printer”: 12th SEATUC symposium, OS03-07, March 2018. 査読有り

[3] 南條光哉, R. Khun-in, 高木真寛, Y. Jiraraksopakun, A. Bhatranand, 横井秀樹, “機械的に誘導された長周期光ファイバグレーティングの評価”: 第78回応用物理学会学術講演会, 7a-PA5-9, September 2017.

[4] R. Khun-in, K. Nanjo, Y. Jiraraksopakun, A. Bhatranand, and H. Yokoi, “3D printed mechanically induced long-period fiber grating for power attenuation”: 第78回応用物理学会学術講演会, 7a-PA5-10, September 2017.

[5] R. Khun-in, K. Nanjo, Y. Jiraraksopakun, A. Bhatranand, and H. Yokoi, “3D printed mechanically induced long-period fiber grating for optical sensing”: 第 4 回グリーンイノベーションシンポジウム, pp. 94-96, February 2017.

CHAPTER 1 INTRODUCTION

1.1 Background

Optical communication plays a big role in world-wide connection as it transports fast data transmission from a transmitter to a receiver at very far distance, so called telecommunication. Optical fiber is selected for a medium to carry the light as a carrier from one side to another side. It comes together with the development of optoelectronics technology. Back into 1970, scientists from Corning Glass Works successfully produced the first low-loss single mode fiber with its attenuation less than 20 dB/km [1]. It was the revolution of transporting information in form of optics through the optical fiber for the telecommunication. Several years later until the present era, the possible minimum attenuation of the optical fiber is 0.14 dB/m for the ultra-low loss optical fiber reported by Hasegawa et al. in 2018 [2]. Optical fiber consists of two major types, a single-mode fiber and a multimode fiber. Their characteristics follow their name as the single-mode fiber lets the only single mode of light ray travel along the fiber and the multimode fiber allows several mode of light ray propagating along the fiber simultaneously. Regarding to the single-mode fiber, not only the low attenuation of the optical signal can be transported along the fiber, but also higher bandwidth can travel for a long distance comparing with the multimode fiber because the single-mode fiber has less modal dispersion. The single-mode fiber has more efficiency to be selected as a transmission medium for the observation of optical band spectrum for any situations occurred on the optical fiber.

Apart from the telecommunication, sensors based on the optical fiber become widespread in many fields of application such as mechanical measurements [3-7], chemical properties and biosensors [8-10], temperature sensors [11-13], and medical applications [14-16]. The dimension of an optical fiber is compact to replace at any structure and anywhere. Some fiber types are also patient to the harsh environment. Any faults or any changes occurred on that structure can be detected from the movement or an alteration of an optical fiber. In addition, several light waves can be transmitted through the fiber from the broadband light source. Some of its wavelengths are considered as noises or interference to the transmission performance. There are methodologies to change the fiber structure to such a kind of sensor to perform as a light wave filter, controllable filter, in which it is commanded to filter out the specific light wavelength from the broadband range. The aforementioned structure of the fiber is called fiber grating.

Fiber grating is a kind of fiber that contains altered structure at specific points along the fiber with the same period. It is used as a sensor to several physical phenomena for both measurement and

detection. The fabrication of the fiber grating structure on to the optical fiber has been developed to increase its sensing accuracy to the target environment. The technology of fiber grating fabrication becomes simpler and uses fewer equipment to perform the grating structure on the optical fiber. Further details of fiber grating are described in a following section.

1.2 History of fiber grating

In 1978, Hill et al. discovered the photosensitivity in the germanium-doped silica fiber to find out the non-linear effect inside the optical fiber at Canadian Communications Research Center (CRC) in Ottawa, Canada [17]. The procedure was taken by irradiating an Argon-ion laser with its wavelength of 488 nm into germanium-doped fiber's core layer. The refractive index of the fiber core was permanently changed from the high intensity of the laser and then formed as a grating index inside core layer. When the light was transmitted through this fiber, the intensity of reflected light would be increased. This is called self-induced grating [18]. Later in 1981, Lam and Garside studied the relationship between the magnitude of refractive index change inside core layer and the square power of Argon-ion laser with its wavelength of 488 nm [19]. In 1987, Stone reported the photosensitivity of an optical fiber from the concentration of germanium-doped into the optical fiber's core layer [20].

The self-induced grating fabricated by Hill et al. had its inscribing Argon-ion laser at the wavelength only 488 nm or it was called Bragg wavelength. That wavelength was not compatible with the usage at communication range. The Bragg wavelength came from Bragg grating which was named after William Lawrence Bragg formulated the conditions for X-ray diffraction [21]. In 1989, Meltz et al. solved the problem by proposing new fabrication technique by using UV irradiation at the wavelength of 244 nm. Two coherent beams induced the periodic modulation of the refractive index of the core layer by exposing the interference pattern. This was the grating formation from outside the fiber called transverse holographic method [22]. This method was flexible for writing the grating structure on the fiber at any period by controlling the angle between two coherent UV beams.

After Meltz et al. proposed the external writing to grating structure on the fiber, several methods had been developed to fabricate the grating structure. It was found out that interferometric method had more flexible setup to create the fiber grating. The setup supported both amplitude-splitting and wavefront-splitting to fabricate the interference of the photosensitive fiber. The amplitude-splitting was selected to fabricate several grating periods by adjusting an angle between two interfering beams. The wavefront-splitting was selected to create the grating structure inside an optical fiber, but this method used fewer equipment than the amplitude-splitting one.

The interference method was inspired to study the photosensitivity of the fiber such as prism interferometer [23] and Lloyd's interferometer [24]. Later, new techniques to fabricate the grating structure were proposed such as phase mask technique [25,26], femtosecond laser technique [27,28], and point-by-point technique [29]. All fabrication techniques, however, the target of fiber grating was to reflect partial light out of an optical link. Further details of conventional techniques of fiber grating will be described in Chapter 2.

1.3 Fiber grating categories

Fiber grating structure is the periodic change of the refractive index of core layer inside an optical fiber. Generally, it contains two major types, fiber Bragg grating (FBG) and long-period fiber grating (LPFG).

1.3.1 Fiber Bragg grating (FBG)

Fiber Bragg grating (FBG) is also called the short-period fiber grating. Its periodic grating structure or grating period relies in sub-micron unit. The purpose of FBG structure is to reflect back the partial wavelength of light while the rest of wavelength can transmit through the fiber. The fabrication of FBG inside fiber's core layer is done by UV irradiation. The reflected wavelength at specific position is called Bragg wavelength (λ_B) [30]. Bragg wavelength can be defined by the relationship with grating period in Eq. 2.1.

$$\lambda_B = 2n_{eff}\Lambda \tag{1.1}$$

where n_{eff} and Λ represent the effective refractive index of core layer inside a single-mode fiber and grating period, respectively. The wavelengths other than Bragg wavelength have weak reflected power because of the phase mismatch over grating length. Bragg wavelength is shifted when the effective refractive index of the core layer is changed. The FBG structure is shown in Fig. 1.1.

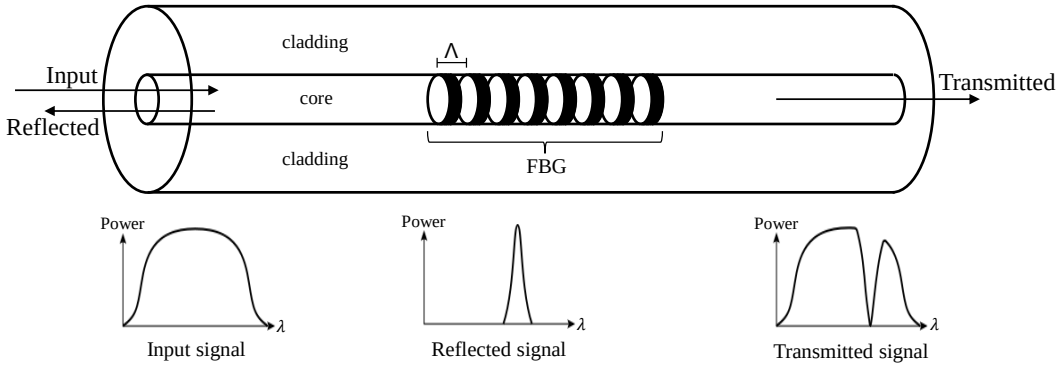

Figure 1.1 The structure of fiber Bragg grating [31].

1.3.2 Long-period fiber grating (LPFG)

In 1983, Youngquist et al. observed the mode coupling in the birefringence fiber by creating the periodic perturbation on the polarization axis of the birefringence fiber [32]. The periodic structure was made by the crystalline plastic as its shape was a comb. The experimental results showed the relationship between the attenuated wavelength and the periodic structure. Later in 1986, Blake et al. discovered the coupling of linear polarized (LP) light between fundamental mode LP_{01} and coupled mode LP_{11} by the use of grating structure from a copper wire with its diameter of 0.25 mm [33]. The characteristic of coupling mode was in the form of attenuation loss inside an optical fiber. In 1990, Hill et al. found out the new grating fabrication method by using UV laser for the point by point writing on the side of the fiber [34]. In addition, in 1991, Bilodeau et al. could observe the coupling from LP_{01} mode to LP_{02} mode with the narrow bandwidth of the attenuation loss [35]. After the observation of mode coupling inside an optical fiber was proposed, it came up with the new type of fiber grating as long-period fiber grating (LPFG). In 1996, Vengsarkar et al. proposed the first LPFG with its period ranging between 100 and 1,000 μm [36]. The LPFG structure brought to the attenuation loss in form of resonant wavelength. The relationship between the resonant wavelength and the grating period is expressed as

$$\lambda = \left[n_{eff,core} - n_{eff,clad}^{i} \right] \Lambda \tag{1.2}$$

where $n_{eff,core}$ and $n_{eff,clad}^{i}$ represent the effective refractive index of fundamental core mode and coupled cladding mode at *i*th order, respectively. The λ refers to the resonant wavelength from each coupling of *i*th order cladding modes. The LPFG structure is displayed in Fig. 1.2. In comparison with FBG structure, LPFG structure has lower insertion loss, easier fabrication method, and better wavelength tenability.

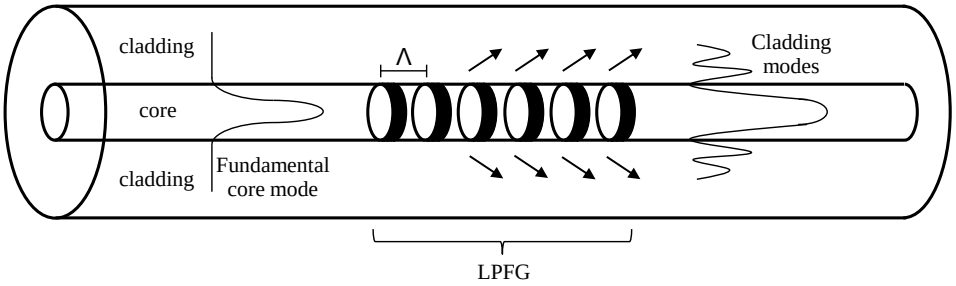

Figure 1.2 The structure of long-period fiber grating [37].

Fundamentally, the correlation between the resonant wavelength and the grating period is clarified as a phase matching curve as plotted in Fig. 1.3 which is the phase matching curve of an LPFG in SMF-28 model single-mode fiber. The largest $d\lambda/d\Lambda$, the highest order of cladding mode

has the highest sensitivity [38-40]. Under the same grating period inside an optical fiber, the fundamental core mode can be coupled to several cladding modes simultaneously resulting to different resonant wavelengths corresponding to each of coupled cladding modes. From the phase matching curve, the slope $d\Lambda/d\lambda$ progressively decreases from lower order mode to higher order mode, so the shorter grating period results to the higher coupled mode.

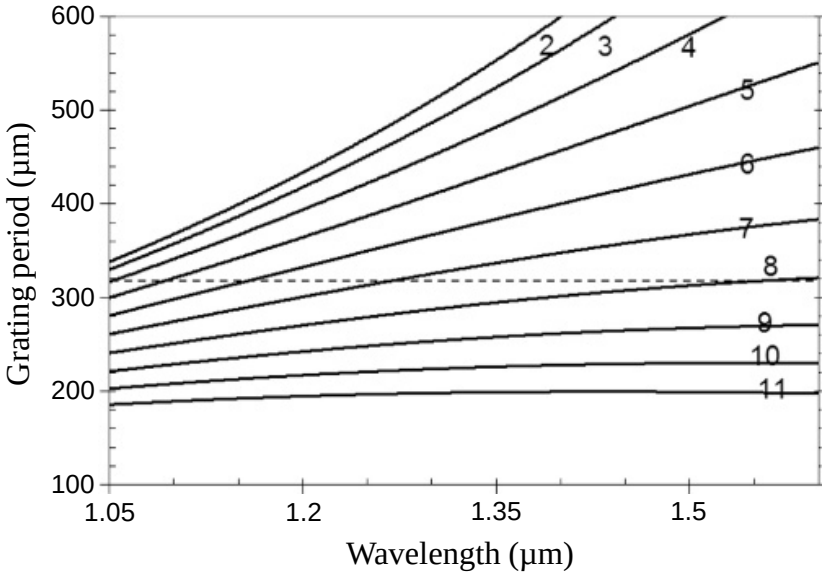

Figure 1.3 Phase matching curve of SMF-28 single-mode fiber [41].

1.4 Scope of research

Only the fiber grating type of LPFG is conducted in this research. Several conventional methods to fabricate LPFG structure on to a single-mode fiber used many equipment and tools for the setup and fabrication procedure. Moreover, those fabrication methods permanently altered the fiber structure from the laser irradiation which means that the fiber could not be used for another purpose anymore. The major outline of this research focuses on the simpler method to create an LPFG structure on to a bare single-mode fiber by using a specific designed LPFG structure device which is called three dimensional (3D) printed LPFG device. The characteristics of resonant wavelengths from the perturbation of the device are observed in term of attenuation magnitude and resonant wavelength shift trend. In the another word, the term of perturbation in case of this research is performed by directly pressing on the fiber of the device. The 3D printed LPFG device also contains several grating periods from the tilt angles of the device respect to the fiber axis. Therefore, resonant wavelength shift can be observed from these various grating periods.

The main objective of this research is the presentation of the new method to create the LPFG structure inside the fiber which integrates with the technology of the 3D printing material. The

resolution of the 3D printing is brought to very few microns and it meets the condition to create the LPFG device at the resolution of hundred microns. The big difference from conventional mechanically induced techniques is that the dimension and the unique grating period of the LPFG device can be customized to the appropriate size for the right usage. Moreover, the formation of the LPFG structure on the fiber is temporary when the 3D printed LPFG device is only pressed.

Resonant wavelength is the characteristic of power attenuation at specific wavelength from broadband wavelength as a spectral dip. It is resulted from the coupling from the core mode to the cladding mode. The simulation of electric field distribution along the fiber axis is observed by FullWAVE (Synopsys Inc.) software to see the characteristic of coupling at each grating pitch. The structural size of the optical fiber and the grating period needs to be adjusted in the simulation due to the limitation of the computer's performance to reduce the unnecessary simulation time. Moreover, the input light is available only for individual wavelength, so the resonant wavelength from the experiment is selected for the input light wavelength. The main factor is the refractive index difference (Δn) that affects the intensity of field distribution when the light reaches the grating pitch.

1.5 Organization of the dissertation

This research presents the mechanically induced technique to produce the LPFG structure on the optical fiber by using 3D printed LPFG device. The benefit of this device is the temporary LPFG structure can be created on the optical fiber. Resonant wavelengths from various situation by the perturbation of 3D printed LPFG devices are observed to figure out its trend for the selective optical wavelength filter. In addition, those resonant wavelengths from the experiment are selected for the simulation of the electric field distribution through the LPFG structure designed in FullWAVE (Synopsys Inc.) software as the distribution of electric field profile yields the attenuation of an optical power passing through LPFG structure.

This dissertation is composed of six chapters as follows.

Chapter 1 Introduction, sensor based optical fiber has been used widely and rapidly in few decades. The history of fiber grating and development is described in this chapter. There are two main types of the fiber grating, FBG and LPFG. The scope of research targets to the characteristics of LPFG and its fabrication by using 3D printed LPFG device.

Chapter 2 Literature review on the fabrication of LPFG, this research is motivated from the conventional method on fabricating LPFG structure into the fiber structure. They are point-by-point, phase mask, femtosecond laser, CO_2 laser, arc discharge, and etching discharge technique. Those conventional methods permanently changed the fiber structure after the fabrication. There is also

another method that temporarily changes the fiber structure when the LPFG structure is applied, it is mechanically induced technique.

Chapter 3 Coupling theory of LPFG, this chapter presents the corresponding parameters and formulas to the coupling mode of the fiber from the applied LPFG structure. In addition, the graphic of linear polarized (LP) are also displayed. These mode coupling characteristics are in the form of resonant wavelengths in practical way.

Chapter 4 Experimental setup, results and discussion, all related equipment and machines to create an LPFG structure on the single-mode fiber are described. Moreover, the experimental setup and the procedure to apply the perturbation on the optical fiber with several grating periods are also described. The 3D printed LPFG devices with several grating periods at every 10 μm and with the tilt angles are applied on the fiber to observe resonant wavelengths. Lastly, experimental results and discussion are clarified to claim the usage of 3D printed LPFG device.

Chapter 5 Electric field distribution along grating structure, resonant wavelengths from the coupling modes inside an optical fiber relates to the optical attenuation when the light transmits through an LPFG as the optical power leaks from the core layer to the cladding layer. The magnitude of electric field and the direction of field distribution when the field passes each grating pitch are observed. The discussion is also described in this chapter.

Chapter 6 Conclusion, the summary of both experiment and simulation of LPFG are described that they reach the research scope and it is useful for the sensing application device. The suggestion of the future work by using this device is also guided in this chapter.

Reference

[1] D. B. Keck, and P. C. Schultz, "**Method of producing optical waveguide fibers**," U.S. Patent 3,711,262, issued May 11, 1970.

[2] T. Hasegawa, Y. Tamura, H. Sakuma, Y. Kawaguchi, Y. Yamamoto, and Y. Koyano, "**The first 0.14-dB/km ultra-low loss optical fiber**," SEI Technical Review, no. 86, pp. 18-22, April 2018.

[3] A. W. Domanski, "**Application of optical fiber sensors in mechanical measurements**," IEEE Instrumentation and Measurement Technology Conference, Ottawa, Canada, pp. 700-702, May 1997.

[4] D. A. Drake, R. W. Sullivan, and J. C. Wilson, "**Distributed strain sensing from different optical fiber configurations**," Inventions, vol. 3, no. 4, 67, September 2018.

[5] W. Blazejewski, P. Gasior, and J. Kaleta, "**Application of optical fibre sensors to measuring the mechanical properties of composite materials and structures**," Adv. in Composite Materials – Ecodesign and Analysis, IntechOpen, pp. 221-246, March 2011.

[6] G. Marchi, V. Baier, P. Alberton, R. Burgkart, A. Aszodi, H. Clausen-Schaumann, and J. Roths, "**Microindentation sensor system based on an optical fiber Bragg grating for the mechanical characterization of articular cartilage by stress-relaxation**" Sensors and Actuators B: Chemical, vol. 252, pp. 440-449, November 2017.

[7] R. Martinek, J. Nedoma, M. Fajkus, and R. Kahankova, "**Fiber-optic Bragg sensors for the rail applications**," Int. J. Mech. Eng. Rob. Res., vol. 7, no. 3, pp. 292-295, May 2018.

[8] M. Yin, B. Gu, Q. An, C. Yang, Y. L. Guan, and K. Yong, "**Recent development of fiber-optic chemical sensors and biosensors: Mechanisms, materials, micro/nano-fabrications and applications**," Coordination Chemistry Reviews, vol. 376, pp. 348-392, December 2018.

[9] M. Pospisilova, G. Kuncova, and J. Trogi, "**Fiber-optic chemical sensors and fiber-optic bio-sensors**," Sensors, vol. 15, no. 10, pp. 25208-25259, October 2015.

[10] F. Chiavaioli, F. Baldini, S. Tombelli, C. Trono, and A. Giannetti, "**Biosensing with optical fiber gratings**," Nanophotonics, vol. 6, no. 4, pp. 663-679, December 2016.

[11] E. Schena, D. Tosi, P. Saccomandi, E. Lewis, and T. Kim, "**Fiber optic sensors for temperature monitoring during thermal treatments: An overview**," Sensors, vol. 16, no. 7, 1144, July 2016.

[12] Q. Lin, N. Zhao, K. Yao, Z. Jiang, B. Tian, P. Shi, and F. Chen, "**Ordinary optical fiber sensor for ultra-high temperature measurement based on infrared radiation**," Sensors, vol. 18, no. 11, 4071, November 2018.

[13] P. Liu, M. P. Buric, K. Byerly, S. R. Moon, M. Nazmunnahar, S. Simizu, A. M. Leary, R. B. Beddingfield, C. Sun, P. Zandhuis, M. E. McHenry, and P. R. Ohodnicki, "**Real-time monitoring of temperature rises of energized transformer cores with distributed optical fiber sensors**," IEEE Trans. Power Del., vol. 34, no. 4, pp. 1588-1598, April, 2019.

[14] S. Poeggel, D. Tosi, D. Duraibabu, G. Leen, D. McGrath, and E. Lewis, "**Optical fibre pressur sensors in medical applications**," Sensors, vol. 15, no. 7, pp. 17115-17148, July 2015.

[15] F. Fateh, R. L. Sharma, "**A review on optical fiber sensors for biomedical sensing**," Int. J. Sci. & Eng. Res., vol. 8, no. 3, pp. 1439-1442, March 2017.

[16] A. G. Leal-Junior, C. A. R. Diaz, L. M. Avellar, M. J. Pontes, C. Marques, and A. Frizera, "**Polymer optical fiber sensors in healthcare applications: A comprehensive review**," Sensors, vol. 19, no. 14, 3156, July 2019.

[17] K. O. Hill, Y. Fujii, D. C. Johnson, and B. S. Kawasaki, "**Photosensitivity in optical fiber waveguides: Application to reflection filter fabrication**," Appl. Phys. Lett., vol. 32, pp.647-649, May 1978.

[18] A. Othonos, "**Fiber Bragg gratings**," Rev. Sci. Instrum., vol. 68, 4309, September 1997.

[19] D. K. W. Lam, and B. K. Garside, "**Characterization of single-mode optical fiber filters**," Appl. Opt., vol. 20, no. 3, pp. 440-445, February 1981.

[20] J. Stone, "**Photorefractivity in GeO_2-doped silica fibers**," J. Appl. Phys., vol. 62, no. 11, pp. 4371-4374, December 1987.

[21] W. L. Bragg, G. M. Caroe, and H. B. Hartley, "**Sir William Bragg, F. R. S. (1862-1942)**," Notes Rec. R. Soc. Lond., vol. 17, no. 2, December 1962.

[22] G. Meltz, W. W. Morey, and W. H. Glenn, "**Formation of Bragg gratings in optical fibers by a transverse holographic method**," Opt. Lett., vol. 14, no. 15, pp. 823-825, August 1989.

[23] B. J. Eggleton, K. A. Ahmed, H. F. Liu, P. A. Krug, and L. Poladian, "**Experimental** demonstration **of compression of dispersed optical pulses by reflection from self-chirped optical fiber Bragg gratings**," Opt. Lett., vol. 19, no. 12, pp. 877-879, June 1994.

[24] H. G. Limberger, P.-Y. Fonkallaz, P. Lambelet, R.-P. Salathe, C. Zimmer, and H. H. Gilgen, "**Optical low-coherence reflectometry (OCLR) characterization of efficient Bragg gratings in optical fiber**," Proceeding of the SPIE, vol. 2044, pp. 272-283, December 1993.

[25] D. Z. Anderson, V. Mizrahi, T. Erdogan, and A. E. White, "**Phase-mask method for volume manufacturing of fiber phase gratings**," Conference on Optical Fiber Communication/ International Conference on Integrated Optics and Optical Fiber Communication, California, USA, paper PD16, February 1993.

[26] K. O. Hill, B. Malo, F. Bilodeau, D. C. Johnson, and J. Albert, "**Bragg gratings fabricated in monomode photosensitive optical fiber by UV exposure through a phase mask**," Appl. Phys. Lett., vol. 62, no. 10, pp. 1035-1037, March 1993.

[27] D. Grobnic, C. Smelser, S. Mihailov, R. Walker, and P. Lu, "**Fiber Bragg gratings with suppressed cladding modes made in SMF-28 with a femtosecond IR laser and phase mask**," IEEE Photonics Technol. Lett., vol. 16, no. 8, pp. 1864-1866, July 2004.

[28] Y. Li, C. R. Liao, D. N. Wang, T. Sun, and K. T. V. Grattan, "**Study of spectral and annealing properties of fiber Bragg gratings written in H_2-free and H_2-loaded fibers by use of femtosecond laser pulses**," Opt. Express, vol. 16, no. 26, pp. 21239-21247, December 2008.

[29] B. Malo, F. Bilodeau, D. C. Johnson, and K. O. Hill, "**Fiber mode converters: Point-by-point fabrication of index gratings, visualization using thermoluminescence, and applications**," Optical Fiber Communication, California, USA, paper WL3, February 1991.

[30] S. Dewra, Vikas, and A. Grover, "**Fabrication and applications of fiber Bragg grating – A review**," Adv. Eng. Tec. Appl., vol. 4, no. 2, pp. 15-25, March 2015.

[31] S. J. Mihailov, "**Fiber Bragg grating sensors for harsh environments**," Sensors, vol. 12, no. 2, pp. 1898-1918, February 2012.

[32] R. C. Youngquist, J. L. Brooks and H. J. Shaw, "**Birefringent-fiber polarization coupler**," Opt. Lett., vol. 8, no. 12, pp. 656-658, December 1983.

[33] J. N. Blake, B. Y. Kim, and H. J. Shaw, "**Fiber-optic modal coupler using periodic microbending**," Opt. Lett., vol. 11, no. 3, pp. 177-179, March 1986.

[34] K. O. Hill, B. Malo. F. Bilodeau, D. C. Kohnson, and I. M. Skinner, "**Efficient mode conversion in telecommunication fibre using externally written gratings**," Electron. Lett., vol. 26, no. 16, pp. 1270-1272, August 1990.

[35] F. Bilodeau, K. O. Hill, B. Malo, D. C. Johnson, and I. M. Skinner, "**Efficient narrowband LP_{01} to LP_{02} mode converters fabricated in photosensitive fibre: Spectral response**," Electron. Lett., vol. 27, no. 8, pp. 682-684, April 1991.

[36] A. M. Vengsarkar, P. J. Lemaire, J. B. Judkins, V. Bhatia, T. Erdogan, and J. E. Sipe, "**Long-period fiber gratings as band-rejection filters**," J. Light. Technol., vol. 14, no. 1, pp. 58-65, January 1996.

[37] C. Silva, J. Coelho, P. Caldas, and P. Jorge, "**Fiber sensing system based on long-period gratings for monitoring aqueous environments**," In M. Yasin, S. Harun, H. Arof (Eds), Fiber Optic Sensors, pp. 317-342, February 2012.

[38] V. Bhatia, "**Properties and sensing applications of long-period gratings**," Ph.D. Thesis in Electrical Engineering, Virginia Polytechnic Institute and State University, November 1996.

[39] T. Erdogan, "**Cladding-mode resonances in short and long period fiber grating filters**," J. Opt. Soc. Am. A, vol. 14, no. 8, pp. 1760-1773, August 1997.

[40] T. Erdogan, "**Fiber grating spectra**," J. Light. Technol., vol. 15, no. 8, pp. 1277-1294, August 1997.

[41] A. Kapoor, and E. Sharma, "**Long period fiber grating refractive-index sensor: Optimal design for single wavelength interrogation**," Appl. Opt., vol. 48, no. 31, pp. G48-G94, November 2009.

CHAPTER 2 LITERATURE REVIEW ON THE FABRICATION OF LPFG

2.1 Introduction

An optical fiber mainly consists of two layers: core layer and cladding layer. The light transmits through only inside the core layer to reach the destination at another side of the fiber. In some cases, broadband wavelength of light contains partial wavelengths as noises that deteriorate the signal transmission performance. The fiber structure needs to be physically altered to become a partial light wavelength filter. One of the common structure of the fiber is an LPFG. Theoretically, the structure of an LPFG structure is the periodical change of the refractive index of core layer inside an optical fiber which has a longer period than the initial FBG. Those periodic changes of the refractive index lead to the coupling modes of light from fundamental core mode to cladding modes [1], so that partial wavelengths of light are filtered out regarding to each of coupling modes while the rest can pass through the LPFG structure. Practically, the fabrication of an LPFG structure into the optical fiber keeps developing for not only the higher accuracy of its performance, but also the simpler technique which uses fewer equipment for the fabrication process and has a lower cost of operation.

Several techniques to fabricate an LPFG structure on to the optical fiber have been proposed in many researches. It began from the usage of UV exposure method such as point-by-point technique [2] and amplitude phase mask technique [3,4]. Some examples of the light source for a UV laser consisted of KrF excimer emitting at the wavelength of 242-248 nm [5,6], the second harmonic radiation of a continuous wave Ar ion laser emitting at the wavelength of 244 nm [7], nanosecond pulses from ArF excimer laser emitting at the wavelength of 193 nm [8], frequency quadrupled and tripled Nd:YAG lasers emitting at the wavelength of 266 nm and 355 nm, respectively [9,10], etc. Another type was the usage of non-UV exposure method such as CO_2 laser radiation [11,12], electric arc discharge [13,14], femtosecond laser pulse radiation [15,16], etc. In term of non-UV laser exposure method, it could induce higher refractive index changes inside core layer and it was more suitable technique to write an LPFG structure in any kind of silicon (Si) fibers. In the other hand, the average refractive index of cladding layer was increased resulting to higher loss and this method required more equipment to fabricate an LPFG structure.

The process of fabrication techniques has been developed for better LPFG structure and requires fewer equipment. They were also developed from a permanent fabrication to become a temporary fabrication, so that the fiber is able to be reused for another purposes.

2.2 Fabrication techniques of LPFG structure

The fabrication techniques of an LPFG structure from using the irradiation method to the optical fiber until using the external grating devices to perform a grating structure on the fiber are discussed in following sections. Various equipment setup for the fabrication process of an LPFG structure not only show the variety of the fabrication performance, but also side effects from the implementation. The purpose of the fabrication is to alter the refractive index of fiber's core layer to become a periodic refractive index difference.

2.2.1 Point-by-point technique

Point-by-point technique was the first technique to create the periodic change of the refractive index inside a fiber's core layer. This technique was performed by using a UV irradiation as a fiber mode converter [17]. The periodic change of the refractive index of the core layer inside a fiber by point-by-point technique uses focused pulses from a UV laser relatively moving along the fiber axis with a step of time. The focused pulses from the laser source are adjusted to pass through a slit resulting to increase the refractive index of the core layer at the section of shooting point. The grating pitch appeared on the fiber structure depends on the size of a slit and focusing lens. Partial region of an optical fiber is transformed to a grating structure inside a core layer with a specified period along the fiber axis. The advantage from the fabrication by point-by-point technique is that it is easy to adjust Bragg grating parameters such as the grating period, the size of grating pitch, and the grating length. Therefore, the spectral response corresponding to fabricated LPFG can be controlled by adjusting those related parameters [18,19]. The equipment setup for the fabrication of an LPFG by point-by-point technique is shown in Fig. 2.1.

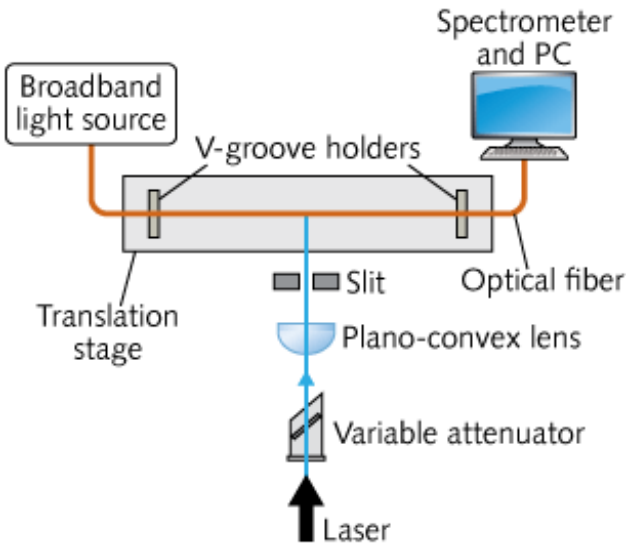

Figure 2.1 LPFG fabrication by point-by-point technique [20].

2.2.2 Phase mask technique

Phase mask technique was developed and proposed six years later after the fabrication by point-by-point technique was carried out by Vengsarkar, et al. in 1996 [9]. The equipment setup for the fabrication process is illustrated in Fig. 2.2. The main point of an implementation is the usage of a UV laser beam impacting on to the optical fiber through the phase mask device. The phase mask contains an array of windows guiding to the diffraction of laser beams with a period of Λ_G on the fiber. During the fabrication, a UV laser beam transmitting through the phase mask device is diffracted into various orders overlapping and optically interfering with each other in the mask vicinity. The UV laser beam interference creates alternating zones of low and high laser intensity where the space between those intensities is equal to the phase mask period or half of its period depending on the exposure geometry. The relationship between the phase mask period (Λ_p) and the grating period fabricated on the fiber (Λ_G) is derived in the following equation [21].

$$\Lambda_p = 2\Lambda_G \tag{2.1}$$

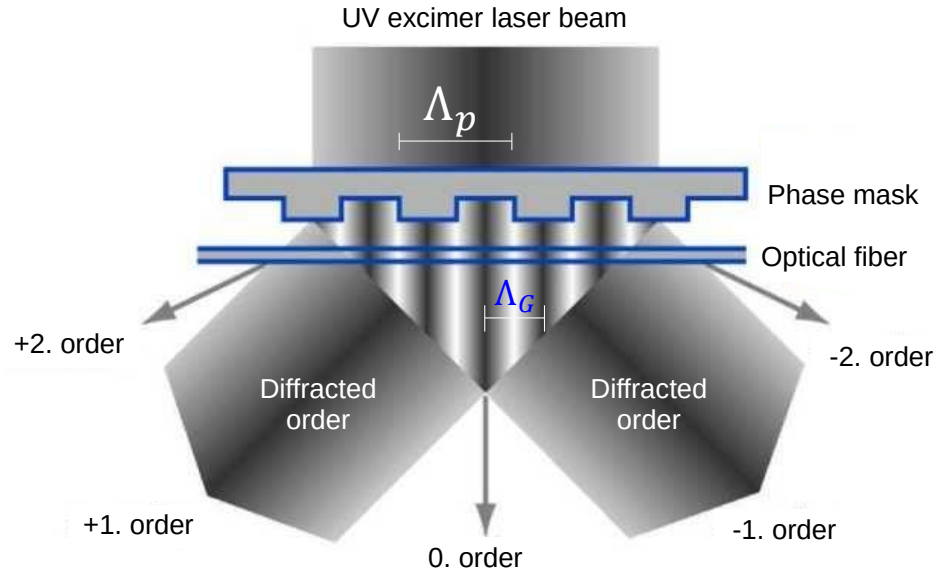

Figure 2.2 LPFG fabrication by phase mask technique [22].

2.2.3 Femtosecond laser technique

The fabrication by using a UV irradiation as a laser induced in the region of visible light and infrared were not successful because they had low photon energy. Only Ge-doped fibers were applicable to the LPFG fabrication by using UV laser irradiation. The photoinduced refractive index change in different types of glasses by using femtosecond laser was proposed by K. M. Davis, et al. in 1996 [23]. The wavelength of 810 nm beam was used to induce the refractive index change of high silica, borate, and soda lime silica glasses. The damaged points, but not cracked, from the induction

by a femtosecond laser were observed at the focal point of the laser in glasses after the irradiation. The damage point in the bulk glass presented higher refractive index than the surrounding glass of the focus point. Moreover, the characteristic of a femtosecond laser could be expressed in term of the two-photon absorption. In 1999, the fabrication of an LPFG structure on the fiber by using femtosecond laser technique was proposed by Kondo, et al. [15] for the first time. The temperature during the fabrication process was found to be stable at higher than 100 °C and the grating structure inside the fiber was more durable than the one fabricated by UV irradiation method.

The experimental setup to fabricate an LPFG structure by using femtosecond laser technique is shown in Fig. 2.3. The femtosecond laser has its wavelength at 800 μm and a single-mode fiber is used as a medium for the process of fabrication. The femtosecond laser is transmitted through a computer control shutter and controlled by microscope objective lens where the focal point lies on the core layer of a fiber. The optical fiber is fixed with a 3-dimensional translation stage (XYZ-stage) controlled by the same computer used with the shutter. The charge-coupled device (CCD) camera is located to detect the laser beam transmitted from the femtosecond laser to the fiber's core layer. While the translation stage is moving along the axis of fiber alignment, the femtosecond laser transmits the laser beam periodically to the fiber's core layer in step with the opening of the shutter. This process results to the periodical refractive index change of the core layer inside a single-mode fiber. The grating period from this process can be measured from the moving step of the translation stage.

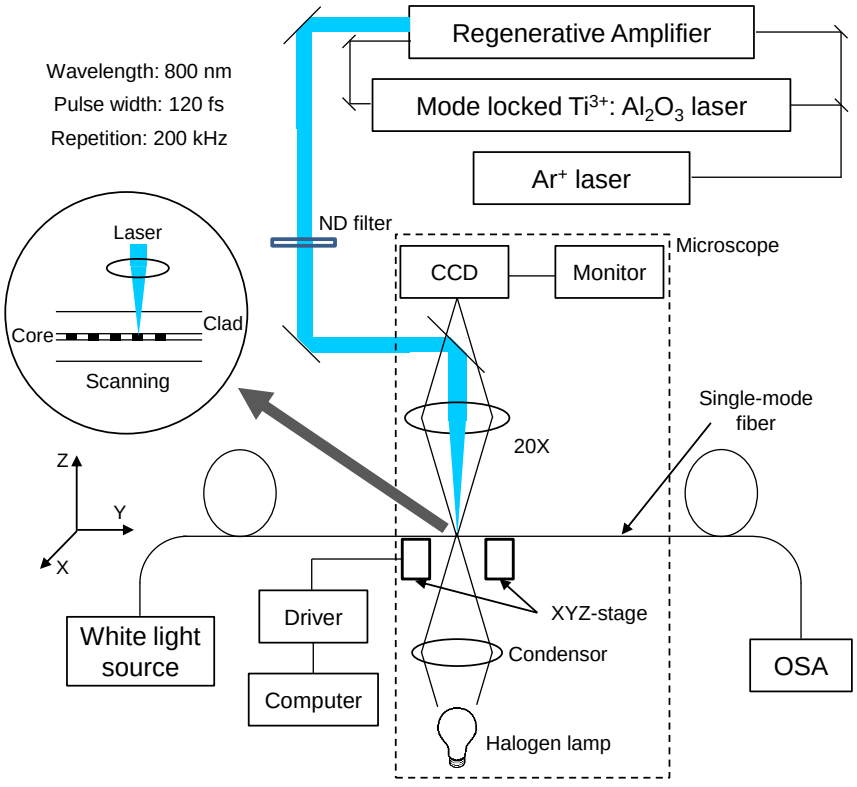

Figure 2.3 LPFG fabrication in single-mode fiber by femtosecond laser technique [24].

Another types of an optical fiber also have a potential to become LPFG by using femtosecond laser technique such as photonic crystal fiber (PCF) and photonic bandgap fiber (PBF). PCF structure requires a very short pulse and a high energy of the femtosecond laser for the fabrication process of an LPFG structure. Fig. 2.4 shows the experimental setup of an LPFG fabrication to the PCF by using femtosecond laser. The gratings appeared in the PCF are created by the periodic physical damage such as microholes inside the fiber. The femtosecond laser is transmitted through a computer control shutter and incident on the fixed PCF aligning on the translation stage. The femtosecond laser beam is focused by a microscope objective, so that the focal point of the laser beam relies on the center of the PCF on its upper surface and the translation stage moves perpendicular to the fiber alignment. The focused beam creates the first microhole on the upper surface of the PCF, then the PCF is moved by the translation stage along the fiber axis with the same step determining the grating period to create the next microhole. The LPFG fabrication in PCF based on the periodic microhole structure is shown in Fig. 2.5.

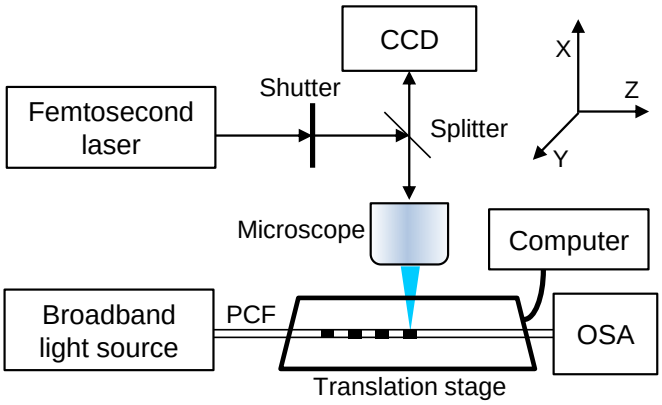

Figure 2.4 LPFG fabrication in PCF by using femtosecond laser [24].

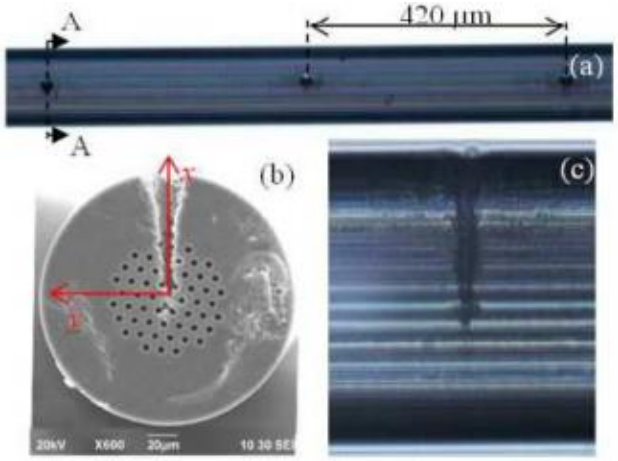

Figure 2.5 (a) Top view section of the LPFG structure in PCF, (b) SEM cross-sectional image of the drilled region, and (c) side view of the drilled region [24].

2.2.4 CO_2 laser technique

CO_2 laser technique to fabricate the LPFG structure was first proposed by D. D. Davis, et al. in 1998 [25]. The fabrication by CO_2 laser technique has more flexible process and lower cost of operation comparing with the UV irradiation technique because there is no photosensitivity inside an optical fiber. This modern technique is suitable for several types of an optical fiber including pure-silica PCF and air-core PBF. The conventional glass fiber is used to fabricate an LPFG structure and the fabrication process is based on the point-by-point technique. The fiber is fixed on the translation stage and periodically moved along the fiber axis under control by the same computer that controls the shutter. The CO_2 laser transmits through the shutter and lens focused on to the optical fiber. The translation stage then moves along the fiber axis corresponding to the moving step and the shutter step with a period to create the grating structure on the fiber. The LPFG fabrication process by using CO_2 laser is illustrated in Fig. 2.6.

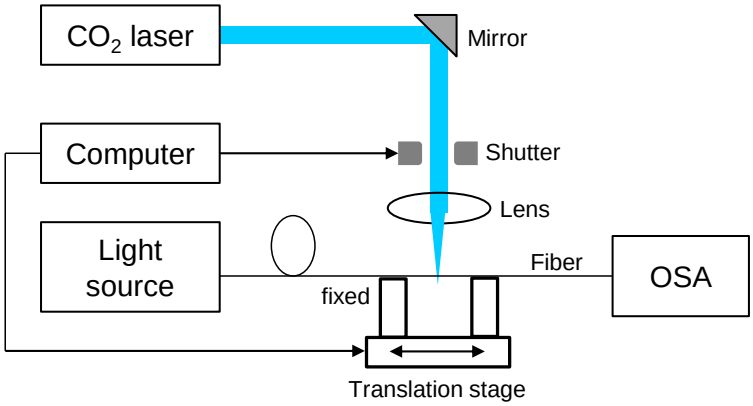

Figure 2.6 LPFG fabrication by using CO_2 laser based on point-by-point technique [26].

From the fabrication setup, both shutter and translation stage are exactly controlled because the vibration of the fiber fixed on the translation stage can occur during the movement affecting an instability and nonrepeatability of the written grating structure. Later, Rao, et al. [27] developed the fabrication process based on 2-dimensional scanning of the CO_2 laser beam in 2003 as illustrated in Fig. 2.7. In this setup, one end of the fiber is fixed while another end is attached to a small weight to create the constant prestrain in the fiber to increase its potential fabrication. The high frequency CO_2 laser scans the laser beam across the fiber along the X direction and then shifts a grating pitch along the Y direction to create next grating pitch along the fiber axis with the period of the moving step in Y direction. From this process, the fiber is fixed, so that there is no any vibration occurred caused by the fiber movement.

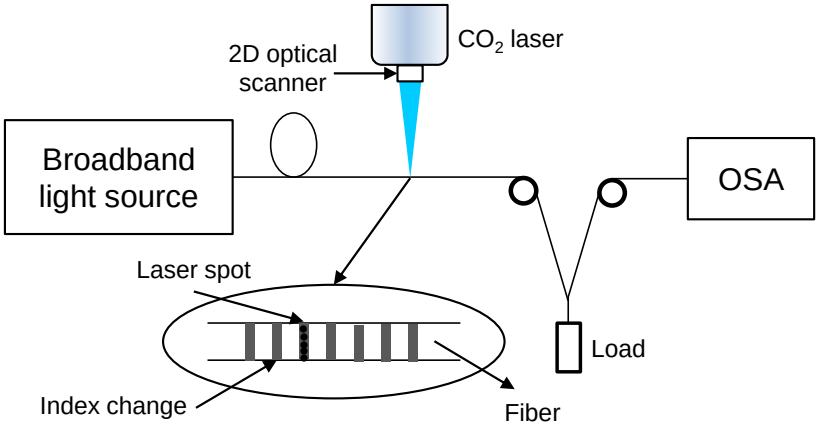

Figure 2.7 LPFG fabrication by using CO_2 laser based on 2-dimensional scanning [27].

The fabrication process had been developed from Fig. 2.7 in which the shutter is setup into the new design. The mirror and lens are added into the setup to reflect the CO_2 laser beam projecting on the fiber. Those additional devices are fixed with the translation stage controlled by the computer together with the shutter. The mirror and lens periodically move instead of the fiber movement. Several parameters such as grating pitch, amount of grating periods, exposure time per period, and amount of exposure cycles can be selected in the software to control the computer. The adapted design from Fig. 2.6 and Fig. 2.7 is developed by adding mirror and lens as shown in Fig. 2.8.

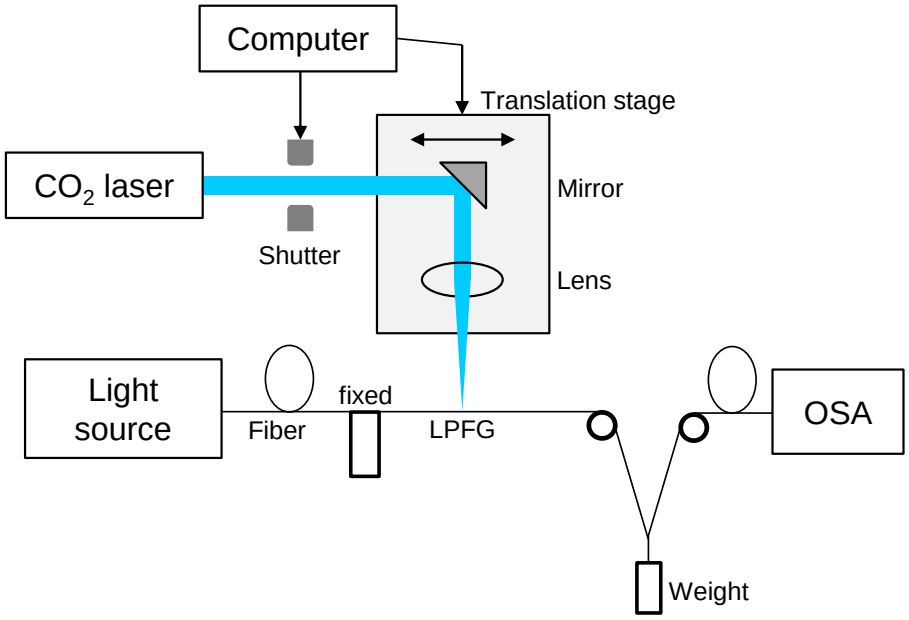

Figure 2.8 The developed design for LPFG fabrication by using CO_2 laser [26].

The refractive index change of a core layer from the fabrication by using CO_2 laser exposure is different from using a UV irradiation as observed from three situations: residual stress relaxation, glass structure change, and physical deformation. These phenomena depend on the structure of each types of the optical fiber.

In 2008, Wang, et al. proposed that the LPFG structure could be written on an air-core PBF by using developed setup of the CO_2 laser technique [28]. The stability of CO_2 laser beam and good repeatability of the scanning process are very critical to fabricate the LPFG structure in an air-core PBF. In case of PCF, it requires higher average laser power and a longer time for the irradiation process. While the CO_2 laser beam is being irradiated to the fiber, the residual stress inside the fiber leads to the refractive index change of the fiber's core layer, the fiber glass structure is also changed from this process. The CO_2 laser irradiation affects the glass volume of the fiber resulting to the modulation of its refractive index. The periodic physical deformation from the irradiation by using CO_2 laser beam is the main process to fabricate an LPFG structure in the PCF and the PBF. The fiber then becomes tapered and elongated affecting the decrease of the fiber diameter as the change of its refractive index. The fiber diameter of the air-core PBF decreases when it is irradiated by using CO_2 laser beam as shown in Fig. 2.9.

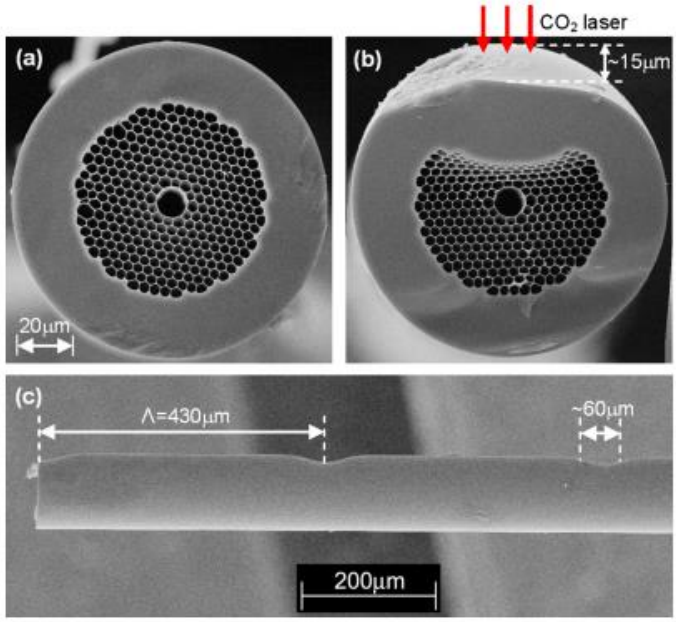

Figure 2.9 The cross-section image of an air-core PBF (a) before and (b) after CO_2 laser irradiation, (c) side view of fabricated LPFG with two periods [28].

2.2.5 Arc discharge technique

Arc discharged technique was proposed by Poole, et al. for the first time in 1994 [29]. The proposed technique contains two main steps to fabricate an LPFG structure. First, the fiber glass surface is cut by using CO_2 laser exposure. Then, the fiber is heated up to its melting point for a short time by using an arc fusion splicer to anneal the fiber. It affects the deformation of the fiber core from the high temperature at the position of arc discharge as illustrated in Fig. 2.10. The annealing from arc discharge aims to the periodic deformation of the core diameter.

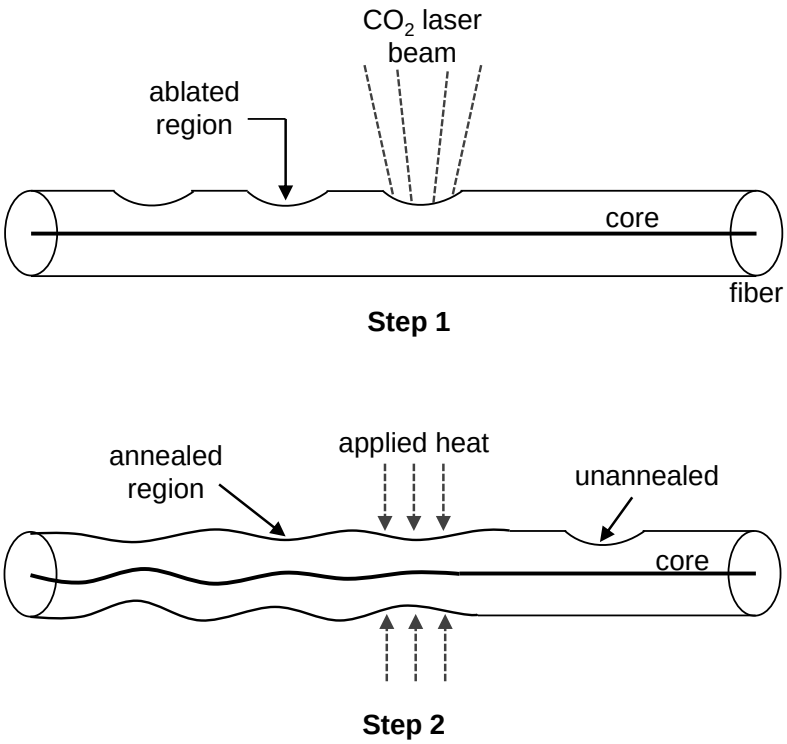

Figure 2.10 Two-step process for creating the periodic deformation of the fiber core [29].

Later in 1999, the new procedure based on the periodic microbend by using an electric arc was proposed by Hwang, et al. [30] as illustrated in Fig. 2.11. From the setup, both ends of the fiber are fixed with the fiber holder. One holder is fixed while another one is displaced in orthogonal direction to the fiber alignment to create the literal stress. The fiber is annealed by using arc discharge method by a pair of electrodes to create the microbending structure as shown in Fig. 2.11(b). The pair of electrodes is moved with a distance of a grating period to create the next microbending structure on the fiber. The amplitude of the microbend on the fiber is controlled by arc duration and arc current that results to the LPFG structure.

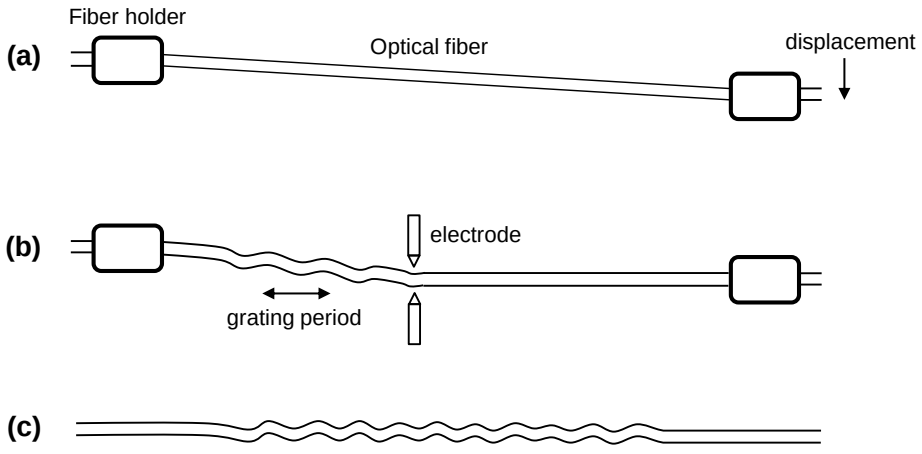

Figure 2.11 LPFG fabrication based on periodic microbend by arc discharge technique [30].

2.2.6 Etching technique

Etching technique was proposed for the first time by Vaziri and Chen in 1992 [31]. From the setup, a small section of a multimode fiber is stressed. Partial sections of the fiber are etched to a smaller diameter. The distance between each of sections refers to the grating period. The stretched region at non-etching section affects to few changes of the spectral output while at the etching section affects to the reduction of the spectral output. The physical diagram of the etched fiber sensing element for the strain gauge is shown in Fig. 2.12.

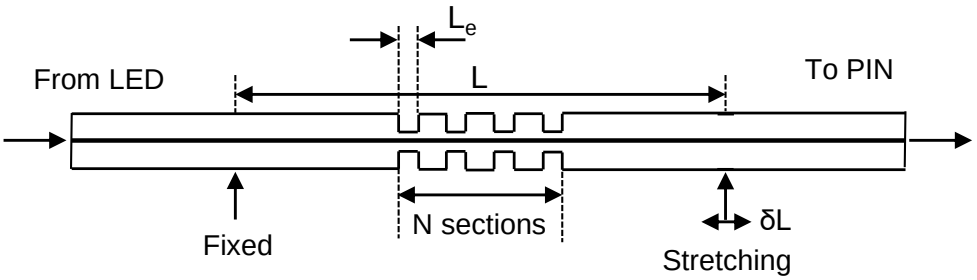

Figure 2.12 Strain gauge with an etched fiber sensing element [31].

In 2012, Chiang and Tsai proposed an inductively coupled plasma (ICP) etching technique to fabricate an LPFG structure [32]. The procedure of the fabrication process by using an ICP is shown in Fig. 2.13. The copper element is used as a mask and the grating pattern is created by a lithography method to become a grating mask. Optical fibers are then covered by a copper grating mask by a chemical technique to remove an epoxy-based negative photoresist. After that, the periodic pattern of a photoresist is created. The optical fiber is then put into a chamber of an ICP to create the periodic notch on the fiber structure while an epoxy-based negative photoresist is being removed by using sulfuric acid. The overall procedures still contain weaknesses that the fiber may be fragile during the process. The notched long-period fiber grating (NLPFG) is finally released. Later in the same year, H.-Y. Wang, et al. [33] proposed the LPFG fabrication by an imprinting lithography technique to increase the strength of the LPFG structure by using etching method. The propose of this research was the application of bending sensors.

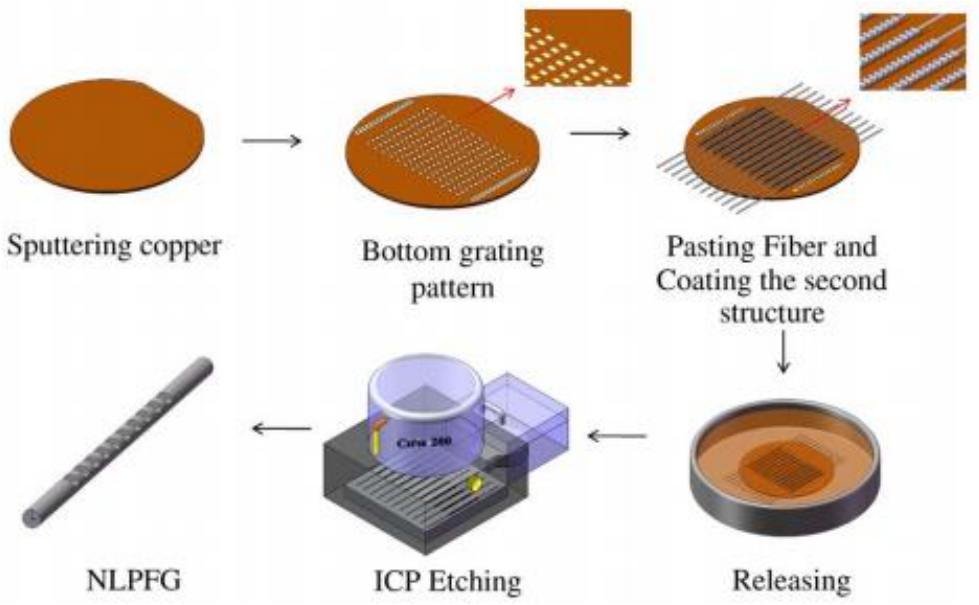

Figure 2.13 The fabrication of NLPFG with etching technique [32].

2.2.7 Mechanically induced technique

The LPFG fabrication by a periodic pressure technique was proposed for the first time by Youngquist, et al. in 1983 [34]. The periodic pressure in the birefringence fiber was created by pressing plastic ridges directly on to the fiber that caused the mode coupling of polarization modes inside the fiber. Later in 1994, this procedure was implemented to couple LP_{01} mode to higher order mode at the wavelength lower than cut-off wavelength of a single-mode fiber. In 2005, Savin, et al. [35] proposed the mechanically induced periodic refractive index modulation for the different mode coupling inside the optical fiber for the first time as shown in Fig. 2.14. The optical fiber is aligned between a flat plate and a groove plate. The groove plate lying above the fiber is directly pressed on to the optical fiber to create the periodic modulation of the refractive index of the fiber. At the pressing point on the fiber by the groove plate, the refractive index modulation affects the photoelastic on the fiber structure. The formation of grating pitch on the fiber structure occurs from the groove period of the groove plate. Therefore, the grating period assigned on the fiber can be selected by changing the groove plate with different groove period. The purpose of this research was the investigation of the relationship between the pressure of the perturbation by the groove plate and the magnitude of resonant wavelength. The coupled mode phenomenon has more strength when the higher pressure of the perturbation is applied and it results to the higher magnitude of the resonant wavelength.

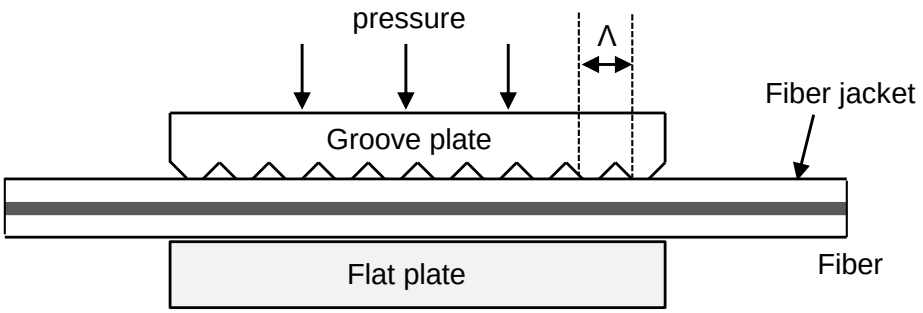

Figure 2.14 LPFG fabrication by mechanically induced technique [35].

There are several types of devices to perform a fabrication of an LPFG structure on the fiber by mechanically induced technique. In 2009, Sakata, et al. [36] proposed another example of the LPFG fabrication by using spherical graphite rods array as devices to perform a grating structure on the fiber. Graphite rods are arranged on the substrate in which the diameter of each graphite rod represents the grating period fabricated on the fiber. The optical fiber is aligned between the silicon wafer designed as a glass plate and graphite rods array. Those graphite rods are pressed on the fiber by the weight of insertion for the perturbation. The modulation of the refractive index of the fiber is performed by the perturbation weight of those graphite rods affecting the photoelastic effect. The LPFG fabrication by using graphite rods array is displayed in Fig. 2.15.

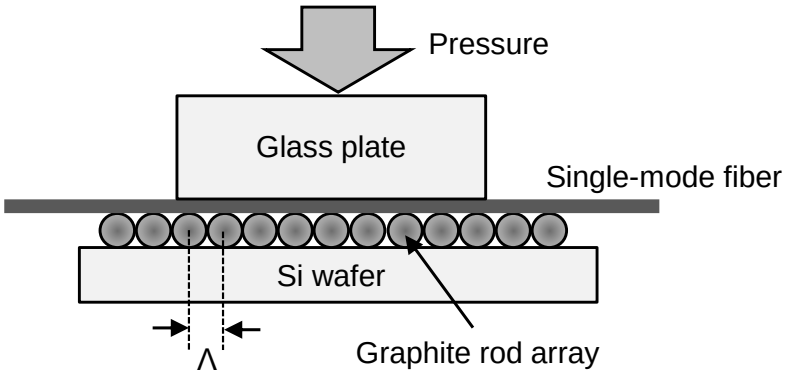

Figure 2.15 LPFG fabrication based on the periodic of graphite rods array [36].

Reference

[1] X. Zhou, S. Shi, Z. Zhang, and Y. Liu, "**Refractive index sensing by using mechanically induced long-period fiber grating**," IEEE Photonics J., vol. 4, no. 1, pp. 119-125, February 2012.

[2] P. J. Lemaire, R. M. Atkins, V. Mizrahi, and W. A. Reed, "**High pressure H_2 loading as a technique for achieving ultrahigh UV photosensitivity and thermal sensitivity in GeO_2 doped optical fiber**," Electron. Lett., vol. 29, no. 13, pp. 1191-1193, June 1993.

[3] H. J. Patrick, C. G. Askins, R. W. McElhalon, and E. J. Friebele, "**Amplitude mask patterned on an excimer laser mirror for high intensity writing of long period fiber gratings**," Electron. Lett., vol. 33, no. 13, pp. 1167-1168, June 1997.

[4] J. A. Rogers, R. J. Jackman, G. M. Whitesides, J. L. Wagener, and A. M. Vengsarkar, "**Using microcontact printing to generate amplitude photomasks on the surfaces of optical fibers: A method for producing in-fiber gratings**," Appl. Phys. Lett., vol. 70, no. 1, pp. 7-9, January 1997.

[5] J. Albert, B. Malo, K. O. Hill, F. Bilodeau, D. C. Johnson, and S. Theriault, "**Comparison of one-photon and two-photon effects in the photosensitivity of germanium doped silica optical fibers exposed to intense ArF excimer laser pulses**," Appl. Phys. Lett., vol. 67, no. 24, pp. 3529-3531, December 1995.

[6] B. Malo, J. Albert, K. O. Hill, F. Bilodeau, D. C. Johnson, and S. Theriault, "**Enhanced photosensitivity in lightly doped standard telecommunication fiber exposed to high fluence ArF excimer laser light**," Electron. Lett., vol. 31, no. 11, pp. 879-880, June 1995.

[7] I. Bennion, A. R. Williams, L. Zhang, K. Sugden, and N. J. Doran, "**UV written in-fiber Bragg gratings**," Opt. Quant. Electron., vol. 28, no. 2, pp. 93-135, February 1996.

[8] B. Guan, H. Tam, S. Ho, S. Liu, and X. Dong, "**Growth of long-period gratings in H_2-loaded fiber after 193-nm UV inscription**," IEEE Photonics Technol. Lett., vol. 12, no. 6, pp. 642-644, July 2000.

[9] A. M. Vengsarksar, P. J. Lemaire, J. B. Judkins, V. Bhatia, T. Erdogan, and J. E. Sipe, "**Long-period fiber gratings as band-rejection filters**," J. Lightwave Technol., vol. 14, no. 1, pp. 58-65, February 1996.

[10] C. Ye, S. James, and R. Tatam, "**Simultaneous temperature and bend sensing with long-period fiber gratings**," Opt. Lett, vol. 25, no. 14, pp. 1007-1009, July 2000.

[11] D. D. Davis, T. K. Gaylord, E. N. Glytsis, and S. C. Mettler, "**CO_2 laser-induced long-period fiber gratings: Spectral characteristics, cladding modes and polarization independence**," Electron. Lett., vol. 34, no. 14, pp. 1416-1417, August 1998.

[12] D. D. Davis, T. K. Gaylord, E. N. Glytsis, and S. C. Mettler, "**Very-high-temperature stable CO_2-laser-induced long-period fiber gratings**," Electron. Lett., vol. 35, no. 9, pp. 740-742, May 1999.

[13] G. Rego, O. Okhotnikov, E. Dianov, and V. Sulimov, "**High-temperature stability of long-period fiber gratings produced using an electric arc**," J. Lightwave Technol., vol. 19, no. 10, pp. 1574-1579, October 2001.

[14] A. Malki, G. Humbert, Y. Ouerdane, A. Boukhenter, and A. Boudrioua, "**Investigation of the writing mechanism of electric-arc-induced long-period fiber gratings**," Appl. Opt., vol. 42, no. 19, pp. 3776-3779, August 2003.

[15] Y. Kondo, K. Nouchi, T. Mitsuyu, M. Watanabe, P. G. Kazansky, and K. Hirao, "**Fabrication of long-period fiber gratings by focused irradiation of infrared femtosecond laser pulses**," Opt. Lett., vol. 24, no. 10, pp. 646-648, June 1999.

[16] F. Hindle, E. Fertein, C. Przygodzki, F. Durr, L. Paccou, R. Bocquet, P. Niay, G. Limberger, and M. Douay, "**Inscription of long-period gratings in pure silica and germane-silicate fiber cores by femtosecond laser irradiation**," IEEE Photonics Technol. Lett., vol. 16, no. 8, pp. 1861-1863, September 2004.

[17] J. N. Blake, B. Y. Kim, and H. J. Shaw, "**Fiber-optic modal coupler using periodic microbending**," Opt. Lett., vol. 11, no. 3, pp. 177-179, April 1986.

[18] G. D. Marshall, M. Ams, and M. J. Withford, "**Point by point femtosecond laser inscription of fiber and waveguide Bragg gratings for photonic device fabrication**," 2nd Pacific International Conference on Applications of Lasers and Optics, Melbourne, Australia, pp. 360-362, April 2006.

[19] R. J. Williams, C. Voigtlander, G. D. Marshall, A. Tunnermann, S. Nolte, M. J. Steel, and M. J. Withford, "**Point-by-point inscription of apodized fiber Bragg gratings**," Opt. Lett., vol. 36, no. 15, pp. 2988-2990, August 2011.

[20] J. Wallace, "**Point-by-point UV exposure makes optimum fiber-optic long-period gratings**," [Online], Available: https://www.laserfocusworld.com/fiber-optics/article/16550079/pointbypoint-uv-exposure-makes-optimum-fiberoptic-longperiod-gratings [2014, July 28].

[21] N. Singh, S. C. Jain, A. K. Aggarwal, and R. P. Bajpai, "**Fiber Bragg grating writing using phase mask technology**," J. Sci. Ind. Res., vol. 64, no. 2, pp. 108-115, February 2005.

[22] R. Delmadahl, and K. Buchwald, "**An interference lithography based production system enables pushbutton fabrication of fiber Bragg gratings (FBGs) for remote fiber sensing**," [Online], Available: https://www.laserfocusworld.com/fiber-optics/article/16547082/optics-fabrication-fiber-bragg-grating-fabrication-system-is-automated [2016, February 17].

[23] K. M. Davis, K. Miura, N. Sugimoto, and K. Hirao, "**Writing waveguides in glass with a femtosecond laser**," Opt. Lett., vol. 21, no. 21, pp. 1729-1731, November 1996.

[24] S. Liu, L. Jin, W. Jin, D. Wang, C. Liao, and Y. Wang, "**Structural long period gratings made by drilling micro-holes in photonic crystal fibers with a femtosecond infrared laser**," Opt. Express, vol. 18, no. 6, pp. 5496-5503, March 2010.

[25] D. D. Davis, T. K. Gaylord, E. N. Glytsis, S. G. Kosinski, S. C. Mettler, and A. M. Vengsarkar, "**Long-period fibre grating fabrication with focused CO_2 laser pulses**," Electron. Lett., vol. 34, no. 3, pp. 302-303, March 1998.

[26] Y. Wang, "**Review of long period fiber gratings written by CO_2 laser**," J. Appl. Phys., vol. 108, no. 8, pp. 081101-081101-18, November 2010.

[27] Y.-J. Rao, Y.-P. Wang, Z.-L. Ran, and T. Zhu, "**Novel fiber-optic sensors based on long period fiber gratings written by high-frequency CO_2 laser pulses**," J. Lightwave Technol., vol. 21, no. 5, pp. 1320-1327, June 2003.

[28] Y. Wang, W. Jin, J. Ju, H. Xuan, H. L. Ho, L. Xiao, and D. Wang, "**Long period gratings in air-core photonic bandgap fibers**," Opt. Express, vol. 16, no. 4, pp. 2784-2790, March 2008.

[29] C. D. Poole, and H. M. Presby, "**Two-mode fiber spatial-mode converter using periodic core deformation**," Electron. Lett., vol. 30, no. 17, pp. 1437-1438, September 1994.

[30] I. K. Hwang, S. H. Yun, and B. Y. Kim, "**Long-period fiber gratings based on periodic microbends**," Opt. Lett., vol. 24, no. 18, pp. 1263-1265, September 1999.

[31] M. Vaziri, and C.-L. Chen, "**Etched fiber as strain gauges**," J. Lightwave Technol., vol 10, no. 6, pp. 836-841, July 1992.

[32] C.-C. Chiang, and L. Tsai, "**Perfectly notched long-period fiber grating filter based on ICP dry etching technique**," Opt. Lett., vol. 37, no. 2, pp. 193-195, January 2012.

[33] H.-Y. Wang, S.-M. Chuo, C.-Y. Huang, and L. A. Wang, "**Embedded corrugated long-period fiber gratings, for sensing applications**," Appl. Opt., vol. 51, no. 10, pp. 1453-1458, April 2012.

[34] S. J. Mihailov, "**Fiber Bragg grating sensors for harsh environments**," Sensors, vol. 12, no. 2, pp. 1898-1918, December 2012.

[35] S. Savin, M. J. F. Digonnet, G. S. Kino, and H. J. Shaw, "**Tunable mechanically induced long-period fiber gratings**," Opt. Lett., vol. 25, no. 10, pp. 710-712, June 2000.

[36] H. Sakata, H. Yoshimi, and Y. Otake, "**Wavelength tenability of L-band fiber ring lasers using mechanically induced long-period fiber gratings**," Opt. Commun., vol. 282, no. 6, pp. 1179-1182, March 2009.

CHAPTER 3 COUPLING THEORY OF LPFG

3.1 Introduction

This chapter presents the related theories behind the phenomenon of the coupling characteristic from the fundamental mode to several cladding modes inside an optical fiber. The following expression about the coupling is based on the step-index single-mode fiber with three layers: core layer, cladding layer, and the surrounding medium. Erdogan described the coupling mode in both core and cladding layers in 1997 [1]. Moreover, the light propagation mode is also discussed.

3.2 Characteristic equation of core and cladding modes

The fundamental property of the fiber grating is considered from the phase matching condition as expressed by [2]

$$\beta_1 - \beta_2 = \Delta\beta = \frac{2\pi}{\Lambda} \tag{3.1}$$

where both β_1 and β_2 are the propagation constants of coupled modes and Λ is the grating period. The phase matching condition of the LPFG is obtained in consideration of the coupling from fundamental core mode to the cladding modes at i^{th} order. Therefore, from the equation (3.1), it is rewritten as

$$\beta_{core} - \beta_{clad}^{i} = \Delta\beta = \frac{2\pi}{\Lambda} \tag{3.2}$$

where β_{core} and β_{clad}^{i} are the propagation constants of fundamental core mode and cladding modes at i^{th} order, respectively. The value of $\Delta\beta$ is small in case of LPFG, hence the grating period is very large. In contrast, for the case of FBG, the value of $\Delta\beta$ is large and the grating period is small (less than 1μm). The relationship between the propagation constant (β) and the effective refractive index (n_{eff}) of the fiber is [3]

$$\beta = \frac{2\pi}{\lambda} n_{eff} \tag{3.3}$$

The phenomenon of mode coupling inside an optical fiber mainly relies upon the effective refractive indices of core and cladding modes. From these parameters, substituting the equation (3.3) into the equation (3.2), the relationship between the grating period and the resonant wavelength can be observed as

$$\lambda = \left[n_{eff,core} - n_{eff,clad}^{i} \right] \Lambda \tag{3.4}$$

where λ is the resonant wavelength, Λ is the applied grating period, $n_{eff,core}$ and $n_{eff,clad}^{i}$ are the effective refractive indices of fundamental core mode and cladding mode at i^{th} order. In order to calculate the effective refractive index, assume that the core mode is not affected by the surrounding medium at all. The cladding layer is considered to be infinity as far as the core mode concerns. The expression of the mode calculation is in term of radial and azimuthal vector components due to the possible overlap between fundamental core mode field and cladding mode field. The characteristic equation of the fundamental core mode is derived as the following equation [1]

$$V\sqrt{1-b}\,\frac{J_1\left(V\sqrt{1-b}\right)}{J_0\left(V\sqrt{1-b}\right)} = V\sqrt{b}\,\frac{K_1\left(V\sqrt{b}\right)}{K_0\left(V\sqrt{b}\right)} \tag{3.5}$$

where J_m is the first class Bessel function of m^{th} order, K_m is the modified Bessel function of the second class of m^{th} order, V is represented as a V-number or a normalized frequency, and b is the normalized propagation constant. The expression of the normalized frequency is shown below

$$V = \frac{2\pi a}{\lambda_0} NA = \frac{2\pi a}{\lambda_0}\sqrt{n_1^2 - n_2^2} \tag{3.6}$$

where a is the radius of a core layer, λ_0 is the free space wavelength, and NA is the numerical aperture where n_1 and n_2 refer to the refractive indices of core and cladding layer, respectively. The characteristic of the normalized propagation constant (b) and the normalized frequency (V-number) is shown in Fig. 1.

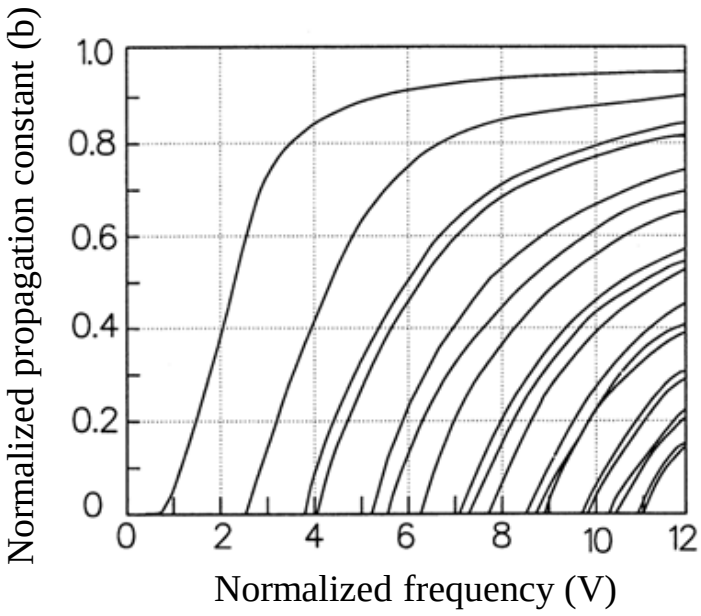

Figure 3.1 The relationship between the normalized propagation constant and the V-number [6].

The regular single-mode propagation operates through the single mode fiber when the V-number is less than or equal to 2.4048 [4]. The characteristic equation of cladding modes is defined with several parameters in the following equation [1]

$$\frac{1}{\sigma_2}\frac{u_2\left(J\cdot K+\frac{\sigma_1\sigma_2 u_{21}u_{32}}{n_2^2 a_1 a_2}\right)\cdot p_m(a_2)-K\cdot q_m(a_2)+J\cdot r_m(a_2)-\frac{1}{u_2}s_m(a_2)}{-u_2\cdot\left(\frac{u_{32}}{n_2^2 a_2}J-\frac{u_{21}}{n_1^2 a_1}K\right)\cdot p_m(a_2)+\frac{u_{32}}{n_1^2 a_2}q_m(a_2)+\frac{u_{21}}{n_1^2 a_1}r_m(a_2)} \tag{3.7}$$

$$=\sigma_1\frac{u_2\left(\frac{u_{32}}{a_2}J-\frac{n_3^2\cdot u_{21}}{n_2^2\cdot a_1}\right)\cdot p_m(a_2)-\frac{u_{32}}{a_2}q_m(a_2)-\frac{u_{21}}{a_2}\cdot r_m(a_2)}{u_2\cdot\left(\frac{n_3^2}{n_2^2}J\cdot K+\frac{\sigma_1\sigma_2 u_{21}u_{32}}{n_1^2 a_1 a_2}K\right)\cdot p_m(a_2)-\frac{n_3^2}{n_1^2}K\cdot q_m(a_2)+J\cdot r_m(a_2)-\frac{n_2^2}{n_1^2\cdot u_2}s_m(a_2)}$$

where these parameters in the equation (3.7) are clarified by the following relations [1]

$$\sigma_1=\frac{im}{\eta}\cdot n_{eff,clad}\ ;\ \sigma_2=im\cdot\eta\cdot n_{eff,clad} \tag{3.8a}$$

$$u_{21}=\frac{1}{u_2^2}-\frac{1}{u_1^2}\ ;\ u_{32}=\frac{1}{w_3^2}-\frac{1}{u_2^2} \tag{3.8b}$$

$$u_1=\frac{2\pi}{\lambda}\sqrt{n_1^2-n_{eff,clad}^2}\ ;\ u_2=\frac{2\pi}{\lambda}\sqrt{n_2^2-n_{eff,clad}^2}\ ;\ w_3=\frac{2\pi}{\lambda}\sqrt{n_{eff,clad}^2-n_3^2} \tag{3.8c}$$

$$J=\frac{1}{2}\frac{J_{m-1}\left(u_1a_1\right)+J_{m+1}\left(u_1a_1\right)}{u_1J_m\left(u_1a_1\right)};\ K=-\frac{1}{2}\frac{K_{m-1}\left(w_3a_2\right)+K_{m+1}\left(w_3a_2\right)}{w_3K_m\left(w_3a_2\right)} \tag{3.8d}$$

$$p_m\left(r\right)=J_m\left(u_2r\right)Y_m\left(u_2a_1\right)-J_m\left(u_2a_1\right)Y_m\left(u_2r\right)$$

$$q_m\left(r\right)=\frac{1}{2}J_m\left(u_2r\right)\left(Y_{m-1}\left(u_2a_1\right)-Y_{m+1}\left(u_2a_1\right)\right)-Y_m\left(u_2r\right)\left(J_{m-1}\left(u_2a_1\right)-J_{m+1}\left(u_2a_1\right)\right)$$

$$r_m\left(r\right)=\frac{1}{2}Y_m\left(u_2a_1\right)\left(Y_{m-1}\left(u_2r\right)-Y_{m+1}\left(u_2r\right)\right) \tag{3.8e}$$

$$s_m\left(r\right)=\frac{1}{4}\left(J_{m-1}\left(u_2r\right)-J_{m+1}\left(u_2r\right)\right)\left(Y_{m-1}\left(u_2a_1\right)-Y_{m+1}\left(u_2a_1\right)\right)$$

$$-\left(J_{m-1}\left(u_2a_1\right)-J_{m+1}\left(u_2a_1\right)\right)\left(Y_{m-1}\left(u_2r\right)-Y_{m+1}\left(u_2r\right)\right)$$

where Y_m is the second class of the Bessel function, η is the vacuum impedance, and m is the azimuthal mode number. By solving equation (3.6) and (3.7), the effective refractive indices of both core and cladding layers can be found.

3.3 Coupled mode equations of LPFG

The coupling between forward propagation modes are considered in case of an LPFG structure. The only one forward propagating core mode and forward propagating cladding modes is derived in the following equation [5]

$$\frac{dA_{core}\left(z\right)}{dz}=i\sum_m B_m\left(z\right)C_{core,m}\left(z\right) \tag{3.9a}$$

$$\frac{dB_j\left(z\right)}{dz}=iA_{core}\left(z\right)C_{j,core}+\sum_{m\neq j}B_m\left(z\right)C_{j,m}\left(z\right) \tag{3.9b}$$

Assuming that the periodic induction of the refractive index is much lower than the initial condition or non-induction, the coupling coefficient of the propagation mode can be approximated as derived in the following equation [5]

$$C_{core,m}=\frac{k}{2\eta_0}\int_{A_\infty}n\left(r\right)\delta n\left(r,z\right)\hat{e}_{core}^{*}\left(r\right)\cdot\hat{e}_m^{*}\left(r\right)e^{-i\left(\beta_{core}-\beta_m\right)z}dA \tag{3.10}$$

where $C_{m,core}=\left(C_{core,m}\right)^*$, $\hat{e}_m^{*}\left(r\right)$ is the normalized electric field, dA is the differential area, and the integration is taken along the infinite area. The parameter $\delta n\left(r,z\right)$ or the uniform refractive index

induction of a three-layered waveguide corresponding to core layer, cladding layer, and surrounding medium, respectively can be expressed as [5]

$$\delta n(r,z)=\begin{cases}\delta n_{core}e^{i\left(\frac{2\pi}{\Lambda}z+\phi_{\infty}\right)} & r\le a_1\\ \delta n_{clad}e^{i\left(\frac{2\pi}{\Lambda}z+\phi_{clad}\right)} & a_1\le r\le a_2\\ 0 & r>a_2\end{cases} \tag{3.11}$$

The coupling coefficient of the propagation can be expressed as [5]

$$C_{core,m}=\frac{k}{2\eta_0}e^{-i\Delta z+i\phi_{core}}\left\{n_1\delta n_{core}I_{1m}+n_2\delta n_{clad}I_{2m}\right\} \tag{3.12}$$

where

$$\Delta=\left(\frac{2\pi}{\Lambda}-\frac{2\pi\Delta n_{eff,core,m}}{\lambda}\right) \tag{3.13}$$

and

$$\begin{aligned}I_{1m}&=\int_0^{a_1}\hat{e}^{*}_{core}(r)\cdot\hat{e}_m(r)\,rdr\\ I_{2m}&=\int_{a_1}^{a_2}\hat{e}^{*}_{core}(r)\cdot\hat{e}_m(r)\,rdr\end{aligned} \tag{3.14}$$

From equations (3.12) and (3.13), some propagation constant parameters are discussed as $\beta_{core}-\beta_m=\frac{2\pi\left(n_{eff,core}-n_{eff,clad}\right)}{\lambda}=2\pi\Delta n_{eff,core,m}$. They are discussed in terms of the effective refractive indices between the core and the cladding modes. The integrals expressed in equation (3.14) show the overlap factors between core and cladding modes which is determining the changes in the optical spectrum when some factors and environments are changed along the fiber structure such as fiber dimension, external refractive index, temperature, and fiber stress. Those factors all affects the change of refractive indices of both core and cladding modes.

According to the analysis of the amplitude of core and cladding modes, only the single coupling to cladding mode is considered. Therefore, after differentiating equations (3.9a) and (3.9b) and then solving the resultant equation, the results are [5]

$$A_{core}(z) = A_1 \cos\left(\sqrt{\left(\frac{\Delta}{2}\right)^2 + \left|C_{core,m}\right|^2}\, z\right) e^{-i\frac{\Delta}{2}z} + B_1 \sin\left(\sqrt{\left(\frac{\Delta}{2}\right)^2 + \left|C_{core,m}\right|^2}\, z\right) e^{-i\frac{\Delta}{2}z} \tag{3.15a}$$

$$B_m(z) = A_2 \cos\left(\sqrt{\left(\frac{\Delta}{2}\right)^2 + \left|C_{core,m}\right|^2}\, z\right) e^{i\frac{\Delta}{2}z} + B_2 \sin\left(\sqrt{\left(\frac{\Delta}{2}\right)^2 + \left|C_{core,m}\right|^2}\, z\right) e^{i\frac{\Delta}{2}z} \tag{3.15b}$$

From this point, the specific boundary conditions in LPFG is considered where $A_{co}(0) = 1$ and $B_m(z) = 0$ in which the results are [5]

$$A_{core}(z) = \left(\begin{array}{c} \cos\left(\sqrt{\left(\frac{\Delta}{2}\right)^2 + \left|C_{core,m}\right|^2}\, z\right) \\ +i\frac{\Delta}{2\sqrt{(\Delta/2)^2 + \left|C_{core,m}\right|^2}} \sin\left(\sqrt{\left(\frac{\Delta}{2}\right)^2 + \left|C_{core,m}\right|^2}\, z\right) \end{array} \right) e^{-i\frac{\Delta}{2}z} \tag{3.16a}$$

$$B_m(z) = i\frac{C_{core,m}}{\sqrt{(\Delta/2)^2 + \left|C_{core,m}\right|^2}} \sin\left(\sqrt{\left(\frac{\Delta}{2}\right)^2 + \left|C_{core,m}\right|^2}\, z\right) e^{i\frac{\Delta}{2}z - \phi} \tag{3.16b}$$

The transmittance of the core mode is [3]

$$T_{core}(z) = \cos^2\left(\sqrt{\left(\frac{\Delta}{2}\right)^2 + \left|C_{core,m}\right|^2}\, z\right) + \frac{(\Delta/2)^2}{(\Delta/2)^2 + \left|C_{core,m}\right|^2} \sin^2\left(\sqrt{\left(\frac{\Delta}{2}\right)^2 + \left|C_{core,m}\right|^2}\, z\right) \tag{3.17}$$

in which it is used only with the uniform LPFG structure with a step change. Practically, the refractive index change is not that much perfect as an ideal case such as for arc discharge technique, the area affected by an electric arc span is higher than 300 μm and it is asymmetric in both longitudinal and transverse directions. Therefore, the creation of an LPFG structure inside the fiber is challenging. The only way to observe the quality of the LPFG is the analysis from the observed resonant wavelength as the result from the coupling efficiency regarding to the effective refractive indices of both core and cladding layer.

3.4 Light propagation modes

The light generally propagates only inside the core layer of a fiber as resulted from an internal reflection because of the different refractive index between core and cladding layer. The cylindrical axis in term of *r*,*ϕ*,*z* is used to define the mode propagation inside the step index fiber. The normalized index difference (Δ) is expressed as

$$\Delta = \frac{n_1 - n_2}{n_1} \tag{3.18}$$

where n_1 and n_2 are the refractive indices of core and cladding layer, respectively. In case of the normalized index difference less than one percent, it is clarified as the scalar approximation or the weakly guiding approximation. Two independent sets of modes, x-polarized and y-polarized, have the same propagation constant (β) and they are referred as the linear polarized (LP) modes. The relationship between the propagation constant (β) and the free space wave number $\left(k_0\right)$ is expressed in the following equations [7,8]

$$\beta = \frac{\omega n}{c} \tag{3.19}$$

$$k_0 = \frac{\omega}{c} = \frac{2\pi}{\lambda_0} \tag{3.20}$$

where λ_0 is the free space wavelength and c is the speed of light in vacuum. The cylindrical analysis shows that the only transverse coordinate r and ϕ are chosen to solve an electric field and a magnetic field boundary conditions at the core-cladding region where the radial part (r) is divided into two distinct modes as the guided mode and the radiation mode. Both guided and radiation modes are discussed in the following equations [9]

$$n_2^2 < \frac{\beta^2}{k_0^2} < n_1^2 \tag{3.21}$$

$$\beta^2 = k_0^2 n_2^2 \tag{3.22}$$

The fundamental core mode is generally defined as LP_{01} mode. This is the only mode that can be propagated through the single-mode fiber. The higher order modes are defined as LP_{lm} mode where l and m represent the number of radial and azimuthal zeros of a particular mode, respectively. The power distribution pattern of light is categorized as shown in Fig. 3.2.

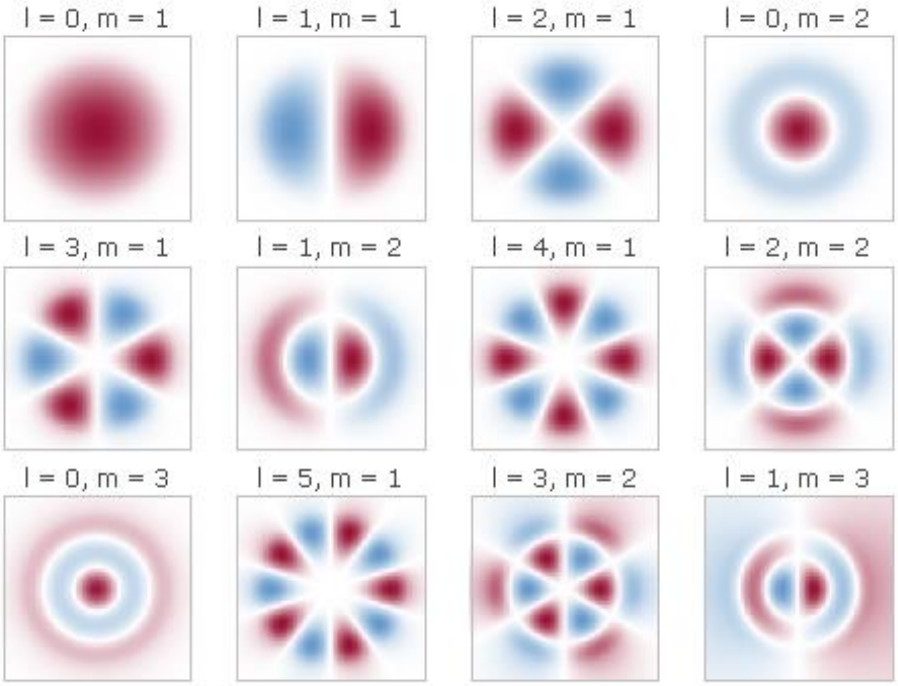

Figure 3.2 Power distribution pattern of LP modes [6].

The V-number determines that how many modes can propagate through the optical fiber. The cut-off wavelength is defined at the position where the normalized propagation constant (*b*) is zero. The wavelength longer than this cut-off wavelength will not be able to propagate through this optical fiber. The state of single-mode propagation is defined when the V-number or normalized frequency is less than 2.4048. The cut-off wavelength (λ_c) is expressed as

$$\lambda_c = \frac{2\pi a}{2.4048} NA = \frac{2\pi a}{2.4048} \sqrt{n_1^2 - n_2^2} \tag{3.23}$$

referred from the equation (3.6) for the single-mode operation.

Reference

[1] T. Erdogan, "**Cladding-mode resonances in short- and long-period fiber grating filters**," J. Opt. Soc. Am. A, vol. 14, no. 8, pp. 1760-1773, August 1997.

[2] V. Bhatia, and A. M. Vengsarkar, "**Optical fiber long period gratings sensors**," Opt. Lett., vol. 21, no. 9, pp. 692-694, May 1996.

[3] R. Kashyap, "**Fiber Bragg gratings**," Academic Press, 2010.

[4] A. S. Vasudeva, "**A textbook of engineering physics (kerala)**," S. Chand & Company Ltd., New Delhi, India, 2008.

[5] J. Bures, "**Guided optics: Optical fibers and all-fiber components**," Wiley-VCH, Weinheim, Germany, 2009.

[6] "**Basic optics for optical fiber**," [Online] Available: https://www.fiberoptics4sale.com/blogs/archive-posts/95048070-basic-optics-for-optical-fiber [2017, July 15].

[7] Y. Kokubun, "**Lightwave Engineering**," CRC Press, Florida, USA, 2018.

[8] J. Singh, "**Optical properties of materials and their applications**," John Wiley & Sons Ltd., West Sussex, United Kingdom, 2020.

[9] S. Kumar, and M. J. Deen, "**Fiber optic communications: Fundamentals and applications**," John Wiley & Sons Ltd., West Sussex, United Kingdom, 2014.

CHAPTER 4 EXPERIMENTAL SETUP, RESULTS AND DISCUSSION

4.1 Introduction

This chapter presents all equipment selected for the experiment of using LPFG devices to create the LPFG structure on the single-mode fiber following by the observation of resonant wavelengths and their characteristics for the analysis of the performance by using proposed LPFG devices. Each equipment with its model and its specification are described in details. The observation of the resonant wavelength from applying an LPFG structure contains three main parts: the transmitter, the medium, and the receiver. The transmitter section is the light source emitting light pulse centering at 1550 nm. The medium section is the bare single-mode fiber without removing the coating layer. The receiver section is the optical spectrum analyzer (OSA) which is able to receive the light wave from 600 to 1750 nm. In addition, the creation procedure of the 3D printed LPFG device by using the high resolution 3D printer is also described. Lastly, the experimental results from a single and simultaneous perturbation by 3D printed LPFG devices with different grating periods and the analysis of the resonant wavelength shifts are expressed in this chapter. The resonant wavelength shifts refer to the tunable wavelength filter by the change of applied grating period on the optical fiber.

4.2 Corresponding equipment

The corresponding equipment and tools with their model and specification are clarified in this section. The same equipment with different model and specification may results to different desired output due to the performance of their functions.

4.2.1 Light source

The general visible light locates in the range between 400 to 700 nm as humans can see with their eyes. The optical communication with the range of telecommunication through an optical fiber requires the light wave signal at around 1550 nm which locates at invisible region. The selected light source is superluminescent diode (SLD-761) emitting broadband light signal with its center at around 1550 nm. Another model of the light source is the one emitting light wave at 1310 nm. This model offers lower optical power comparing with the one operating at 1550 nm. The advantage of the operation wavelength with 1310 nm is that the light source has lower cost and it also offers a good

potential for short distance (up to 10 km). There is a temperature controller box unit (PILOT4-AC) which offers a port of FC connector. The front panel model of the controller box and the SLD light source are shown in Fig. 4.1.

Figure 4.1 Superluminescent diode emitting broadband light wave at 1550 nm.

4.2.2 Single-mode fiber

The single-mode fiber is considered to be used as a transmission medium for the entire experiment and the only single set of a fiber is used to avoid any distortion from the measurement by the receiver. The model of a single-mode fiber is BBG-SM-WF (Hitachi Cable) [1] in which its core and cladding diameter are 0.8 and 125 μm, respectively. The cut-off wavelength (λ_c) is less than or equal to 1260 nm. The fiber attenuation at 1310 and 1550 nm are less than 0.35 and 0.24 dB/km. The coating layer is not removed, so that the diameter of the bare fiber is 250 μm. The fiber is cut from the spool, the coating layer at partial region of both fiber ends are removed by using a stripper and then carefully cut by using a cleaver. Both fiber ends are then inserted to the FC connector kit. One side is connected to the light source, while another side is connected to an OSA. The connecting loss at both sides of FC connectors may occur at both connections. The fiber spool of the single-mode fiber is shown in Fig. 4.2.

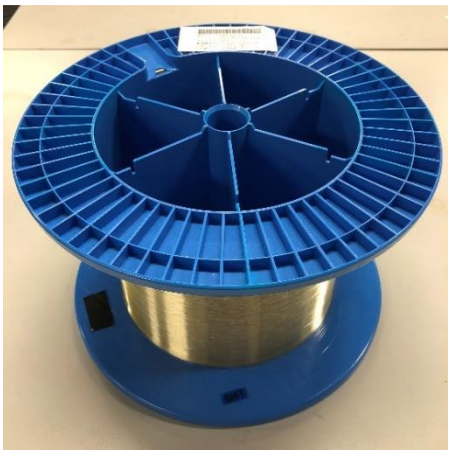

Figure 4.2 Fiber spool of single-mode fiber with total distance of 5 km.

4.2.3 Optical spectrum analyzer

The light signal is received by an optical spectrum analyzer (OSA). The model of the OSA used in the experiment is Anritsu MS9710C [2] supporting the received signal wavelength from 600 to 1750 nm. The port connecting to the fiber is an FC connector type. The display screen shows the relationship between the light wavelength in the unit of nm (x-axis) and the optical power in the unit of dBm (y-axis). The measurement resolution is 0.5 nm. Moreover, the signal peak or the maximum power shown on the screen is automatically located by the machine itself by pressing one button. The spectral data is recorded by the 3.5-inch floppy disc in term of screen display image and text file. The recorded text file of an optical power is in the unit of mW, so it is needed to transform into the unit of dBm by the following formula. The OSA panel is shown in Fig. 4.3.

$$P(dBm) = 10\log\left(P(mW)\right) \tag{4.1}$$

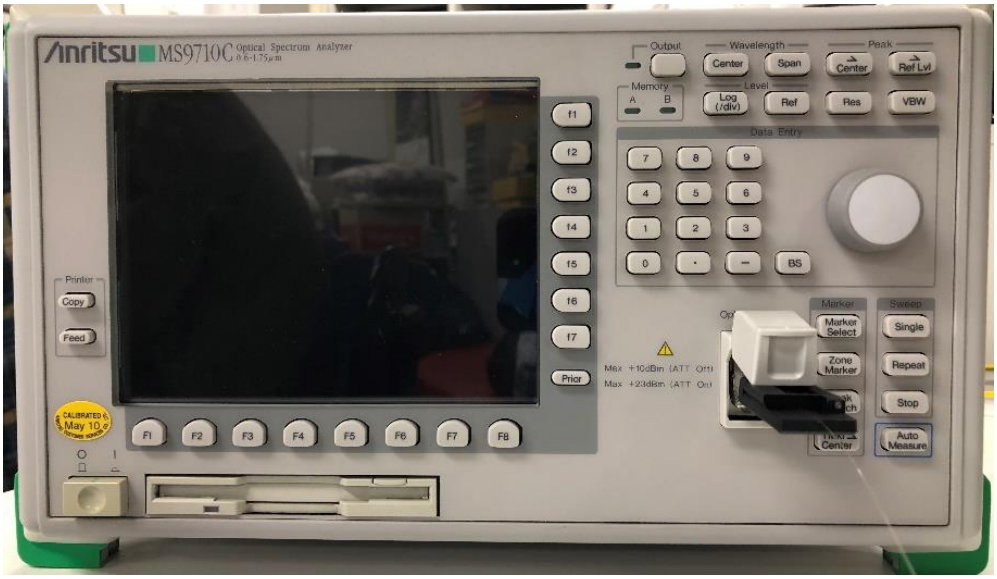

Figure 4.3 Optical spectrum analyzer MS9710C.

4.2.4 Digital force meter

The measurement of the perturbation weight by the 3D printed LPFG device on to an optical fiber is taken by the digital force meter. The model of the digital force meter is Shimpo FGJN-50 [3]. This force meter supports the maximum load of ±50 kg with the resolution of 0.01 kg. The package contains several types of heading tools with several shapes corresponding to the usage in both push and pull direction. The flat heading tool is selected to attach with the digital force meter for the direct pressing on the 3D printed LPFG device in the vertical direction for the experiment. The digital force meter is installed with the test stand to keep the meter floating. The vertical movement of the force

meter is taken by moving the handle located beside the test stand. The setup of the digital force meter is shown in Fig. 4.4.

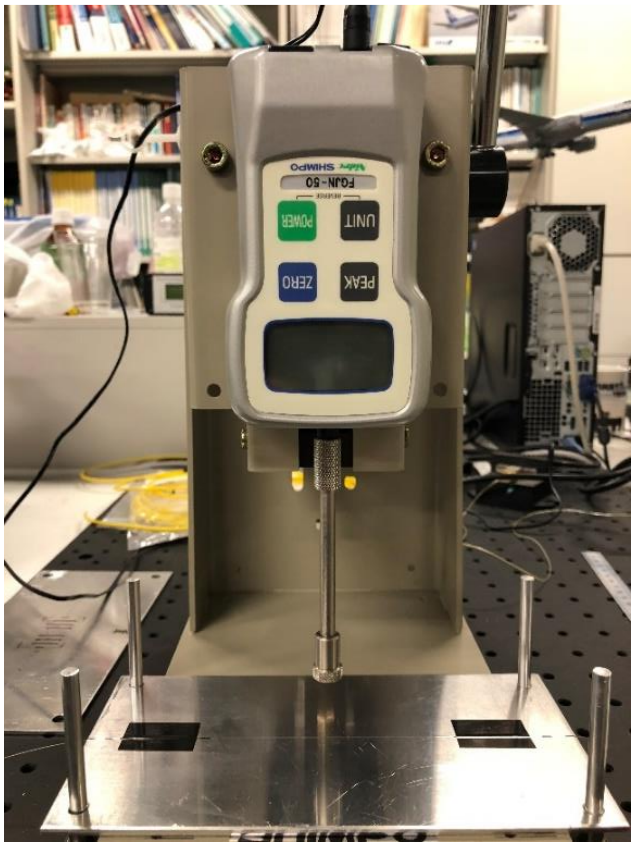

Figure 4.4 Digital force meter installed with the test stand.

4.2.5 3D printed LPFG device

The technology of three-dimensional printing becomes increasingly popular in the recent era. The quality of 3D printed object is rigid to the harsh environment in which it is considered to perform a grating structure on an optical fiber. The resolution of the printing process is going down to the level of few microns supporting the creation of the 3D printed LPFG device. Therefore, it is possible that the 3D printed object has a potential to perform as a 3D printed LPFG device.

The 3D printed LPFG device is designed in Solidworks software as the 3D rectangular shape with the dimension of 4.0 cm long, 2.5 cm wide, and 0.5 cm thick as shown in Fig. 4.5(a). One of its surface is designed as an isosceles triangular crest and trough defining as a grating structure of the object. The aforementioned dimension of the device is the most compact with the experimental equipment, especially the flat heading tool of the digital force meter. The device is printed out by the high resolution 3D printer (Objet Connex500) which offers the minimum resolution of 16 μm as shown in Fig. 4.5(b). The material selected for the printing process is a resin (Polyjet RGD720) [4] in which it has a rigid and translucent structure. The modulus of elasticity relies between 2,000 to

3,000 MPa that is well supporting the perturbation weight by the force meter higher than the expectation at 10 kg. Those periodic grating crests are the only part of the device that directly touch the fiber to change the fiber's refractive index as of the mechanically induced technique. The selected grating period of the 3D printed LPFG begins from 500 to 630 µm at every step of 10 µm. The device with smaller grating period has higher possibility that the grating crests have more curvature than the one with larger grating period. Both single and simultaneous perturbation devices are investigated to find out the position of resonant wavelengths.

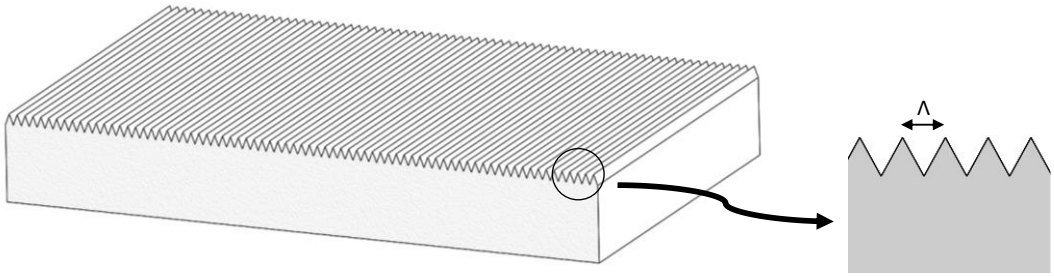

(a)

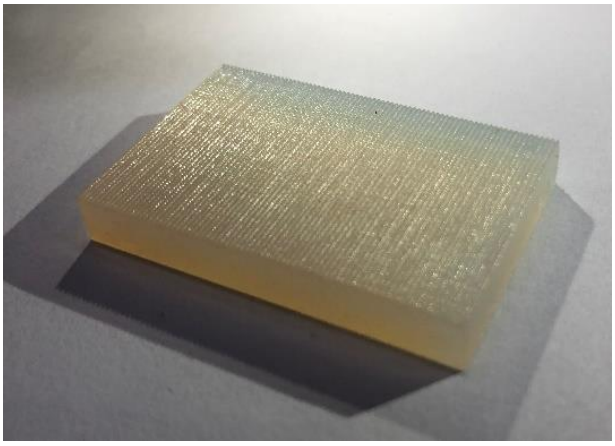

(b)

Figure 4.5 3D printed LPFG device (a) designed in Solidworks and (b) printed by resin material.

4.3 Experimental setup

The setup consists of three main parts as described; the transmitter, the medium, and the receiver. Each equipment is positioned for the experiment as shown in Fig. 4.6. The superluminescent diode light source emits light wave at 1550 nm transmitting through the single-mode fiber and ending up at the OSA as the receiver unit. The single-mode fiber is relaxingly aligned where its partial region

is aligning on the flat aluminum plate installed on the test stand of the digital force meter. Single perturbation contains only one test stand. On the other hand, simultaneous perturbation contains two test stands, so that the fiber is aligned on both test stands simultaneously. The 3D printed LPFG device is placed above the fiber following the fiber axis without any tilt angle. The LPFG structure is induced by moving the handle to lower down the digital force meter with the flat rod and then perturbing or pressing the 3D printed LPFG device. In addition, before performing the grating perturbation, the reference signal of the light source is recorded to each usage of the fiber because the optical power output may be changed due to the connecting loss when the fiber is rejected and reinserted to both light source and OSA.

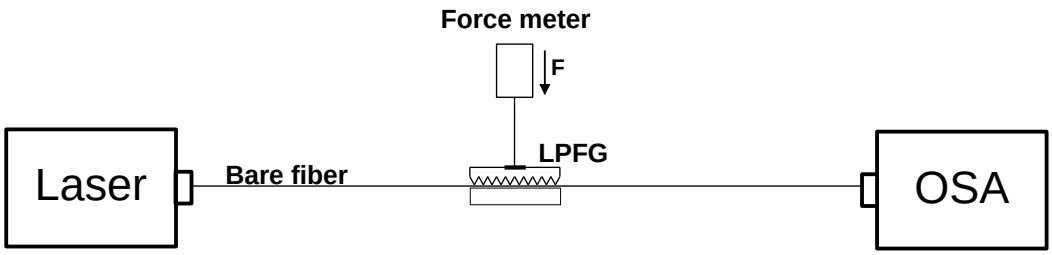

(a)

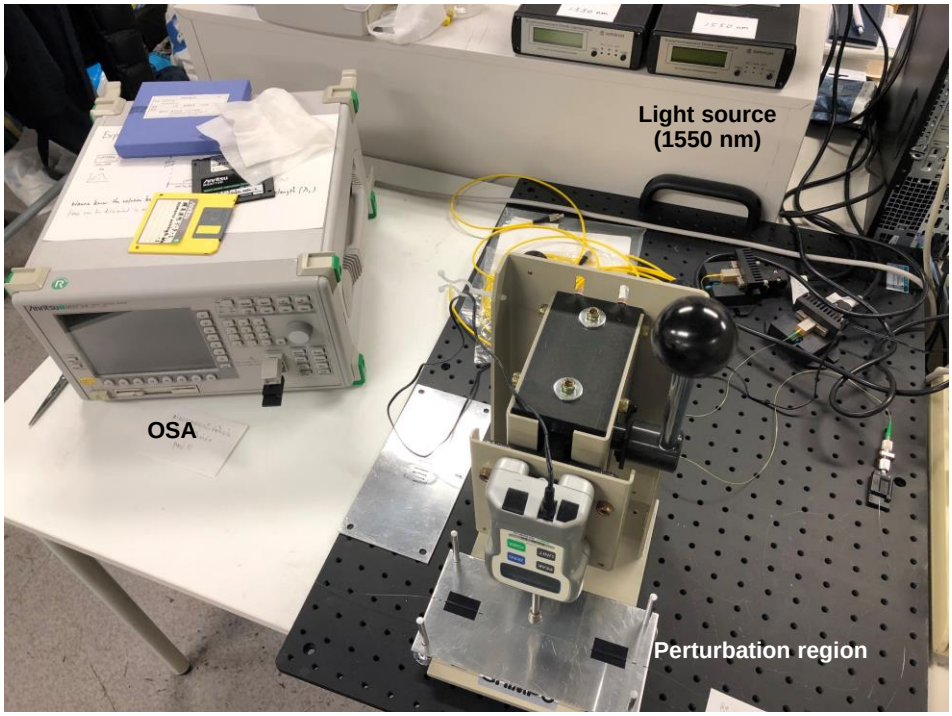

(b)

Figure 4.6 (a) The experimental setup and (b) the setup of the digital force meter.

4.3.1 Reference signal

The uniform broadband light wave from the superluminescent diode light source is recorded by an OSA while the single-mode fiber is not under any environmental effect. In the another word, the fiber is aligned in the relaxation state. The spectral output read by an OSA is displayed in Fig. 4.7 showing the relationship between the optical power (dBm) and the wavelength (nm). The display wavelength covers from 1250 to 1750 nm.

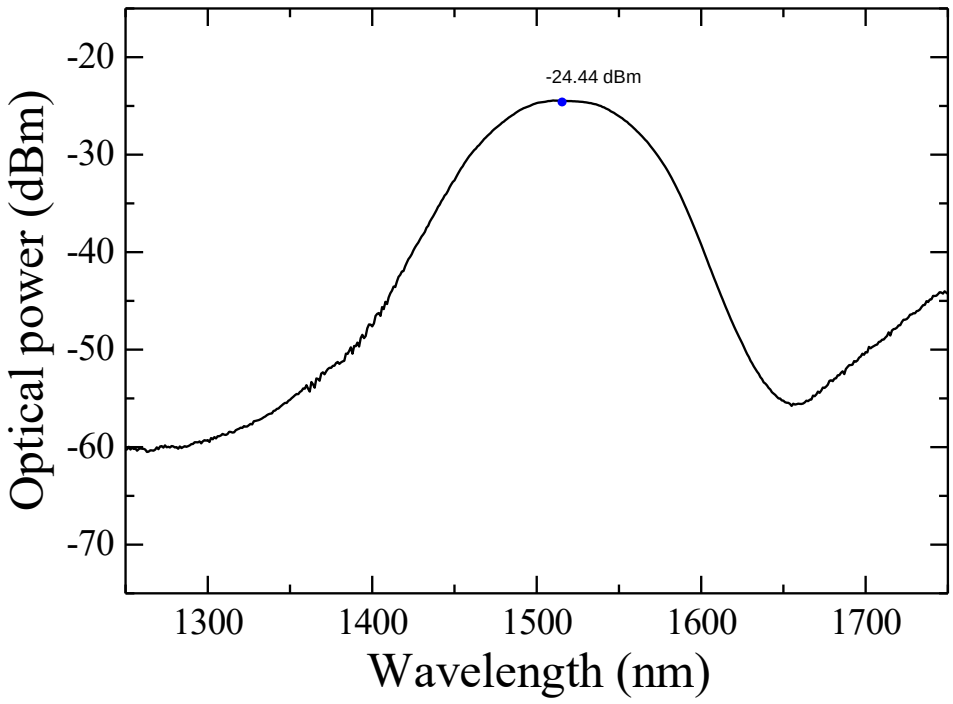

Figure 4.7 The reference spectral output of the light source.

The broadband spectrum has its maximum power of -24.44 dBm at 1510 nm, however the obtained maximum power depends on the connecting loss from an FC connector at both sides. The resonant wavelength can be observed only within this spectral range (approximately 1310 to 1550 nm). The resonant wavelength shift is observed from the change of the grating period of the 3D printed LPFG device. Theoretically, the relationship between the grating period and the resonant wavelength shift is linear as expressed in equation (3.4).

4.4 Single perturbation of 3D printed LPFG device

The creation of the grating structure on the single-mode fiber is performed by the perturbation of 3D printed LPFG devices with different grating periods beginning from 500 to 630 μm at every step of 10 μm. Moreover, the perturbation weights with the step of 1 kg are applied to find out the resonant magnitude. The spectrum displays are shown from Fig. 4.8 to Fig. 4.21.

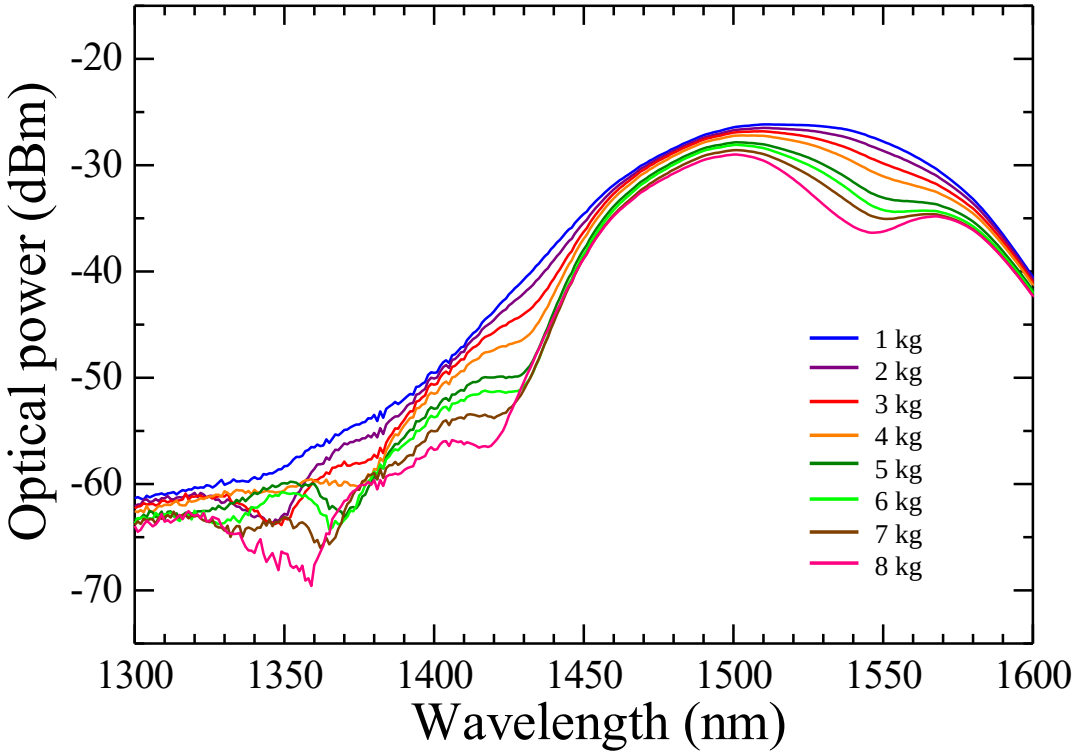

Figure 4.8 The spectral output by 3D printed LPFG device with Λ = 500 µm.

Table 4.1 Resonant wavelength vs perturbation weight by Λ = 500 µm.

	1st resonant λ	**2nd resonant λ**	**3rd resonant λ**	**4th resonant λ**
1 kg	-	-	-	-
2 kg	-	-	-	-
3 kg	-	-	-	-
4 kg	-	-	-	-
5 kg	-	-	1424 nm	1558 nm
6 kg	-	-	1424 nm	1554 nm
7 kg	-	-	1420 nm	1551 nm
8 kg	-	-	1415 nm	1546 nm

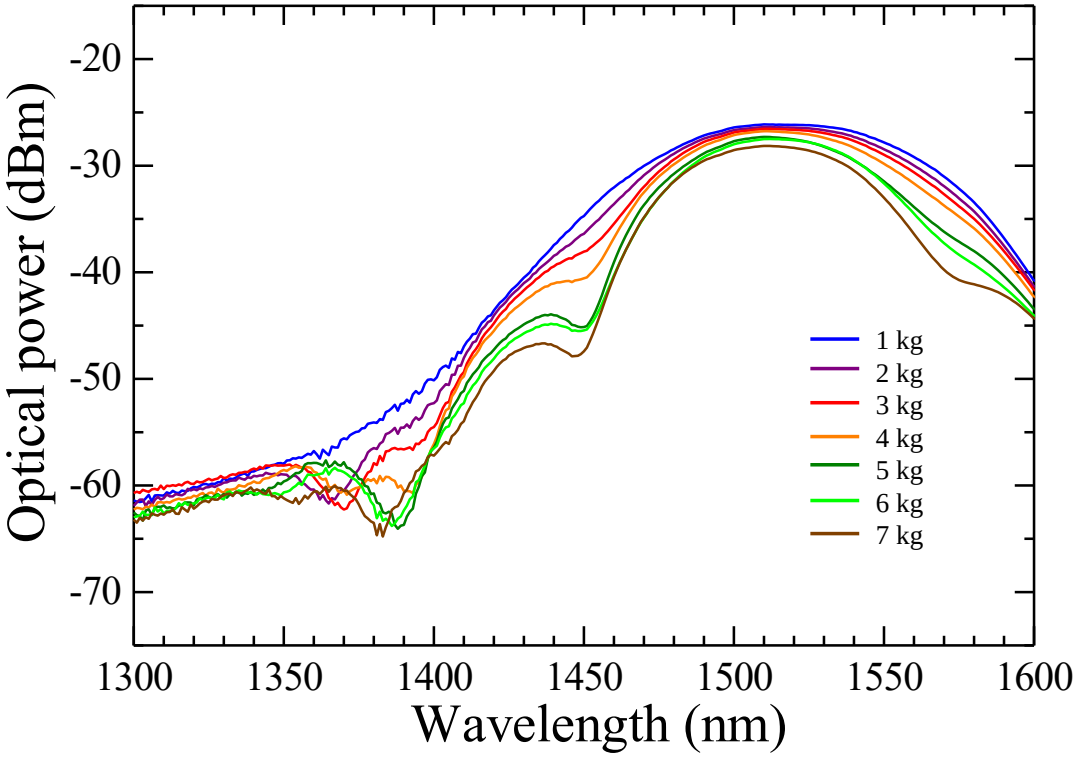

Figure 4.9 The spectral output by 3D printed LPFG device with Λ = 510 µm.

Table 4.2 Resonant wavelength vs perturbation weight by Λ = 510 µm.

	1st resonant λ	**2nd resonant λ**	**3rd resonant λ**	**4th resonant λ**
1 kg	-	-	-	-
2 kg	-	-	-	-
3 kg	-	-	-	-
4 kg	-	-	1450 nm	-
5 kg	-	-	1449 nm	1568 nm
6 kg	-	-	1448 nm	1571 nm
7 kg	-	-	1446 nm	1572 nm

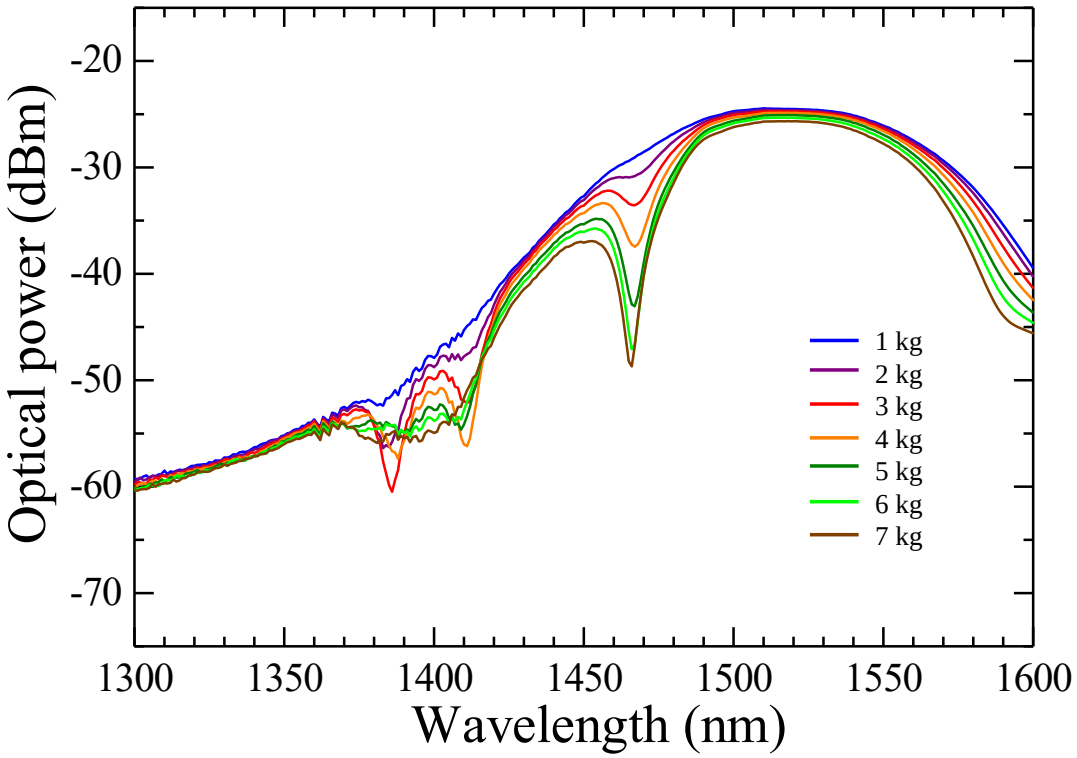

Figure 4.10 The spectral output by 3D printed LPFG device with Λ = 520 µm.

Table 4.3 Resonant wavelength vs perturbation weight by Λ = 520 µm.

	1st resonant λ	**2nd resonant λ**	**3rd resonant λ**	**4th resonant λ**
1 kg	-	-	1463 nm	-
2 kg	-	-	1463 nm	-
3 kg	1386 nm	1411 nm	1467 nm	-
4 kg	1388 nm	1411 nm	1467 nm	1581 nm
5 kg	-	-	1467 nm	1581 nm
6 kg	-	-	1466 nm	1581 nm
7 kg	-	-	1466 nm	1581 nm

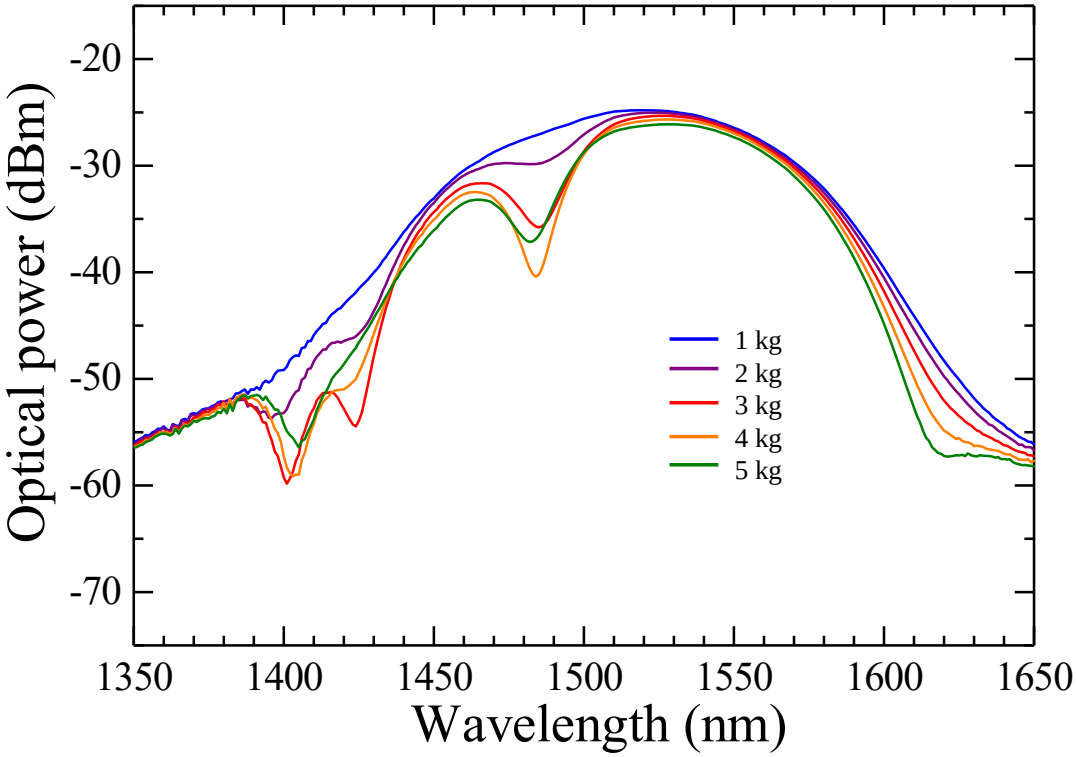

Figure 4.11 The spectral output by 3D printed LPFG device with Λ = 530 µm.

Table 4.4 Resonant wavelength vs perturbation weight by Λ = 530 µm.

	1st resonant λ	**2nd resonant λ**	**3rd resonant λ**	**4th resonant λ**
1 kg	-	-	1487 nm	-
2 kg	1396 nm	1423 nm	1487 nm	-
3 kg	1401 nm	1424 nm	1485 nm	1621 nm
4 kg	1403 nm	1421 nm	1484 nm	1621 nm
5 kg	-	-	1482 nm	1620 nm

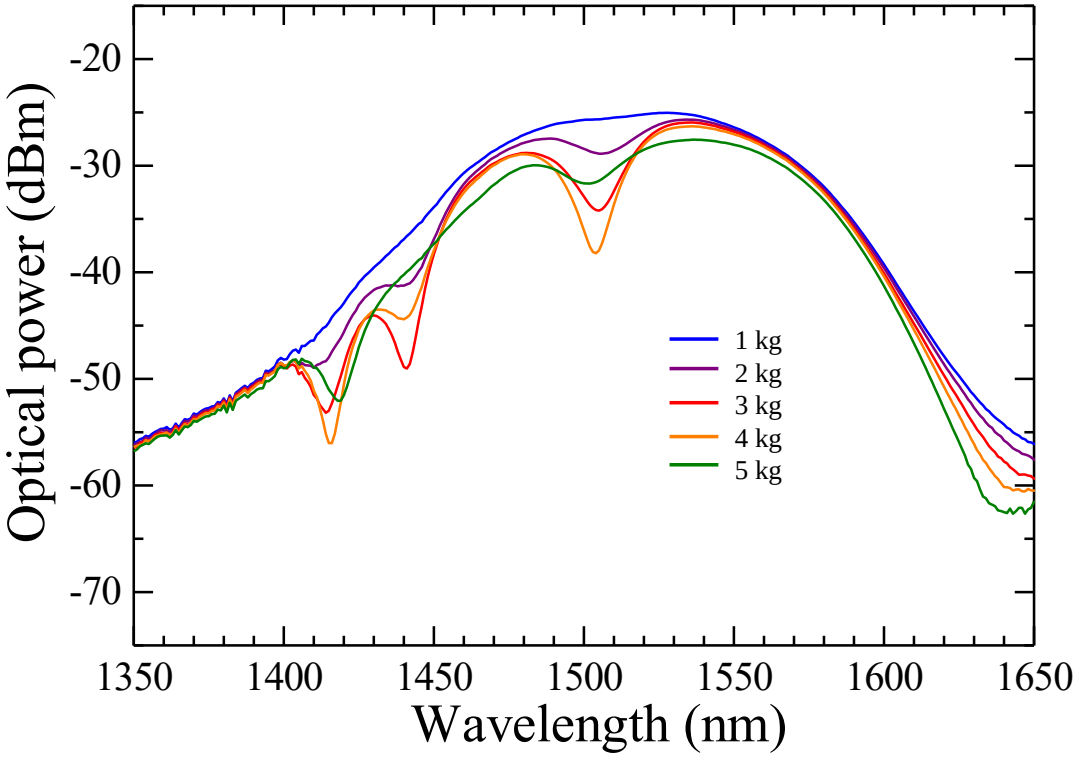

Figure 4.12 The spectral output by 3D printed LPFG device with Λ = 540 µm.

Table 4.5 Resonant wavelength vs perturbation weight by Λ = 540 µm.

	1st resonant λ	**2nd resonant λ**	**3rd resonant λ**	**4th resonant λ**
1 kg	1411 nm	1441 nm	1507 nm	-
2 kg	1411 nm	1439 nm	1506 nm	-
3 kg	1414 nm	1441 nm	1505 nm	1645 nm
4 kg	1416 nm	1440 nm	1504 nm	1644 nm
5 kg	1418 nm	-	1502 nm	1642 nm

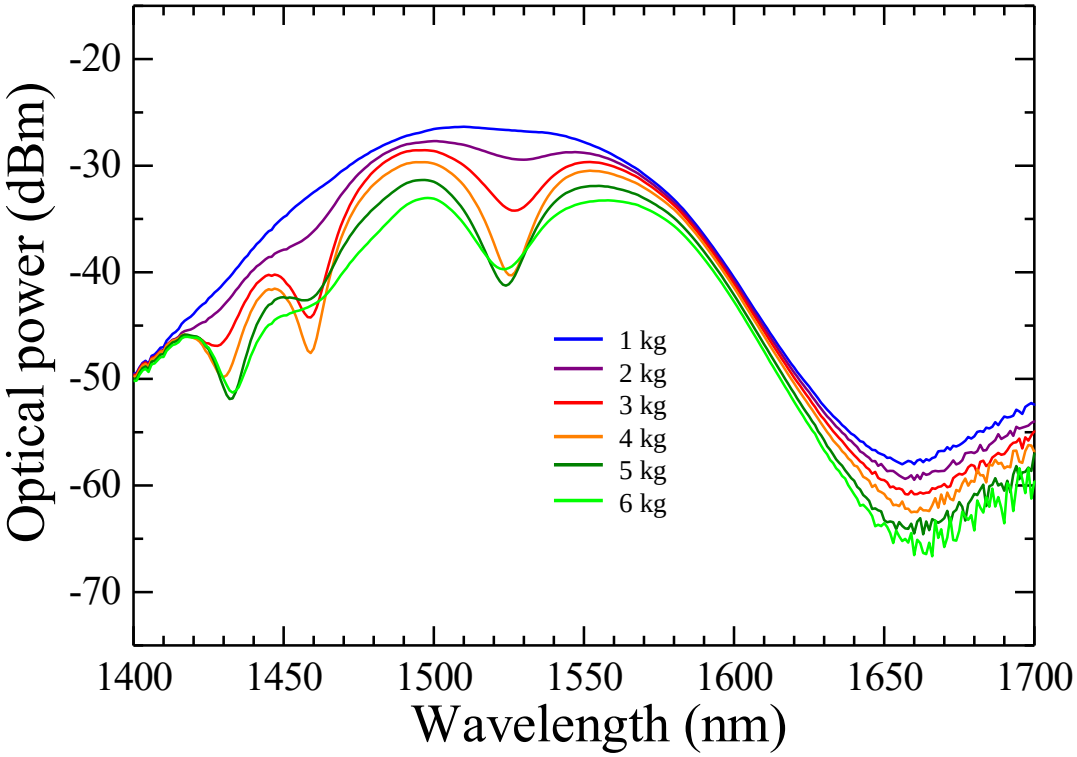

Figure 4.13 The spectral output by 3D printed LPFG device with Λ = 550 µm.

Table 4.6 Resonant wavelength vs perturbation weight by Λ = 550 µm.

	1st resonant λ	**2nd resonant λ**	**3rd resonant λ**
1 kg	1427 nm	1462 nm	1526 nm
2 kg	1427 nm	1458 nm	1530 nm
3 kg	1428 nm	1459 nm	1527 nm
4 kg	1430 nm	1459 nm	1526 nm
5 kg	1432 nm	1457 nm	1524 nm
6 kg	1433 nm	1461 nm	1523 nm

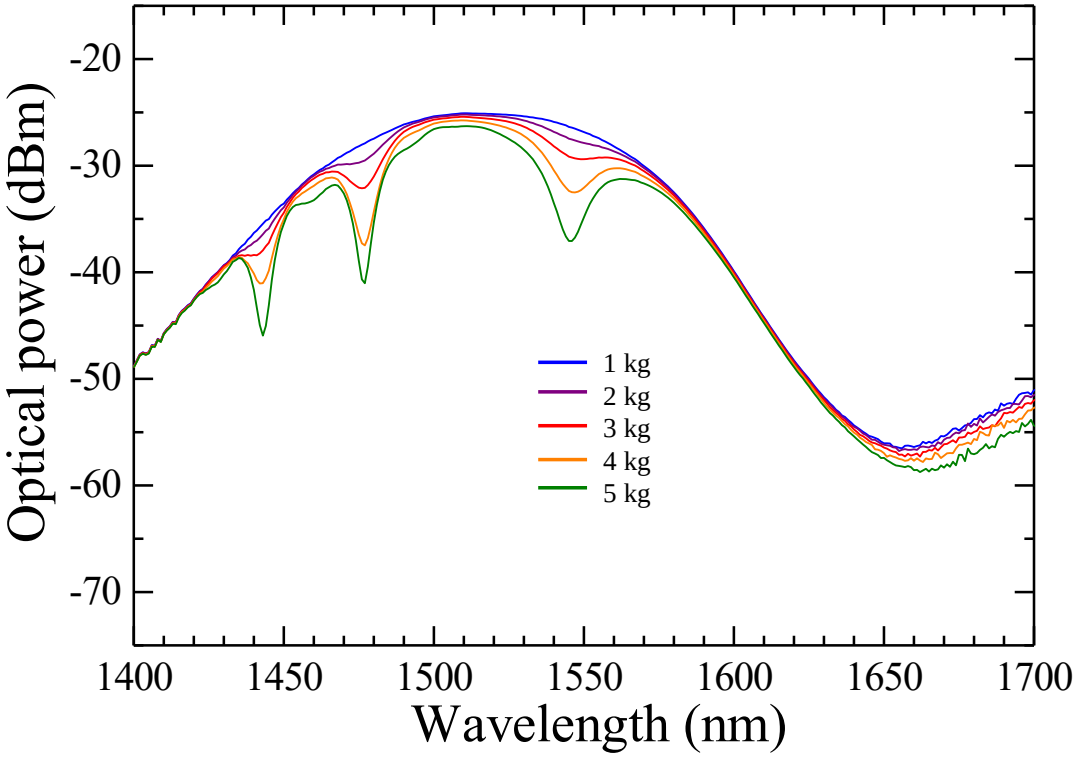

Figure 4.14 The spectral output by 3D printed LPFG device with Λ = 560 µm.

Table 4.7 Resonant wavelength vs perturbation weight by Λ = 560 µm.

	1st resonant λ	**2nd resonant λ**	**3rd resonant λ**
1 kg	1443 nm	1477 nm	1546 nm
2 kg	1442 nm	1476 nm	1546 nm
3 kg	1443 nm	1476 nm	1549 nm
4 kg	1442 nm	1477 nm	1547 nm
5 kg	1443 nm	1477 nm	1546 nm

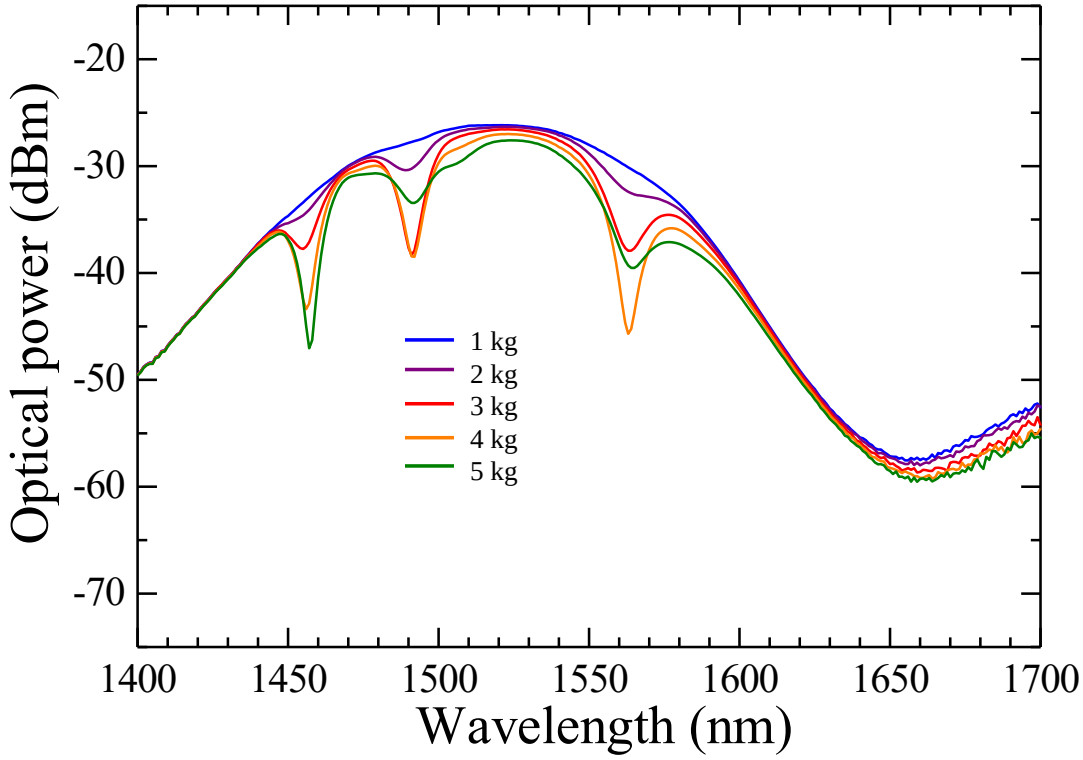

Figure 4.15 The spectral output by 3D printed LPFG device with Λ = 570 µm.

Table 4.8 Resonant wavelength vs perturbation weight by Λ = 570 µm.

	1st resonant λ	**2nd resonant λ**	**3rd resonant λ**
1 kg	1454 nm	1487 nm	1563 nm
2 kg	1454 nm	1489 nm	1563 nm
3 kg	1455 nm	1491 nm	1563 nm
4 kg	1456 nm	1492 nm	1563 nm
5 kg	1457 nm	1492 nm	1565 nm

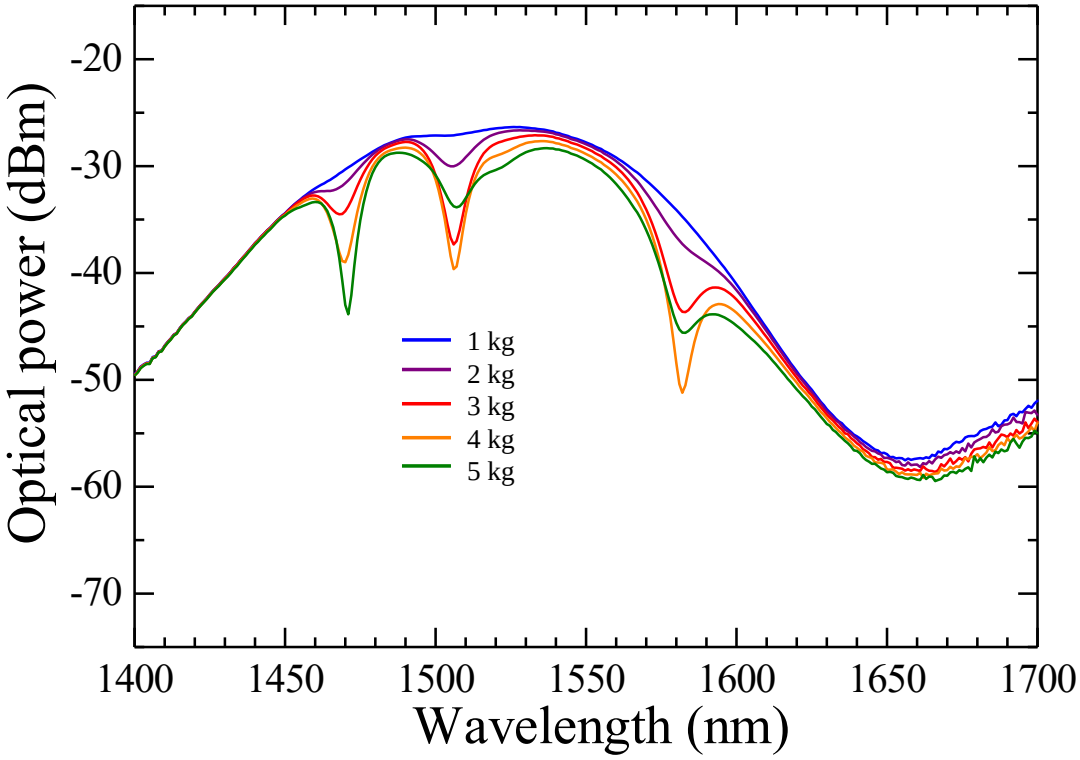

Figure 4.16 The spectral output by 3D printed LPFG device with Λ = 580 µm.

Table 4.9 Resonant wavelength vs perturbation weight by Λ = 580 µm.

	1st resonant λ	**2nd resonant λ**	**3rd resonant λ**
1 kg	1468 nm	1506 nm	-
2 kg	1469 nm	1506 nm	1582 nm
3 kg	1468 nm	1506 nm	1583 nm
4 kg	1470 nm	1506 nm	1582 nm
5 kg	1471 nm	1507 nm	1583 nm

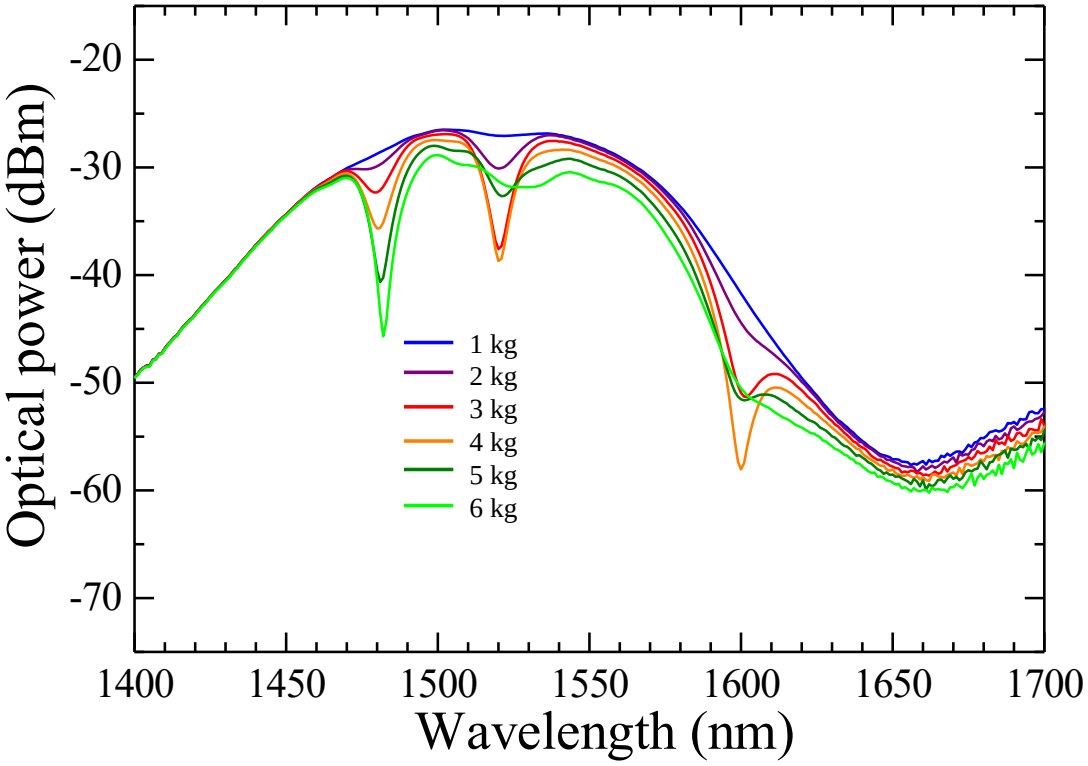

Figure 4.17 The spectral output by 3D printed LPFG device with Λ = 590 µm.

Table 4.10 Resonant wavelength vs perturbation weight by Λ = 590 µm.

	1st resonant λ	**2nd resonant λ**	**3rd resonant λ**
1 kg	1479 nm	1521 nm	-
2 kg	1479 nm	1520 nm	1600 nm
3 kg	1479 nm	1520 nm	1601 nm
4 kg	1480 nm	1520 nm	1600 nm
5 kg	1481 nm	1521 nm	1601 nm
6 kg	1482 nm	-	1600 nm

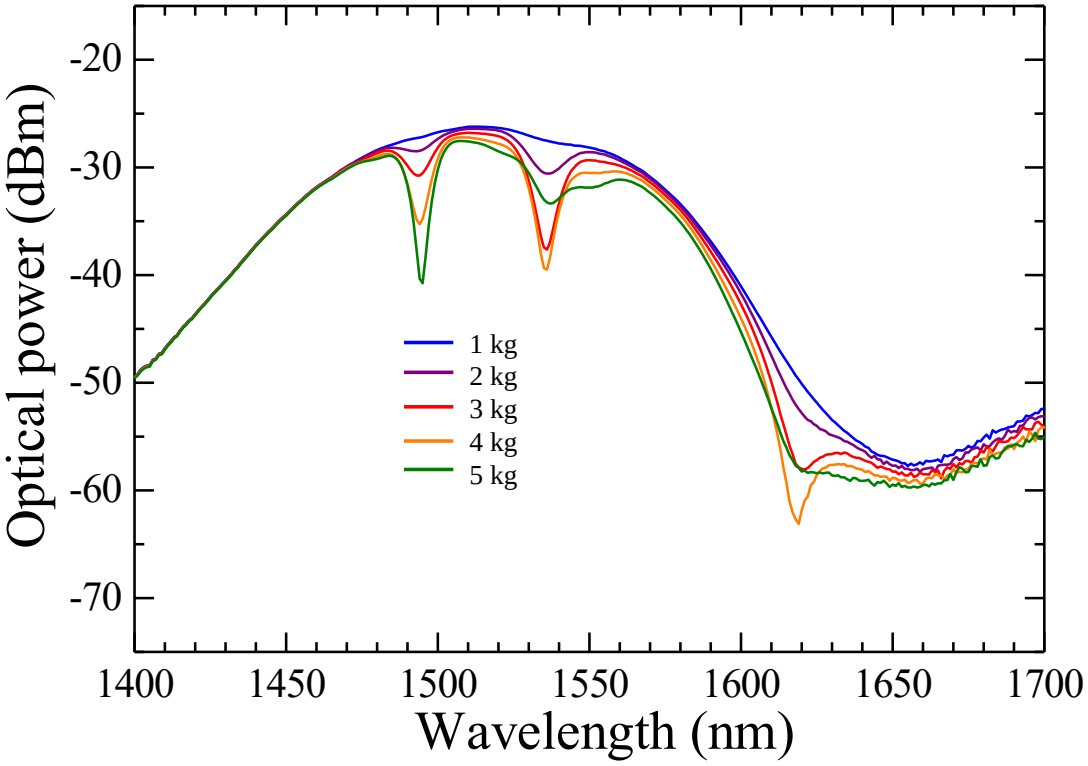

Figure 4.18 The spectral output by 3D printed LPFG device with Λ = 600 µm.

Table 4.11 Resonant wavelength vs perturbation weight by Λ = 600 µm.

	1st resonant λ	**2nd resonant λ**	**3rd resonant λ**
1 kg	1494 nm	1536 nm	-
2 kg	1493 nm	1536 nm	1621 nm
3 kg	1494 nm	1536 nm	1621 nm
4 kg	1494 nm	1536 nm	1619 nm
5 kg	1495 nm	1537 nm	1621 nm

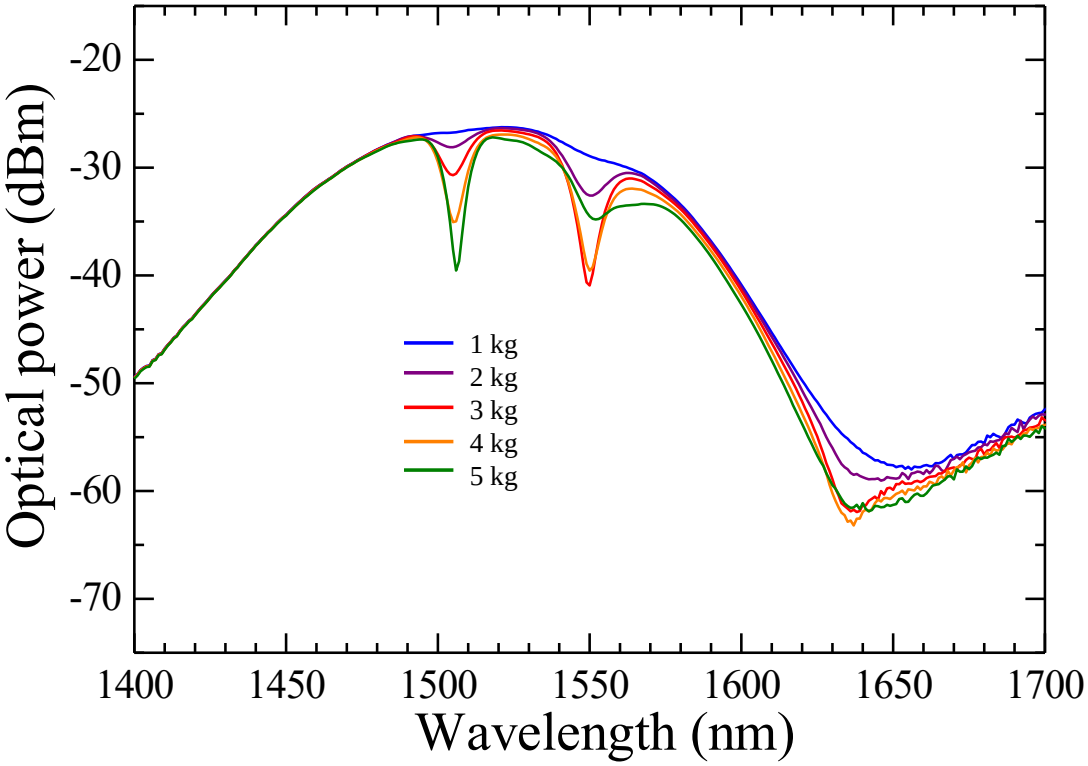

Figure 4.19 The spectral output by 3D printed LPFG device with Λ = 610 μm.

Table 4.12 Resonant wavelength vs perturbation weight by Λ = 610 μm.

	1st resonant λ	**2nd resonant λ**	**3rd resonant λ**
1 kg	1503 nm	1550 nm	-
2 kg	1504 nm	1551 nm	-
3 kg	1505 nm	1550 nm	1636 nm
4 kg	1505 nm	1550 nm	1637 nm
5 kg	1506 nm	1552 nm	1639 nm

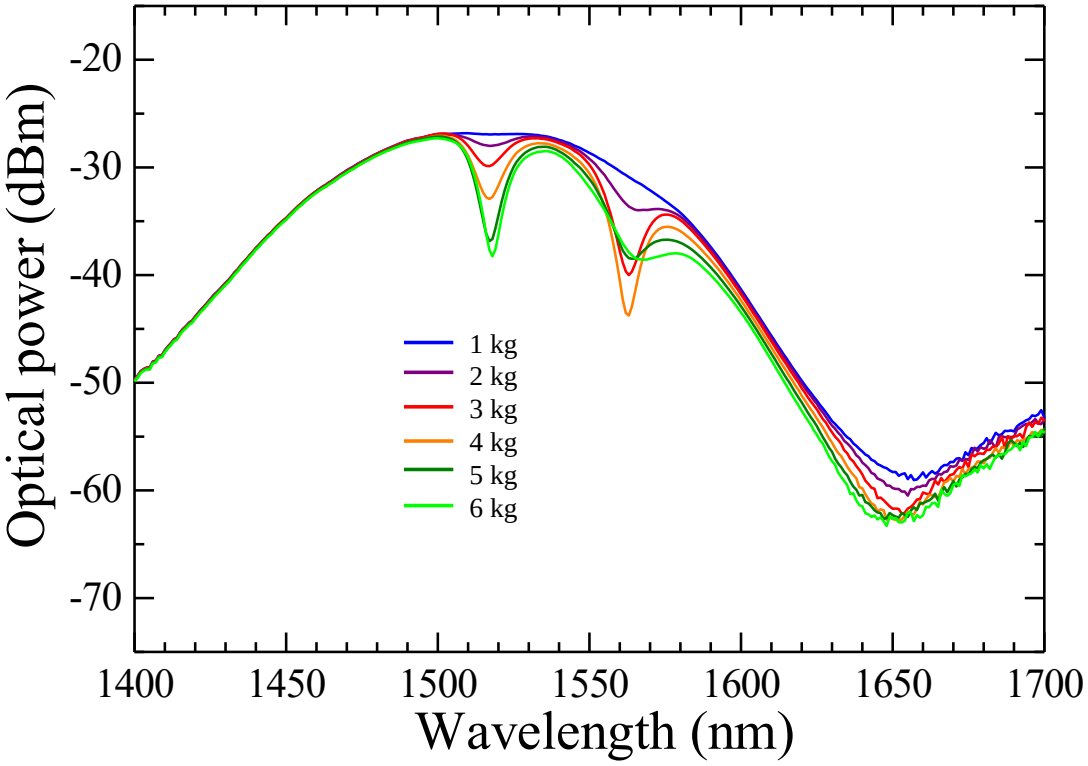

Figure 4.20 The spectral output by 3D printed LPFG device with Λ = 620 µm.

Table 4.13 Resonant wavelength vs perturbation weight by Λ = 620 µm.

	1st resonant λ	**2nd resonant λ**
1 kg	1517 nm	1564 nm
2 kg	1517 nm	1566 nm
3 kg	1517 nm	1563 nm
4 kg	1517 nm	1563 nm
5 kg	1517 nm	1564 nm
6 kg	1518 nm	1568 nm

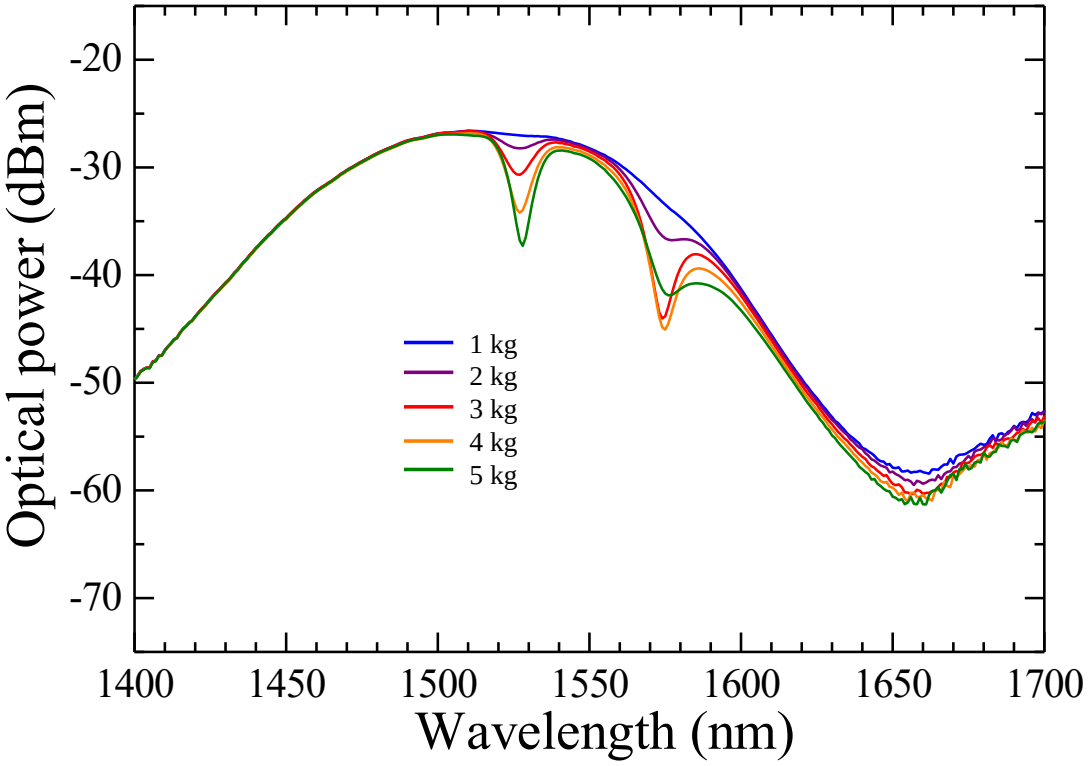

Figure 4.21 The spectral output by 3D printed LPFG device with Λ = 630 µm.

Table 4.14 Resonant wavelength vs perturbation weight by Λ = 630 µm.

	1st resonant λ	**2nd resonant λ**
1 kg	1527 nm	1575 nm
2 kg	1527 nm	1577 nm
3 kg	1527 nm	1574 nm
4 kg	1527 nm	1575 nm
5 kg	1528 nm	1576 nm

The single perturbation of the 3D printed LPFG device with different grating periods from 500 to 630 μm give several spectral output with different positions of resonant wavelengths regarding to each of perturbed devices. The spectral band from the light source limits the availability of the appearance of resonant wavelengths, so that some of longer grating periods give the output showing only two resonant bands while shorter grating periods show up for three and four resonant bands. The clearance of the resonant wavelength is also depending on the optical power at the position where the resonant wavelength locates. Resonant wavelengths at low power region are undefined.

The spectral output from the perturbation by a 3D printed LPFG device with 500 and 510 μm show that first two resonant wavelengths are undefined due to the low power region. In addition, the printed grating structure is very small in which it can result to the unstable periodic grating pitch during the printing process along the whole device. There is a big shift at the third resonant bands which are also resulted from the applied grating structure from the device when higher perturbation weight is pressed on the fiber. The fourth resonant bands have the weakest coupling strength comparing with another three resonant bands. The perturbation weight higher than 8 kg results to the decrease of resonant magnitude and the attenuation of the whole spectrum.

The spectral output from the perturbation by a 3D printed LPFG device with 520 μm shows clearer resonant wavelengths. First two resonant bands can be observed from the perturbation weight of 3 and 4 kg while another weights result to undefined resonant band. The third resonant bands rely on the higher optical power region, so that it is more clearly observed than of shorter grating periods. The characteristic of the fourth resonant bands are as same as the perturbation by shorter grating periods, but their magnitudes are more related to the perturbation weight. The perturbation weight higher than 7 kg results to all decrease of resonant magnitude and the attenuation of the whole signal.

The spectral output from the perturbation by a 3D printed LPFG device with 530 and 540 μm show that first two resonant wavelengths can be mostly observed to all dedicated perturbation weight. The magnitude of third resonant bands are not in uniform due to the periodic grating pitch along the whole device is not stable when higher perturbation weight is applied. The fourth resonant bands begin to appear at low power region in which low perturbation weight is undefined, but their magnitudes are still in uniform related to the perturbation weight. The perturbation weight higher than 5 kg results the attenuation of the whole signal.

The spectral output from the perturbation by a 3D printed LPFG device with 550 and 560 μm show only three resonant bands in which the fourth one is already out of the valid spectral range. The perturbation weight of 5 and 6 kg to the device with 550 μm let the whole spectrum begin to attenuate as observed at the range from between the second and the third resonant band. In addition, the grating

structure of the LPFG device has large grating pitch when higher perturbation is applied. The 3D printed LPFG device with 560 μm has uniform grating structure resulting to that the resonant wavelengths and their magnitudes are uniform. The perturbation weight higher than 6 kg from the applied LPFG device of 550 μm period and perturbation weight higher than 5 kg from the applied LPFG device of 560 μm period results to the attenuation of the whole spectrum.

The spectral output from the perturbation by a 3D printed LPFG device with the rest of grating periods until 630 μm show uniform resonant bands. Each of resonant wavelengths is corresponding to the applied grating period on the fiber. The spectra from the perturbation by grating periods of 620 and 630 μm contain only two resonant wavelengths while the third one is already out of the observed band or undefined. The higher perturbation weight than the assigned maximum weight to the perturbation by each grating device results to the attenuation of the whole signal. The different applied maximum weight depends on the grating structure on the optical fiber.

4.4.1 Discussion

The resonant wavelengths corresponding to the perturbation by each grating period of the 3D printed LPFG device show that those resonant wavelengths shift to the right or to the longer wavelength when longer grating period is applied on the fiber. The resonant wavelength at each position refers to each coupling mode to cladding layer as they have different mode orders of coupling. The amount of resonant wavelengths once appeared depends on the spectral range from the light source. In the other hand, broader spectrum band is able to show more resonant wavelengths. The plot of resonant shifts corresponding to grating periods is shown in Fig. 4.22.

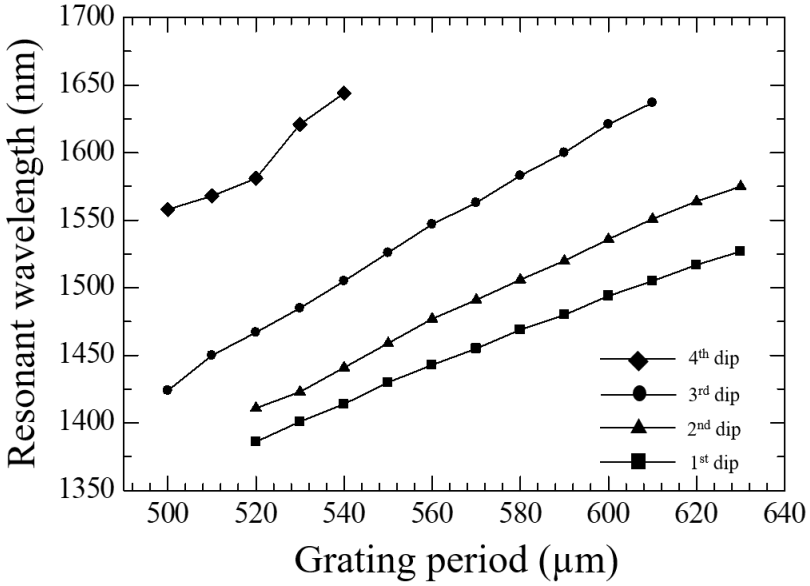

Figure 4.22 Resonant wavelength shift trend.

Figure 4.22 shows the total amount of four resonant wavelength shifts regarding to different applied grating periods of the device. The resonant shift is a linear function which is following the equation (3.4). The linear function between the resonant wavelength and the grating period is determined by the constant value of the differential effective refractive indices between core and cladding mode $\left(\delta n_{eff}\right)$ from the perturbation by the device. The constant values, δn_{eff} of the first to the third resonant wavelengths are 1.2857×10^{-3}, 1.5287×10^{-3}, and 1.9406×10^{-3}, respectively. In addition, the second and the third resonant wavelength shift are 18.9% and 50.9% of the first resonant wavelength shift, respectively. The third resonant wavelength has the longest shift whereas it yields the highest sensitivity. The coefficient of determination (R^2) is used to express the linearity of the trend. The value of R^2 for those three resonant wavelengths are 0.9979, 0.9975, and 0.9987, respectively. The third resonant shift has the highest linearity as well. The fourth resonant is considered as unclear because the band strength is very weak and they have low resonant magnitude resulting to that the linear trend of the fourth one is undefined from the perturbation of 3D printed LPFG devices.

The characteristic of resonant wavelength magnitude or its dip magnitude relating to each of perturbation weight depends on the grating pitches along the whole device in which they become wider when higher weight is applied on the fiber. The wider grating pitch results to the wider bandwidth of resonant wavelength. When the induced grating pitch is very close to the next one, it results to the attenuation of the whole spectral band of the transmitted signal. In addition, the magnitude or the dip is different to all resonant wavelengths at the same perturbation weight because each of coupling modes has different coupling strength and it is also depending on grating pitches.

4.5 Selected simultaneous perturbation of 3D printed LPFG devices

The resonant wavelengths from the perturbation by a single 3D printed LPFG device at every 10 μm grating period from 500 to 630 μm have been observed. In case of simultaneous perturbation of two devices, two grating periods are selected not to let resonant bands from the perturbation by both LPFG devices locate close to each other. The pair of 3D printed LPFG devices of 520/620, 520/630, 530/630, 530/640, 530/650, 540/630, 540/640, and 540/650 μm are selected to observe resonant wavelengths while both devices are simultaneously applied with the same perturbation weight. The additional force meter stand is added to this experiment set up as shown in Fig. 4.23. The spectral output of the simultaneous perturbation of two 3D printed LPFG devices are shown from Fig. 4.24 to Fig. 4.32.

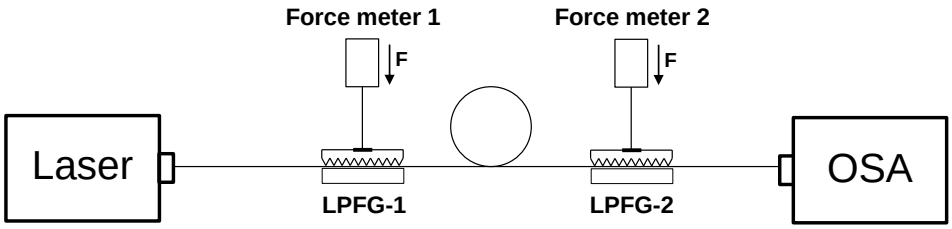

Figure 4.23 Simultaneous perturbation of two 3D printed LPFG devices.

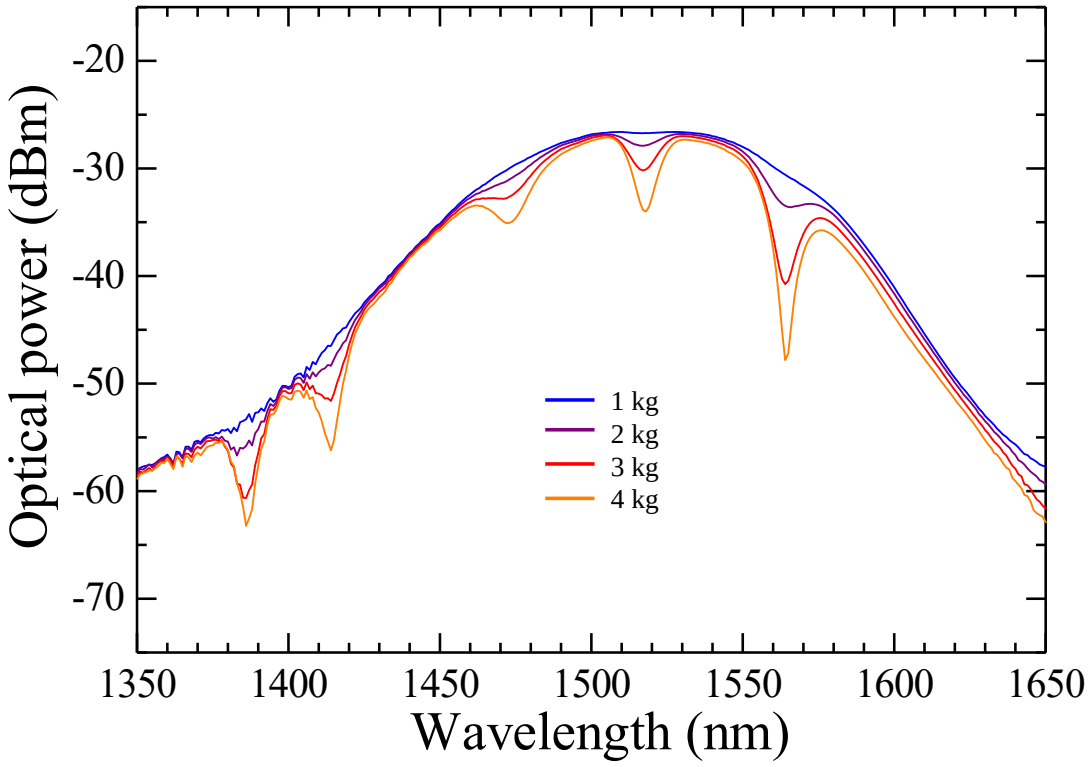

Figure 4.24 The spectral output by 3D printed LPFG devices with Λ = 520 and 620 µm.

Table 4.15 Resonant wavelength vs perturbation weight by Λ = 520 and 620 µm.

	1st resonant λ	**2nd resonant λ**	**3rd resonant λ**	**4th resonant λ**	**5th resonant λ**
1 kg	-	-	1472 nm	1517 nm	1565 nm
2 kg	1383 nm	1412 nm	1472 nm	1517 nm	1566 nm
3 kg	1386 nm	1412 nm	1471 nm	1517 nm	1564 nm
4 kg	1386 nm	1414 nm	1472 nm	1518 nm	1564 nm

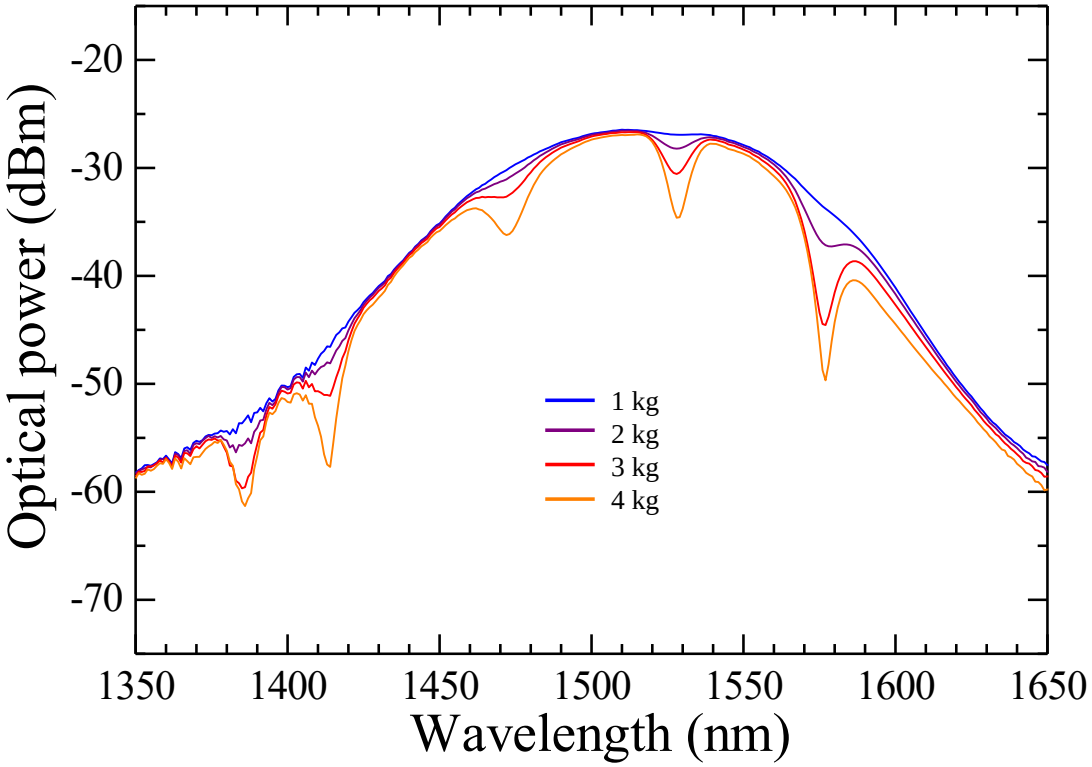

Figure 4.25 The spectral output by 3D printed LPFG devices with Λ = 520 and 630 µm.

Table 4.16 Resonant wavelength vs perturbation weight by Λ = 520 and 630 µm.

	1st resonant λ	**2nd resonant λ**	**3rd resonant λ**	**4th resonant λ**	**5th resonant λ**
1 kg	-	-	1472 nm	1528 nm	1576 nm
2 kg	1385 nm	1413 nm	1472 nm	1529 nm	1579 nm
3 kg	1385 nm	1412 nm	1471 nm	1528 nm	1577 nm
4 kg	1386 nm	1414 nm	1472 nm	1528 nm	1577 nm

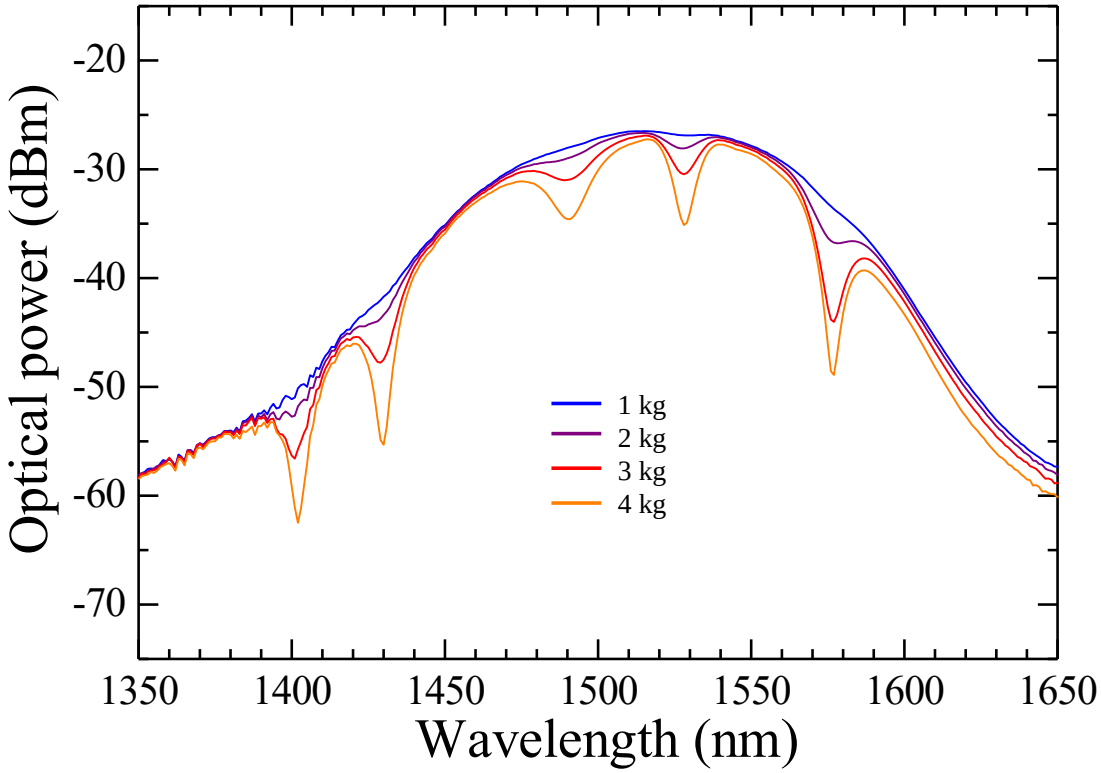

Figure 4.26 The spectral output by 3D printed LPFG devices with Λ = 530 and 630 µm.

Table 4.17 Resonant wavelength vs perturbation weight by Λ = 530 and 630 µm.

	1st resonant λ	**2nd resonant λ**	**3rd resonant λ**	**4th resonant λ**	**5th resonant λ**
1 kg	1401 nm	1429 nm	1490 nm	1528 nm	1576 nm
2 kg	1401 nm	1429 nm	1490 nm	1527 nm	1578 nm
3 kg	1401 nm	1429 nm	1489 nm	1528 nm	1577 nm
4 kg	1402 nm	1430 nm	1490 nm	1528 nm	1577 nm

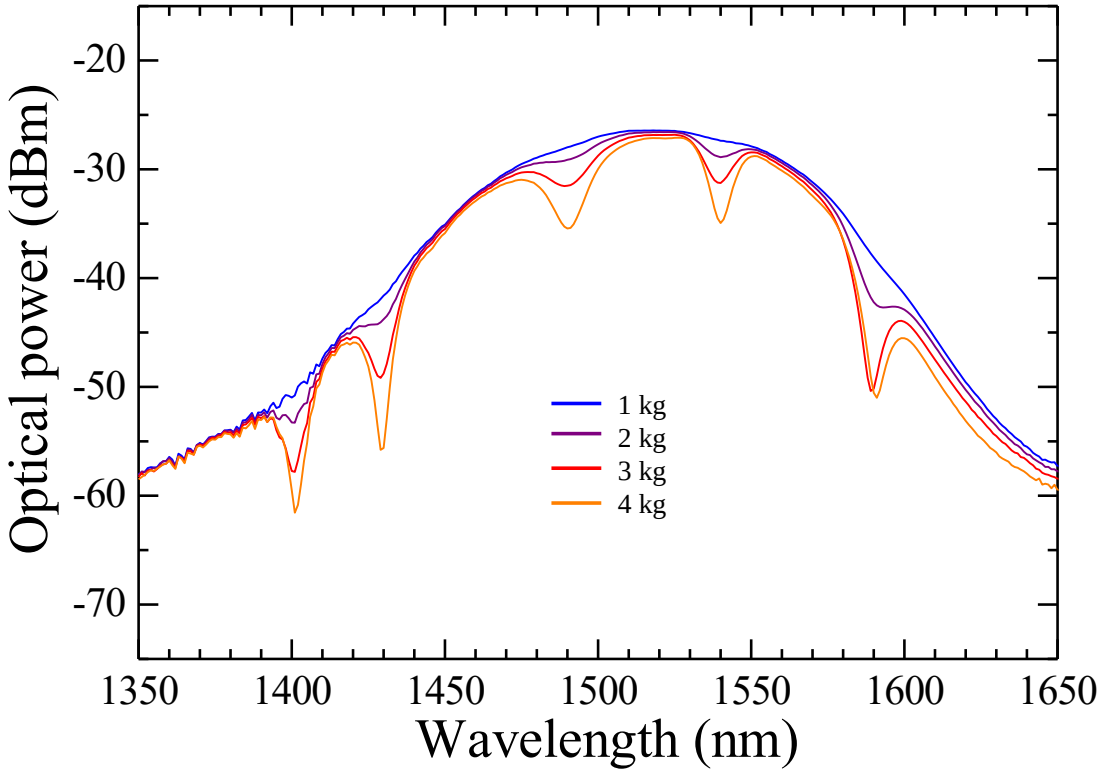

Figure 4.27 The spectral output by 3D printed LPFG devices with Λ = 530 and 640 µm.

Table 4.18 Resonant wavelength vs perturbation weight by Λ = 530 and 640 µm.

	1st resonant λ	**2nd resonant λ**	**3rd resonant λ**	**4th resonant λ**	**5th resonant λ**
1 kg	1401 nm	1429 nm	1490 nm	1540 nm	1590 nm
2 kg	1401 nm	1428 nm	1489 nm	1540 nm	1593 nm
3 kg	1401 nm	1429 nm	1489 nm	1540 nm	1589 nm
4 kg	1401 nm	1430 nm	1490 nm	1540 nm	1591 nm

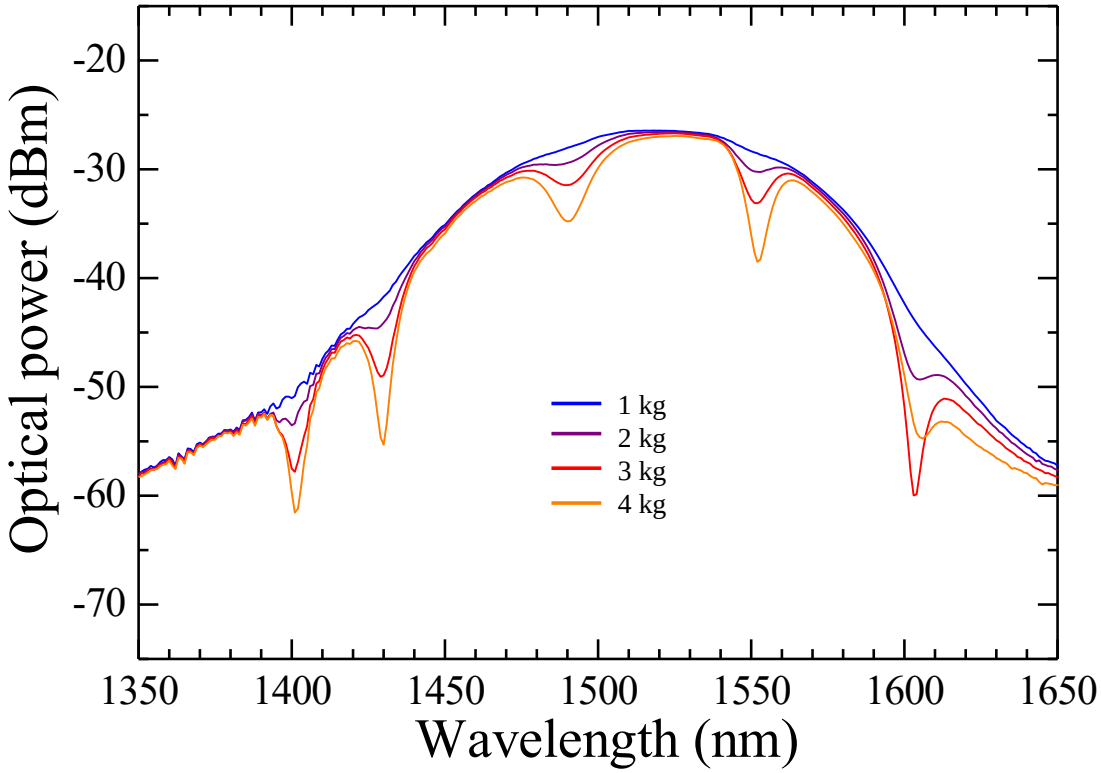

Figure 4.28 The spectral output by 3D printed LPFG devices with Λ = 530 and 650 µm.

Table 4.19 Resonant wavelength vs perturbation weight by Λ = 530 and 650 µm.

	1st resonant λ	**2nd resonant λ**	**3rd resonant λ**	**4th resonant λ**	**5th resonant λ**
1 kg	1401 nm	1429 nm	1490 nm	1552 nm	1604 nm
2 kg	1400 nm	1428 nm	1487 nm	1553 nm	1605 nm
3 kg	1401 nm	1429 nm	1489 nm	1552 nm	1603 nm
4 kg	1401 nm	1430 nm	1490 nm	1552 nm	1606 nm

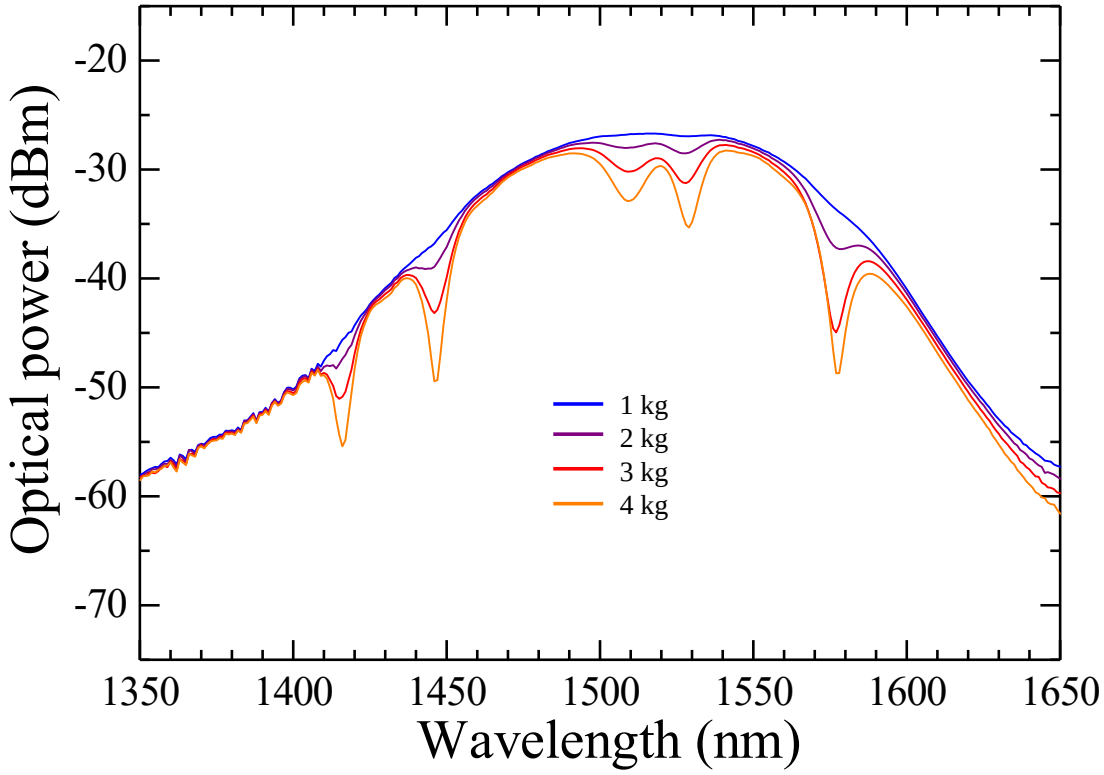

Figure 4.29 The spectral output by 3D printed LPFG devices with Λ = 540 and 630 µm.

Table 4.20 Resonant wavelength vs perturbation weight by Λ = 540 and 630 µm.

	1st resonant λ	**2nd resonant λ**	**3rd resonant λ**	**4th resonant λ**	**5th resonant λ**
1 kg	1416 nm	1446 nm	1508 nm	1528 nm	1576 nm
2 kg	1415 nm	1445 nm	1508 nm	1527 nm	1579 nm
3 kg	1415 nm	1446 nm	1509 nm	1528 nm	1577 nm
4 kg	1416 nm	1446 nm	1509 nm	1529 nm	1577 nm

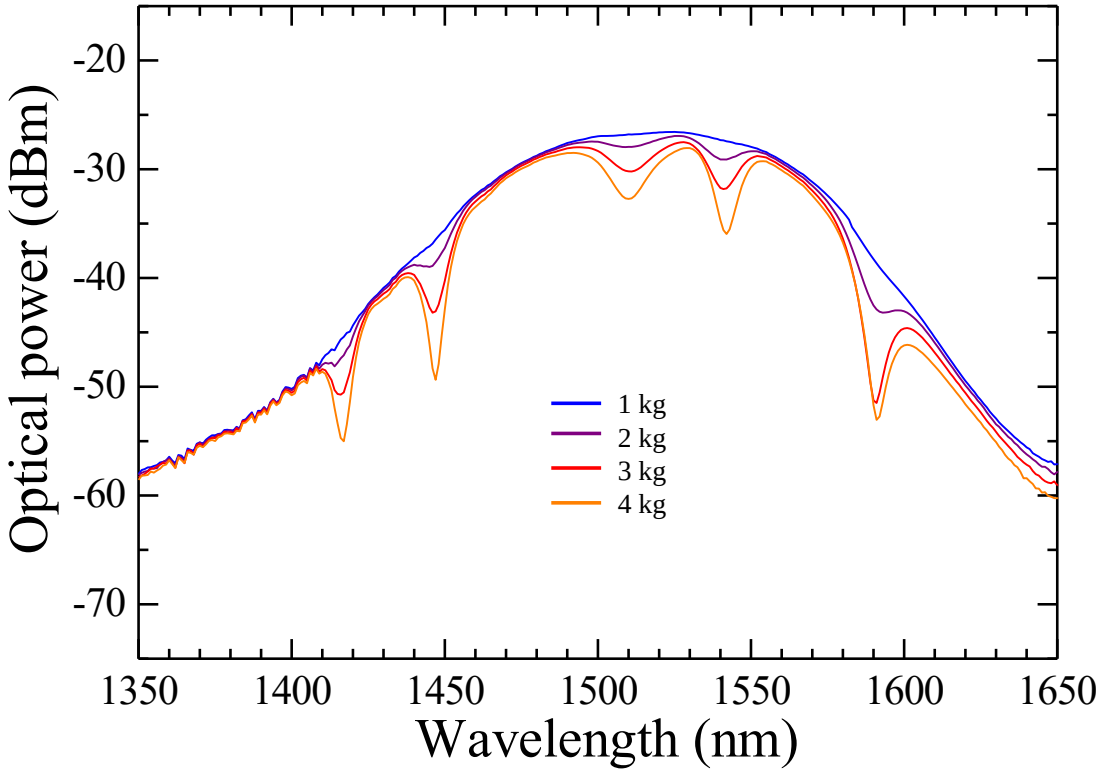

Figure 4.30 The spectral output by 3D printed LPFG devices with Λ = 540 and 640 µm.

Table 4.21 Resonant wavelength vs perturbation weight by Λ = 540 and 640 µm.

	1st resonant λ	**2nd resonant λ**	**3rd resonant λ**	**4th resonant λ**	**5th resonant λ**
1 kg	1416 nm	1446 nm	1509 nm	1541 nm	1592 nm
2 kg	1416 nm	1445 nm	1509 nm	1542 nm	1593 nm
3 kg	1416 nm	1446 nm	1511 nm	1541 nm	1591 nm
4 kg	1416 nm	1447 nm	1510 nm	1542 nm	1591 nm

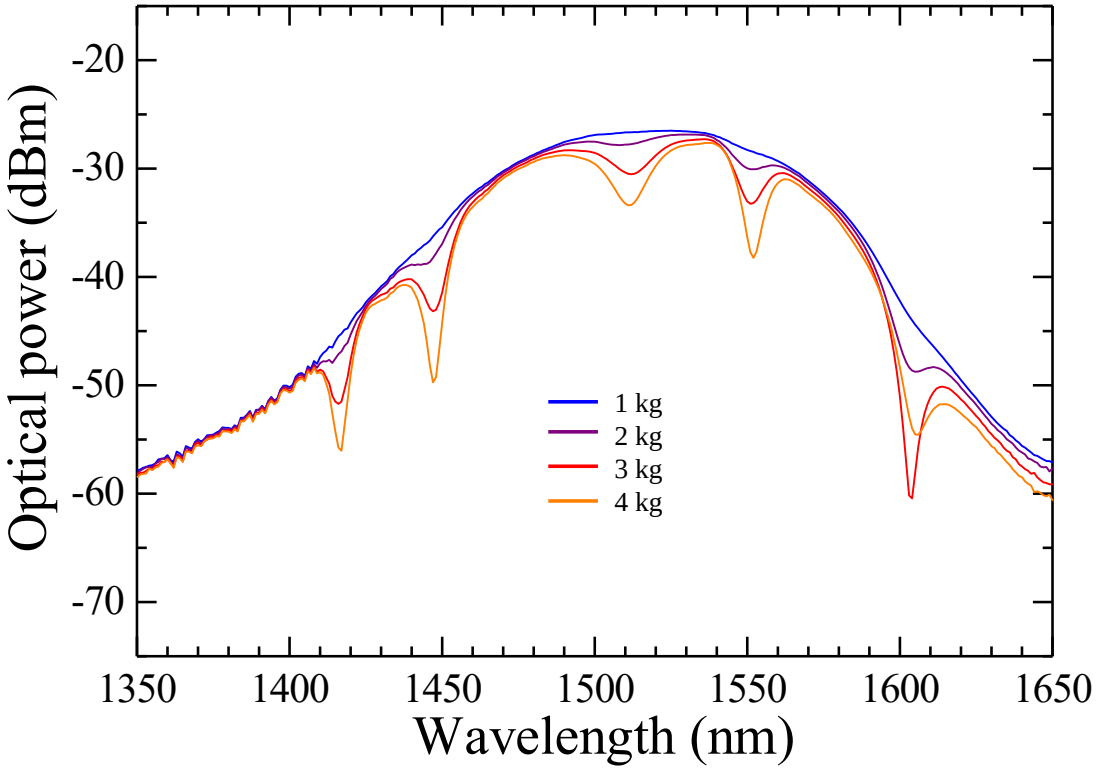

Figure 4.31 The spectral output by 3D printed LPFG devices with Λ = 540 and 650 µm.

Table 4.22 Resonant wavelength vs perturbation weight by Λ = 540 and 650 µm.

	1st resonant λ	**2nd resonant λ**	**3rd resonant λ**	**4th resonant λ**	**5th resonant λ**
1 kg	1416 nm	1446 nm	1509 nm	1551 nm	1604 nm
2 kg	1416 nm	1446 nm	1508 nm	1551 nm	1605 nm
3 kg	1416 nm	1447 nm	1512 nm	1551 nm	1604 nm
4 kg	1417 nm	1447 nm	1511 nm	1552 nm	1606 nm

4.5.1 Discussion

The simultaneous perturbation of two 3D printed LPFG devices with different grating period shows the results of five resonant wavelengths in which first three resonant bands belong to the perturbation of the LPFG device with lower grating period while the rest of two resonant wavelength bands belong to the perturbation of the LPFG device with higher grating period. The position of perturbation where the fiber is pressed by LPFG devices have no matter on the occurrence of resonant wavelengths. The LPFG structure can be applied at anywhere along the entire fiber. In case of this experiment, both 3D printed LPFG devices can be alternatively replacing each other to perform the grating structure. When the perturbation weight is increased, the resonant wavelengths may slightly shift a little due to the applied grating pitches along the LPFG device in practical way. The variation of resonant magnitude depends on the perturbation of each LPFG device separately. More amount of 3D printed LPFG devices can be added up to the system in case of using a light source with broader band of light wave. The perturbation of both LPFG devices with 540 and 630 μm shows the spectral result that there is a little interference between the third and fourth resonant bands where both resonant bands belong to the perturbation of different LPFG devices (third band belong to 540 μm grating period and fourth band belong to 630 μm grating period). Therefore, the appearance of resonant wavelengths to the perturbation of each LPFG device is independent to each other unless the coupling modes of the light propagation from the perturbation by both LPFG devices are locating at the same wavelength or very close to each other.

4.6 The perturbation of 3D printed LPFG device with tilted angle

The resonant shift from the perturbation of a single 3D printed LPFG device shows that it is linear function with the grating period of the device. The width of 2.5 cm supports the tilt angle to expand the grating period of the device. The expansion of grating period $\left(\Lambda_e\right)$ is expressed as

$$\Lambda_e = \frac{\Lambda}{\cos\theta} \tag{4.2}$$

where θ is the tilt angle. Additional equipment to support the rotation of the fiber axis alignment instead of tilting the LPFG device is the 3D printed fiber rotator as shown in Fig. 4.32. The selected grating period of the LPFG device for this perturbation is 550 μm. The fiber axis is rotated by the 3D printed fiber rotator from its initial axis (0 degree) to 25 degrees with an increment of 5 degrees. The perturbation weight selected to observe resonant wavelengths is fixed at 4.5 kg. The resonant wavelengths to all perturbations are shown in Fig. 4.33.

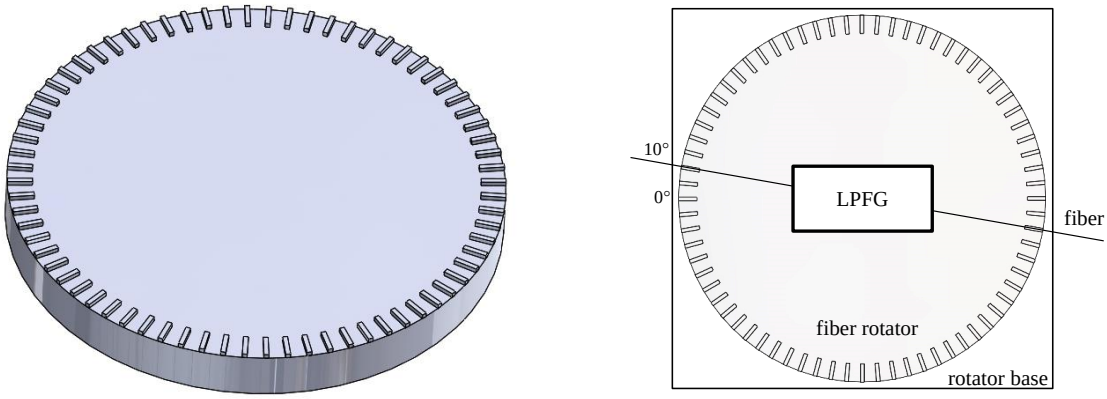

(a) (b)

Figure 4.32 (a) 3D printed fiber rotator and (b) fiber alignment on the rotator.

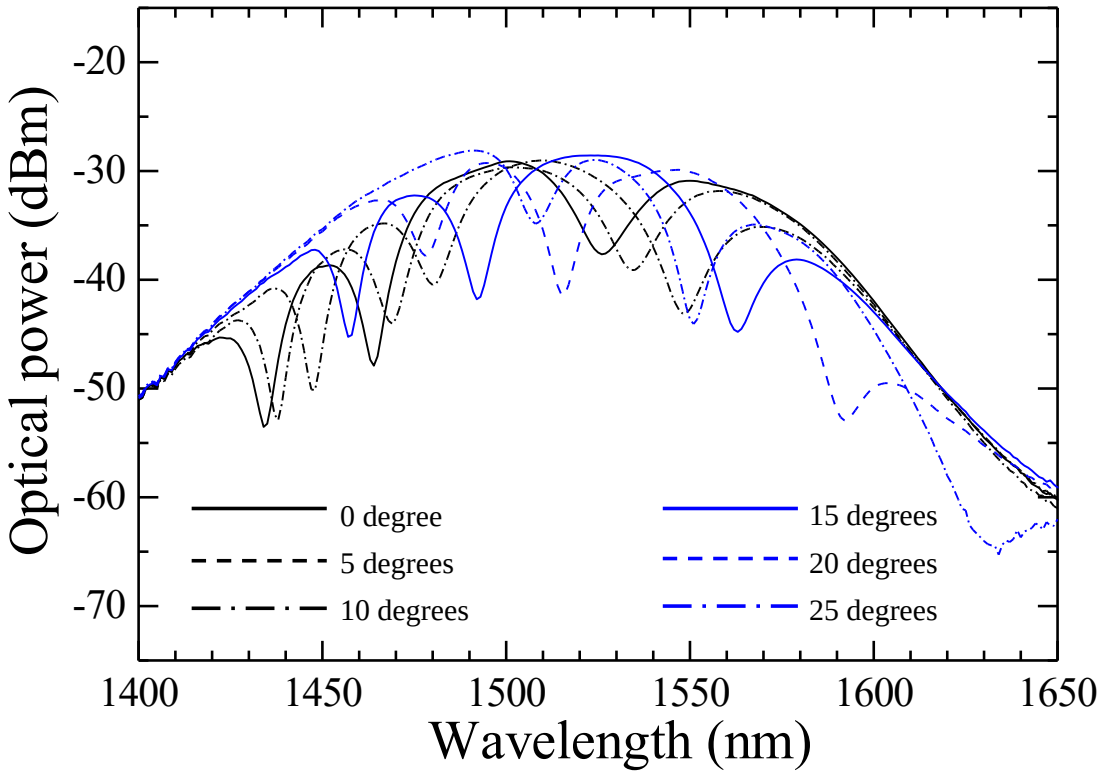

Figure 4.33 The resonant wavelength shift from tilted LPFG device at every 5 degrees.

4.6.1 Discussion

The perturbation of a 3D printed LPFG device with the grating period of 550 μm shows that all resonant wavelengths shift to the right corresponding to the expansion of the grating period of the LPFG device. The trend of resonant wavelength shift related to the expanded grating period is clarified in Fig. 4.34 and Table 4.23.

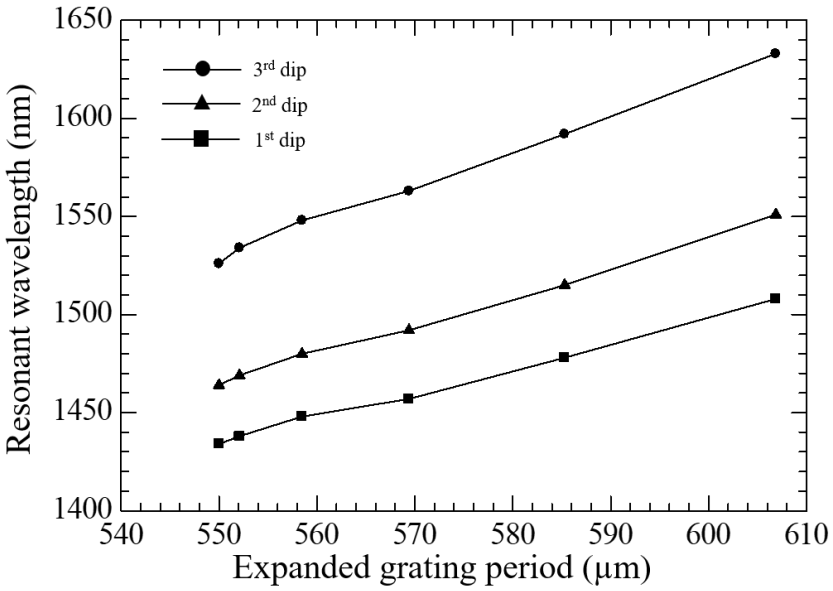

Figure 4.34 Resonant wavelength trend from tilted LPFG device.

Table 4.23 Resonant wavelength vs tilt angle of 550 μm Λ LPFG device.

Tilt angle	Expanded Λ	1st resonant λ	2nd resonant λ	3rd resonant λ
0°	550.00 μm	1434 nm	1464 nm	1526 nm
5°	552.10 μm	1438 nm	1469 nm	1534 nm
10°	558.48 μm	1448 nm	1480 nm	1548 nm
15°	569.40 μm	1457 nm	1492 nm	1563 nm
20°	585.30 μm	1478 nm	1515 nm	1592 nm
25°	606.86 μm	1508 nm	1551 nm	1633 nm

The expansion of the grating period by tilting the device at every 5 degrees is in the trend of exponential. However, when the resonant wavelength shifts are observed from the experiment, the shifts corresponding to the expanded grating period due to tilting the LPFG device show that the shift trend is still a linear function as same as the single perturbation does. From the experimental results, the average shifts of three resonant wavelengths determined by δn_{eff} are 1.2666 x10^{-3}, 1.4843 x10^{-3}, and 1.8194 x10^{-3}, respectively. Moreover, the linearity defined by the coefficient of determination (R^2) of three resonant wavelengths are 0.9959, 0.9965, and 0.9967, respectively. In comparison with the single perturbation, the δn_{eff} of all shifts are slightly lower because the tilted device performing the grating structure on the fiber offers different strain on the fiber surface when it is pressed by those

grating pitches of the device. The tilted device yields larger induced refractive index of the induced section resulting to the smaller grating expansion as it should be. Nevertheless, the perturbation by rotating the optical fiber with some angles and then pressing the LPFG device on to the fiber show that even the small value of expanded grating period still results to the linear shift of all resonant wavelengths. In case of the perturbation with any grating periods of the LPFG device, they may result to the linear shift of resonant wavelengths as well.

The grating structure on the optical fiber performed by pressing the 3D printed LPFG device made by resin material has a potential to filter out partial wavelength from the broadband wavelength. The main characteristic to create the LPFG structure on the fiber is the periodic change of the refractive index of the fiber's core layer to lead the coupling from fundamental core mode to cladding modes when the light is propagated through the fiber. Conventional methods to create the LPFG structure had a high potential of the fabrication of LPFG, but those methods required several equipment setup and they permanently changed the fiber structure. The mechanically induced method to fabricate the LPFG structure uses an external device to create the fiber structure in which the fiber becomes LPFG only when the corresponding device is perturbed or pressed on the fiber. The advantage of this fabrication technique is that the fiber can be reused to the next perturbation or other purpose. The technology of 3D printing becomes more popular in the recent era. The 3D printed object contains high accuracy of its resolution and it is resistant to the harsh environment. The 3D printed LPFG device has a simple design and its dimension is compatible with the fiber. The designed grating period can be an option for the selection to appropriate usage relating to the available range of the light wave. In addition, the design of grating pitch, sharpen or curved design, plays a big role to the characteristic of resonant wavelengths and the requirement of the maximum perturbation weight. The FWHM bandwidth of the resonant wavelength is varied by the size of applied grating pitch. The sharpness of the grating pitch affects the maximum perturbation weight in which more sharpen grating pitch lowers the maximum applied weight it the fiber can be broken more easily than the perturbation by curved grating pitch. The perturbation of the 3D printed LPFG device with different specifications of the fiber may result to different resonant wavelength because they have different refractive indices of core and cladding layers. However, the resonant wavelength shift is still the linear function with the change of the grating period. Lastly, the resonant wavelength can be controlled by the selection of the grating period of the 3D printed LPFG device.

Reference

[1] "**Chapter 5 Optical Fiber**," [Online] Available: www.towa-denshi.co.jp/hikari.pdf [2018, March 23].

[2] "**Anritsu MS9710C Optical Spectrum Analyzer 600 to 1750 nm**," [Online] Available: https://www.upc.edu/sct/ca/documents_equipament/d_125_id-630.pdf [2018, March 23].

[3] "**Economic digital force gauges FGJN series**," [Online] Available: http://www.nidec-shimpokeisoku.jp/en/products/01/01/fgn-b/001.html [2017, May 11].

[4] "**RGD720 transparent material simulating standard plastics**," [Online] Available: http://www.advancedtek.com/wp-content/uploads/2019/10/Data-Sheet-Transparent-RGD720.pdf [2019 , August 10].

CHAPTER 5 ELECTRIC FIELD DISTRIBUTION ALONG GRATING STRUCTURE

5.1 Introduction

This chapter presents the characteristic of electric field distribution to the cladding layer along the fiber axis when the transmitted light with a specific wavelength is propagating through the core layer of the fiber. The observation of those characteristics is taken by the simulation in which the selected software is FullWAVE (Synopsys Inc., Version March 2018) [1]. This software is operated by using finite-difference time-domain (FDTD) technique to solve the Maxwell's equations in optics field [2]. The main purpose of this software relating to the research is to observe the distribution characteristic of an electric field when the light is transmitting through the grating pitches as the periodic change of the fiber's core layer. The real dimension of the fiber and its surrounding cannot be simulated because the simulation time is infinity. All dimension of the fiber is shrunk to support the simulation by the software and not to consume very long time. The electric field distribution to cladding layer from several grating structures with different grating periods are observed.

5.2 Design and parameter setup for simulation

Several parameters corresponding to the fiber and the grating period of the grating structure are set up to simulate the electric field by using FullWAVE (Synopsys, Inc.) The fiber structure is drawn in RSoft CAD as a cylindrical structure representing the fiber's core layer and it is surrounded by the space as shown in Fig. 5.1.

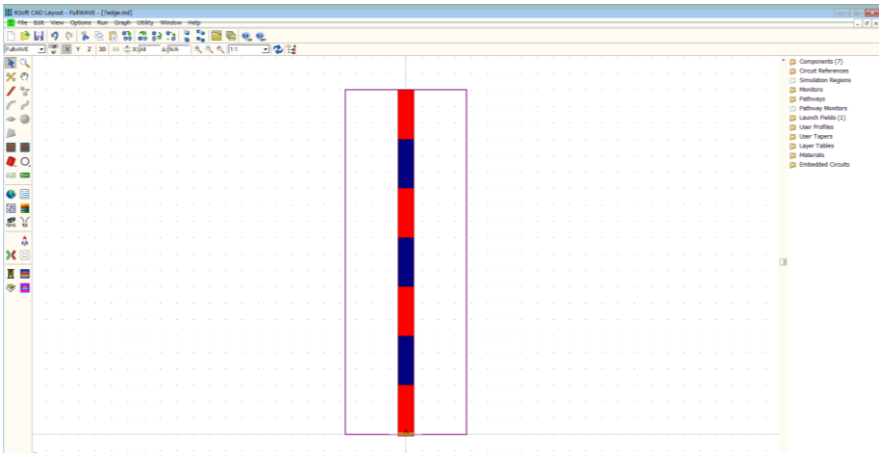

Figure 5.1 The design of grating structure in RSoft CAD software.

The RSoft CAD software is the software used to design the structure and input several parameters to run the simulation of transverse electric (TE) and transverse magnetic (TM) modes. From the cylindrical design structure, it represents the fiber's core layer. Red and blue colors denote the section with different refractive indices. Red section refers to the initial core index and blue section refers to the effective refractive index of the grating pitch. The white space denotes the fiber's cladding layer. The purple boundary corresponds to the spatial domain where the region of simulation takes place. The larger spatial domain consumes longer simulation time. The limitation of the design is that the real dimension of the fiber takes infinite time to run the simulation. The dimension of the design is then shrunk to the size in which it does not take long time for the simulation. The core diameter is set up at 0.8 μm whereas its initial dimension is 8 μm. The grating period is decreased to 100 times, e.g. 500 μm grating period is deducted to only 5 μm for the simulated structure in the software. The length of the fiber varies by the grating period, an amount of grating pitches, and a size of each grating pitch.

The example structure shown in Fig. 5.1 has a dimension of 1x21 μm. The size of the grating pitch is half of the grating period as the length of blue section is as same as the length of red section and this structure contains three grating pitches. The size of the grating pitch is 3 μm and the grating period is 6 μm. In case of the structure for the simulation related to the experiment, some grating periods are selected to observe the electric field distribution characteristic from the transmitted light wavelength as mentioned by the third resonant wavelength. The structure design of the fiber's core layer always begins and ends with the initial refractive index structure (red section), thus the section of grating pitches (blue section) relies between the initial section. The simulation of electric field distribution with the amount of the structure with four grating periods is observed in TE mode. The grating structure with the grating period of 5.2, 5.5, 5.8, and 6.1 μm are selected to observe the electric field distribution along the grating structure. The grating pitch size (blue section) is 1.0 μm. The additional details of those grating structures are clarified in Table 5.1.

Table 5.1 Input parameters to design grating parameters in FullWAVE (Synopsys Inc.).

Input wavelength (nm)	**Grating period (μm)**	**Red section (μm)**	**Blue section (μm)**	**Structure length (μm)**
1467	5.2	4.2	1.0	19.8
1527	5.5	4.5	1.0	21.0
1582	5.8	4.8	1.0	22.2
1639	6.1	5.1	1.0	23.4

Additional parameters are required for the simulation such as refractive indices to all structure parts, grid size of the spatial grid, TE polarization, and 3D structure. The resolution of the simulated results depends on the input grid size along x-, y-, and z-axis. Grid size with greater value consumes longer time, however, the higher resolution of the result can be observed. In addition, the electric field distribution characteristic at the specific point along the structure axis can also be observed. The example of the grating structure with the grating period of 5.3 μm and the grating pitch size of 1.0 μm is shown in Fig. 5.2. The rest of three structures are just only changing the grating period by changing the red section as clarified in Table 5.1. The total length of the fiber is varied by the grating structure. The spatial domain is set at ± 5.31 μm to all design structures to limit the simulation time. Additional parameter setup is found in the appendix.

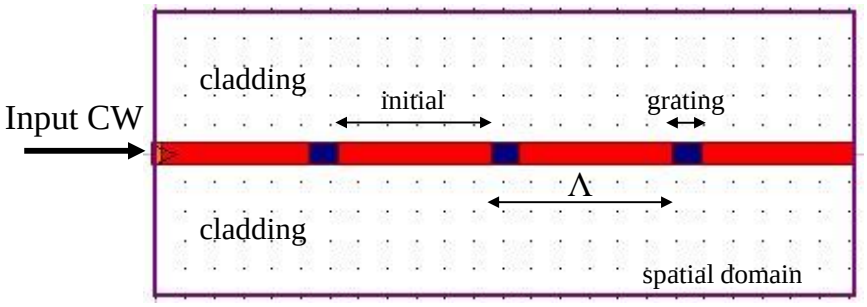

Figure 5.2 Grating structure with 5.3 μm Λ and 1.0 μm pitch.

5.3 Simulation results

The simulation results of all grating structures are expressed in Fig. 5.3 to Fig. 5.6. All grating structures contain 3 grating pitches with 1.0 μm each and 4 initial index sections. The size of the initial index section is varied by the grating period. The refractive index, refers to the specification of standard SMF-28 step index single-mode fiber, of the initial fiber core (red section) is 1.45205 and of the cladding (surrounding the grating structure) is 1.44681. The effective refractive index of the grating section (blue section) has the index difference (Δn) of 0.4. In other words, the effective refractive index of the grating section is 1.84681. The input of an index difference is very high because the structure of the fiber in RSoft CAD is shrunk ten times of its initial size. The input continuous wave (CW) of the transmitted light refers to the third resonant wavelength from the perturbation by corresponding grating periods of the LPFG device. When the light is transmitting through the fiber's core and passing the grating pitch, there is a distribution or the scattering of the light to the cladding layer. The strength of those distributions corresponds the coupling of light from core to cladding layer. The different size of the grating pitch and different input of refractive indices may result to different characteristic of the distribution.

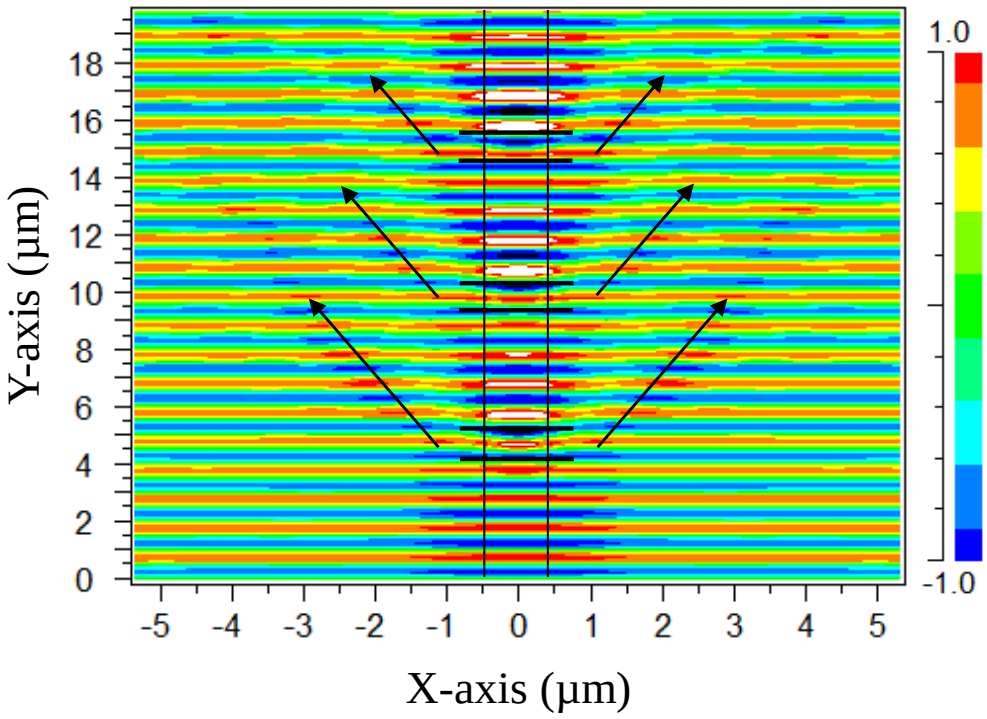

Figure 5.3 Electric field distribution along grating structure with 5.2 µm Λ.

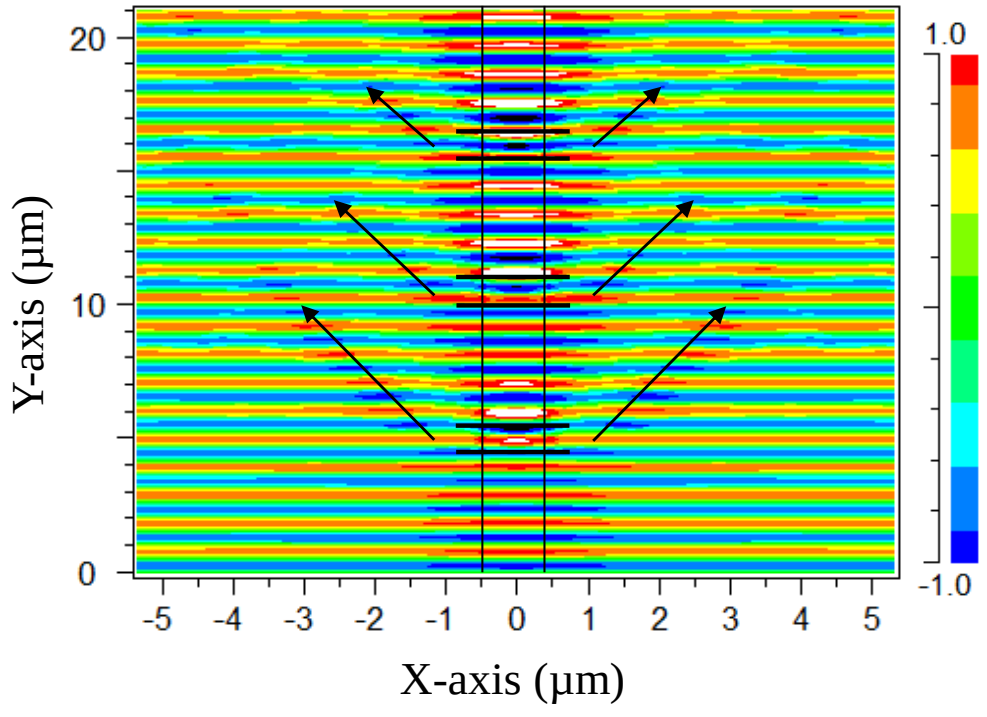

Figure 5.4 Electric field distribution along grating structure with 5.5 µm Λ.

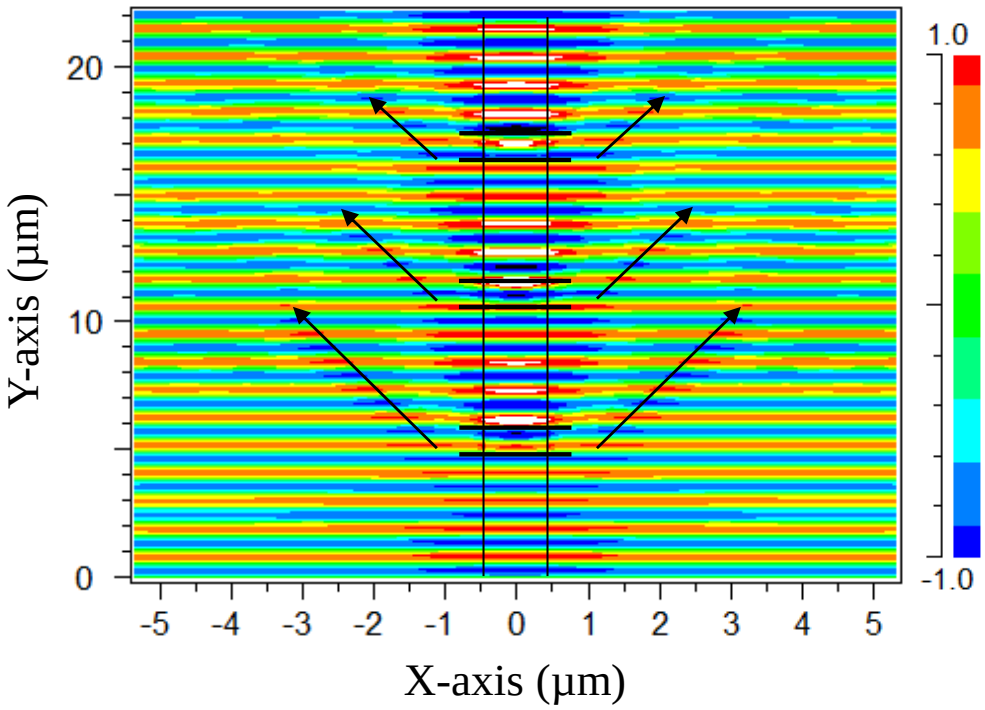

Figure 5.5 Electric field distribution along grating structure with 5.8 µm Λ.

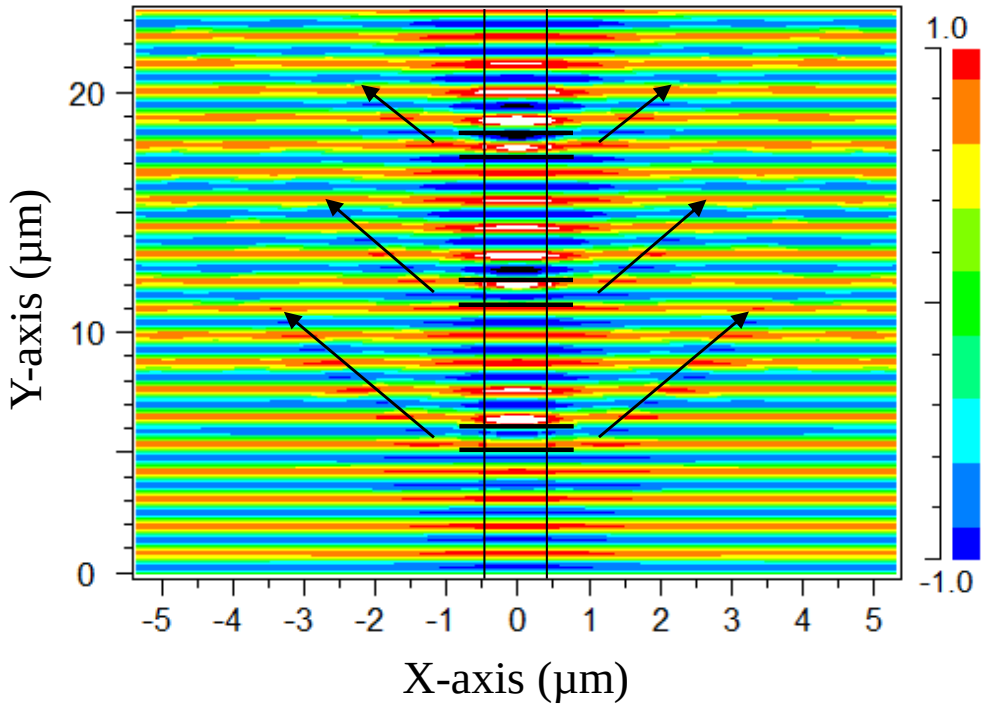

Figure 5.6 Electric field distribution along grating structure with 6.1 µm Λ.

Besides the characteristic of the electric field distribution along the grating structure, the contour of an electric field profile can also be observed at any position along the structure axis. At the first grating pitch, an electric profile is recorded at the middle position of the pitch. At the second pitch, an electric profile is recorded at the boundary between the initial and the grating section (forward). At the last pitch, an electric field profile is recorded at the middle position as same as of the first pitch. Some examples of the profile are shown in following Fig. 5.7 to Fig. 5.10.

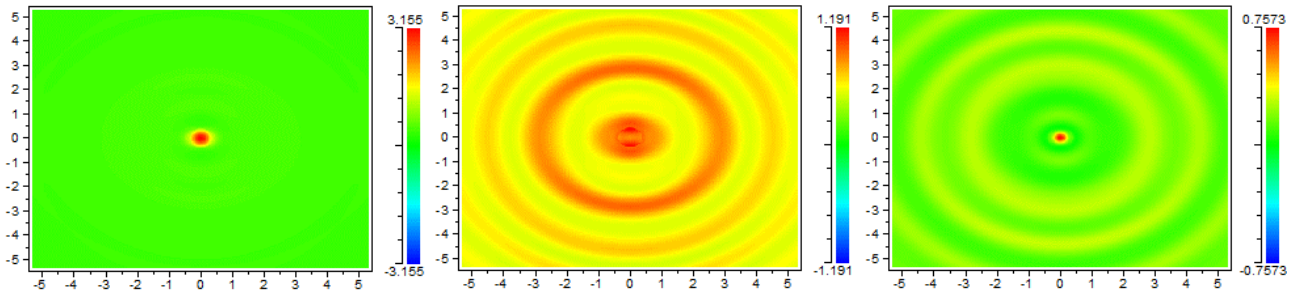

1st grating pitch 2nd grating pitch 3rd grating pitch

Figure 5.7 Electric field profile of the grating structure with 5.2 µm Λ along the structure axis.

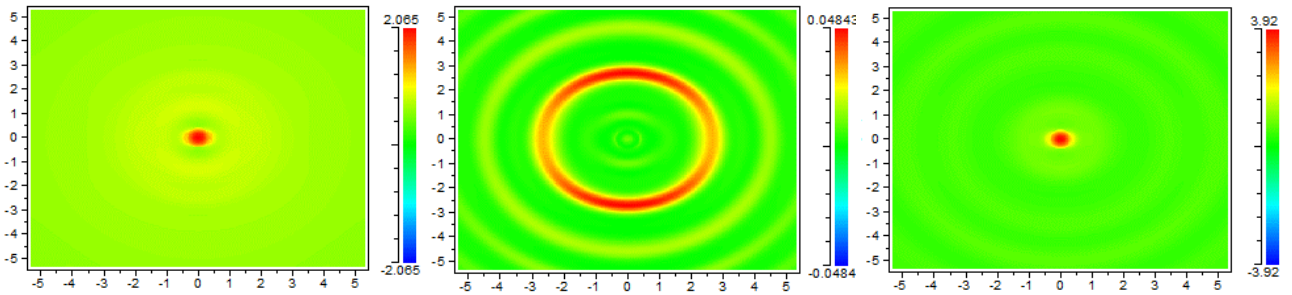

1st grating pitch 2nd grating pitch 3rd grating pitch

Figure 5.8 Electric field profile of the grating structure with 5.5 µm Λ along the structure axis.

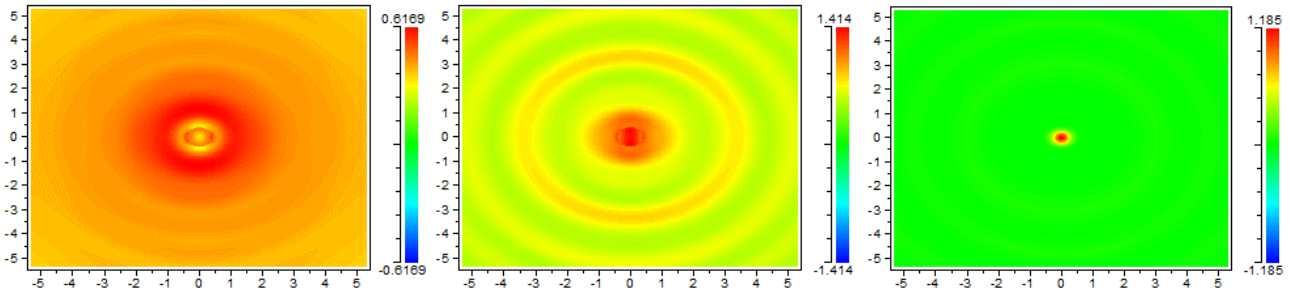

1st grating pitch 2nd grating pitch 3rd grating pitch

Figure 5.9 Electric field profile of the grating structure with 5.8 µm Λ along the structure axis.

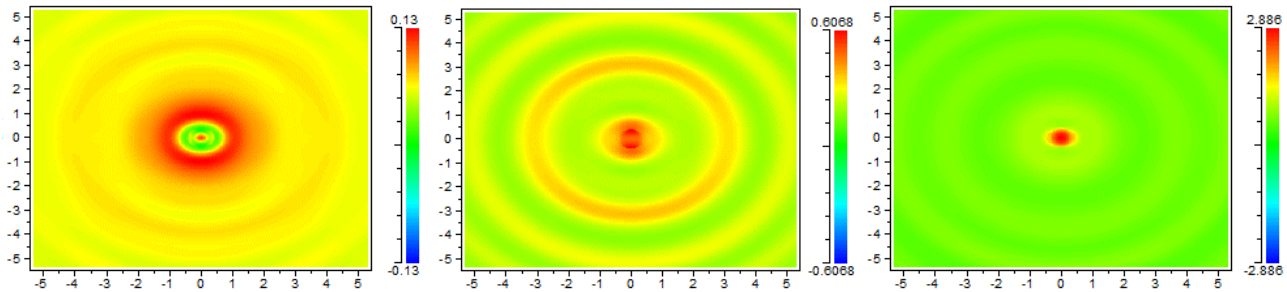

1st grating pitch 2nd grating pitch 3rd grating pitch

Figure 5.10 Electric field profile of the grating structure with 6.1 μm Λ along the structure axis.

The dimension of the results is 5.31x5.31 μm following by the spatial domain of the simulation. The center of those profiles is fiber's core with its diameter of 0.8 μm. Figure 5.7 shows that when the light is transmitting through the first grating pitch, the electric field is still passing through the structure until approaching the second pitch. The coupling to the cladding layer begins and it results to the decreasing of the field magnitude at the core layer, but not the entire field. The third pitch shows that the field is still remaining in the core layer. Figure 5.8 shows that the field at the second pitch mostly relies in the cladding layer while in the third pitch, the field is still in the core layer. The coupling is not complete when it passes the second pitch. Figure 5.9 shows that the coupling begins densely from the first pitch as seen at the surrounding core layer. There is no coupling in the third pitch. Figure 5.10 has a similar profile as of the Fig. 5.9 that there is almost no coupling at the third pitch whereas the first and second pitch do.

5.4 Discussion

The distribution of an electric field scatters to the cladding layer when it transmits through the grating pitch where it has a different refractive index from its original core layer. The input wavelength has its significant to the phase of an electric field. The grating pitch locating on the position where the electric field is in phase will result to the coupling from core layer to cladding layer. In case of that some grating pitch does not have the coupling or the coupling is very low because the field is not in phase to be coupled. The contour of the field profile is observed at each point of section along the structure axis in which it is not observed as a range. The coupling of the field may occur elsewhere within the region of that grating pitch. In addition, the electric field is in phase to the position where the grating pitch locates comes from the corresponding input wavelength at special wavelength, so called the resonant wavelength. The coupling from core to cladding layer is the characteristic that the magnitude of an electric field is increased in the cladding layer while it is decreased in the core layer. This is the attenuation of the resonant wavelength. More amount of grating pitches increases the coupling strength when the corresponding light wavelength is passing through

and when the coupling is totally complete, longer grating length will have no further effect to the coupling anymore.

Every single of input parameters has all effects to the simulation output. Grid size parameter of x-, y-, and z-axis affects the simulation time and the resolution of the simulation result. If one of those parameters is changed, the simulation output or even the field profile will be different from the figures shown above. Refractive indices of the initial core layer, grating pitch and the core surrounding play a vital role to the characteristic of an electric field distribution along the entire grating structure. Practically, those characteristics of electric field distribution are observed as the attenuation of resonant wavelengths from the broadband input wavelength of transmitted light. Therefore, the light coupling from core layer to cladding layer is resonant with the transmitted light through the fiber at a specific wavelength.

Reference

[1] Synopsys Inc., "**RSoft FullWAVE v2018.03 user guide**," 9-13, Optical Solution Groups New York, 2018.

[2] A. Taflove, "**Computational electrodynamics: The finite-difference time-domain method,**" Artech House, Massachusetts, USA, 1995.

CHAPTER 6 CONCLUSION

6.1 Preface

This chapter presents the conclusion of the experiment by using 3D printed LPFG devices to perform the grating structure on the fiber and the simulation of the electric field distribution along the grating structure by using FullWAVE (Synopsys Inc.). The sensor application of the fiber by using 3D printed LPFG device is also clarified. All experimental and simulation results are subjected to only this specific setup which cannot be the standard with the different fiber specification.

6.2 Resonant wavelength from 3D printed LPFG devices

The creation of the LPFG began from the study of the photosensitivity inside the Ge-doped silica fiber. The development of the fiber grating fabrication has been inspired and developed to increase its efficiency for the wavelength filter. Several fabrication techniques began from the irradiation of the laser to change the refractive index of the fiber. In addition, those techniques permanently changed the fiber structure to become LPFG. In the past few years, the fabrication of LPFG structure could be done on the fiber temporarily by using an external device to press or perturb on the fiber. Several devices have been already used to perform the LPFG on the fiber, however, the limitation was that those devices had unique form and shape resulting to the limitation of changing their grating period on the device itself. Moreover, the technology of the 3D printing became popular to various fields and applications. The printing material has also been developed to support and be patient to the harsh environment. The 3D printed LPFG device made by resin was created and its design corresponded to the specific grating period and its dimension for an appropriate to the usage and application.

The purpose of the LPFG structure is the coupling of modes inside the fiber at specific wavelength as it is practically observed as resonant wavelength. Once the LPFG structure is created while perturbing the 3D printed LPFG device on the fiber, there are more than one resonant wavelength due to the coupling from core mode to different cladding modes. However, those resonant wavelengths are varied by the grating period of the applied LPFG device. The perturbation of LPFG devices with several behaviors on the optical fiber proves that the shift of those resonant wavelengths is linear with the change of the grating period as observed by increasing every 10 μm period and tilting the LPFG device every 5 degrees. In addition, the experiment is taken under the stable temperature at around room temperature of 25 °C. The result of those resonant wavelength shifts

shows that the linearity clarified by the coefficient of determination (R^2) is greater than 0.99. These results have proved that the temporary fabrication of an LPFG structure on the optical fiber by using a 3D printed LPFG device has a potential to control the resonant wavelengths. Those phenomena are applicable to the optical sensors such as tunable filter in the optical link. The magnitude of resonant wavelengths is applicable for the weight sensor or intruder sensor to strange object stepping on the sensor area. The perturbation by the LPFG device on the different specification of optical fiber results to different resonant wavelength shifts due to different effective refractive indices of the fiber which affects the coupling mode strength.

6.3 Electric field distribution

The simulation of an electric field distribution by using FullWAVE (Synopsys Inc.) software shows that the electric field from corresponding resonant wavelength as an input to the grating structure scatters to the cladding layer when it transmitted through the first grating pitch where it has different index from the initial core layer of the fiber. Not only the design grating structure is shrunk to few micrometers, but also the index difference between the initial core and the grating pitch is very large to lower the simulation time as it is the limitation of the software. The simulation is done only with a single input wavelength of light, not the broadband wavelength. However, the simulation results follow the theory of coupling from the core mode to cladding mode. When the coupling to cladding mode occurs, the magnitude of the field decreases in the core region. Therefore, when the input wavelength of the transmitted light is resonant with the grating period, the coupling from core to cladding modes occurs.

6.4 Suggestions for the future work

The fabrication of the LPFG structure by using mechanically induced of the 3D printed LPFG devices is successful to the application of tunable wavelength filter. Besides the actual design of the grating pitch with the triangular crest, any design of the crest is possible to create by using a 3D printer such as sinusoidal curve or trapezoid crest. Those different pitches result to different grating structure appeared on the fiber at all. Moreover, the property of the resin material is similar to the metal which increase the efficiency of the resonant wavelength and its attenuation relating to the perturbation weight of the LPFG device. Moreover, the perturbation with the different specification of the fiber is important that the results of resonant wavelengths are different from those in this research. The perturbation under large temperature change may also affects to the resonant wavelength shift as well. It is mandatory to record and observe new resonant wavelength shifts before

the setup is subjected to the application as a sensor. In case of an intruder sensor to the heavy object, it can be applied by adding the weight attenuation to the setup to decrease the weight pressing on the LPFG device and the fiber.

APPENDIX

The parameter setup for the simulation in FullWAVE (Synopsys Inc)

RSoft CAD Layout

1. Global settings window

Model dimension: 3D

Free space wavelength: [1]1.467, [2]1.527, [3]1.582, [4]1.639

Background material: Locally defined

Background index: 1.44681

Index difference: 0.00524

Component width: 0.8

Component height: width

Index profile type: Step

3D structure type: fiber

2. FullWAVE simulation parameters

2.1 Spatial Grid

Domain min: X = -5.31, Y = -5.31, Z = 0

Domain max: X = 5.31, Y = 5.31, Z = [1]19.8, [2]21.0, [3]22.2, [4]23.4

Grid size: [1]0.03, [2]0.03, [3]0.04, [4]0.04 to all X, Y, Z

2.2 FDTD options, Polarization: TE

2.3 Time grid: parameters are automatically generated by the software.

3. Properties for segment (red and blue section)

3.1 Red section (initial core layer)

Material properties: Locally defined

Index difference: delta

Index (img part): alpha

Component width: width

Component height: height

Starting and ending vertex refers to the dimension of the structure along z-axis.

3.2 Blue section (grating ptch)

Material properties: Locally defined

Index difference: 0.4

Index (img part): alpha

Component width: width

Component height: height

Starting and ending vertex refers to the dimension of the structure along z-axis (1.0 μm).

4. Properties for monitor on grating pitch #1, #2, #3

Width: 10.62

Height: 10.62

Length: 0

Phi: 0

Theta: 0

Spatial outputs vs time: E density

X: 0

Y: 0

Z: [1]#1 = 4.7, [1]#2 = 9.4, [1]#3 = 15.1

[2]#1 = 5.0, [2]#2 = 10.0, [2]#3 = 16.0

[3]#1 = 5.3, [3]#2 = 10.6, [3]#3 = 16.9

[4]#1 = 5.6, [4]#2 = 11.2, [4]#3 = 17.8

Remarks:

[1]The simulation of the grating structure with the grating period of 5.2 μm.

[2]The simulation of the grating structure with the grating period of 5.5 μm.

[3]The simulation of the grating structure with the grating period of 5.8 μm.

[4]The simulation of the grating structure with the grating period of 5.2 μm.